International
Progress Report

IPR-02-34

Äspö Hard Rock Laboratory

TRUE Block Scale project

Evaluation of fracture network transport pathways and processes using the Channel Network approach

William Dershowitz
Kate Klise

Golder Associates Inc., Seattle, U.S.A.

December 2002

Svensk Kärnbränslehantering AB
Swedish Nuclear Fuel
and Waste Management Co
Box 5864
SE-102 40 Stockholm Sweden
Tel +46 8 459 84 00
Fax +46 8 661 57 19

Äspö Hard Rock
Laboratory

Report no.
IPR-02-34
No.
F56K
Author
William Dershowitz
Kate Klise
Date
Dec. 2002
Checked by
Anders Winberg
Date
June 2003
Approved
Christer Svemar
Date
2004-02-12

Äspö Hard Rock Laboratory

TRUE Block Scale project

Evaluation of fracture network transport pathways and processes using the Channel Network approach

William Dershowitz
Kate Klise

Golder Associates Inc., Seattle, U.S.A.

December 2002

Keywords: Fractured rock, FracMan, processes, retention, tracer transport, TRUE Block Scale

Abstract

This report presents three studies carried out following the completion of the "Phase C" tracer tests. These studies address the following three aspects of the TRUE Block Scale Hypotheses (Winberg et al., 2000):

a) Hypothesis #1: the validity of the hydro-structural model developed by the project, specifically whether minor changes to the hydro-structural model could provide significant improvement in modeling of hydraulic interference

b) Hypothesis #2: the fracture intersection zone (FIZ) hypothesis, specifically whether the idea of mass loss through fracture intersection zones is a credible possibility, and

c) Hypothesis #3: the nature of transport processes in fracture networks, specifically focusing on the role of immobile zones.

These studies have demonstrated that the advection-dispersion-diffusion concept for transport within fracture networks is reasonably consistent with both hydraulic and transport observations. There are statistical indications that fracture intersections may have special properties for transport, and may possibly serve as flow barriers in some cases. The hydro-structural model used in the project can explain most of the observed hydraulic and transport responses, supporting the validity of that model, with minor modifications.

Evaluation of conservative and sorbing tracer experiments indicate that the hydrostructural model and microstructural model can be used to explain observed tracer retention, without resorting to assumptions of enhanced retention as was indicated by previous studies.

Sammanfattning

Denna rapport presenterar resultaten från tre modelleringsstudier som genomförts efter slutförandet av Phase C-försöken. Dessa studier analyserar tre aspekter av de hypoteser som formulerades inför fältförsöken inom ramen för TRUE Block Scale (Winberg et al., 2003):

a) Hypotes #1: giltigheten och tillämpbarheten av den av projektgruppen utvecklade hydrostrukturella modellen, speciellt om mindre förändringar av den hydrostrukturella modellen kan ge märkbara förbättringar i modelleringen av hydrauliska interferenser

b) Hypotes #2: rollen som skärningszoner mellan sprickor (FIZ) spelar, och specifikt om förlust av spårämnen genom skärningszoner är en möjlighet, och

c) Hypotes #3: transportprocesser i nätverk av sprickor, med speciell tonvikt på den roll som immobila zoner längs transportvägarna spelar.

De utförda studierna har visat att konceptet advektion-dispersion-diffusion för transport i nätverk av sprickor är i stort konsistent med tillgängliga hydrauliska och transportmässiga observationer. Det föreligger statistiska indikationer att skärningszoner mellan sprickor (FIZ) kan ha speciella transportegenskaper, och i vissa fall kan fungera som flödesbarriärer. Den hydrostrukturella modellen som använts inom projektet kan förklara merparten av de noterade hydrauliska och transportmässiga responserna, vilket med smärre modifieringar, stöder giltigheten hos den konstruerade modellen.

Table of Contents

List of Figures

List of Tables

1 Introduction

The hydraulic and tracer tests conducted during 1999 and 2000 for the TRUE Block Scale Project (Andersson et al., 2000a, 2000b, 2001, 2002b) provide a wealth of information to improve the understanding of flow and transport pathways and processes. This report presents three studies carried out following the completion of the "Phase C" tracer tests. These studies address the following three aspects of the TRUE Block Scale Hypotheses (e.g. Andersson et al., 2002b):

a) Hypothesis #1: the validity of the hydro-structural model developed by the project, specifically whether minor changes to the hydro-structural model could provide significant improvement in modeling of hydraulic interference

b) Hypothesis #2: the fracture intersection zone (FIZ) hypothesis, specifically whether the idea of mass loss through fracture intersection zones is a credible possibility, and

c) Hypothesis #3: the nature of transport processes in fracture networks, specifically focusing on the role of immobile zones.

The first study (Chapter 2) addressed the validity and limitations of the "Revised March 2000 Hydro-structural Model" (Hermanson and Doe, 2000). The hydro-structural model was evaluated by simulating hydraulic interference responses within the model. Each discrepancy between measurement and simulation was then investigated and hypotheses were formulated regarding what model limitations could be responsible. The hydro-structural model was investigated with and without background fractures.

The second study (Chapter 3) addressed the hypothesis that mass lost during conservative tracer transport could be related to the occurrence of fracture intersection zone (FIZ) features. To study this, the cause of mass loss in tracer tests was evaluated. The following possibilities were considered: a) the existence of alternative sinks along involved structures, b) evidence that the FIZ provides a hydraulic connection to alternative sinks, and c) experimental error due to truncated time scale or measurement limitations. The FIZ hypothesis was tested where low recovery pathways cross or travel near the fracture intersection zones of Structures 13 and 21 or 20 and 21. The effects of FIZ pipes were also studied for pathways which seemed to experience increased dilution.

The in-situ transport observed in the TRUE Block Scale experiments is the result of combined effects of boundary conditions, the conductive geometry, i.e. the hydro-structural model, and the transport processes active in and along mobile and immobile zones. In order to isolate the effects of transport processes, the third study (Chapter 4) implemented a series of simple linear channel pipe models. These pipe channel models allowed direct evaluation of the range of effective pathway widths and transport apertures consistent with observed in-situ tracer breakthrough. The simple pipe channel models also allowed direct sensitivity studies of the effect of different immobile zone thicknesses and porosities.

2 Hydro-Structural Model Evaluation

2.1 Introduction

This chapter reports on the evaluation of the transmissivity and connectivity of the hydro-structural model (Hermanson and Doe, 2000) based on simulations for hydraulic interference Test A1 (Andersson et al. 2000a). This study was carried out using the FracMan/MAFIC discrete fracture network model (Miller et al., 1999) rather than the channel network model FracMan/PAWorks. The DFN model is a more straightforward implementation of the hydro-structural model. In the DFN model, the entire surface of each structure is discretized into triangles, whereas the CN model builds a set of pipe connections between the fracture intersections on each fracture plane. The DFN model as currently implemented also has greater flexibility for definition of transmissivity fields on fracture planes.

For this study the hydro-structural model was implemented directly using the properties provided by Hermanson and Doe (2000). Two alternatives were studied – a model consisting of deterministic structures alone, and a version including the stochastic background fractures of Andersson et al. (2000a). For each of these alternatives, the study considered (a) possibilities to improve the hydro-structural model by changing structure storativity and transmissivity, and (b) possibilities to improve the hydro-structural model through changes in connectivity.

Figure 2-1 shows the normalized distance drawdown for Test A1. This test has a pumping rate of 2700 ml/min from packer interval KI0025F03:P6 (66.58-74.08 m) (Andersson et al. 2000a). The interesting aspects of this test are as follows:

- responses in Structures 22, 6, and 13 appear as compartmentalized responses, with large drawdown, and little sensitivity to distance from the pumping section
- responses in Structure 19 are very weak
- Structure 21 appears to have a more conventional continuum or network type response, with decreasing response at greater distance from the pumping interval.

The structural model hypothesis (Hypothesis #1) (Winberg et al. 2000) was tested both by direct comparison against the magnitudes of drawdown response, and by its ability to reproduce the observed pattern of response.

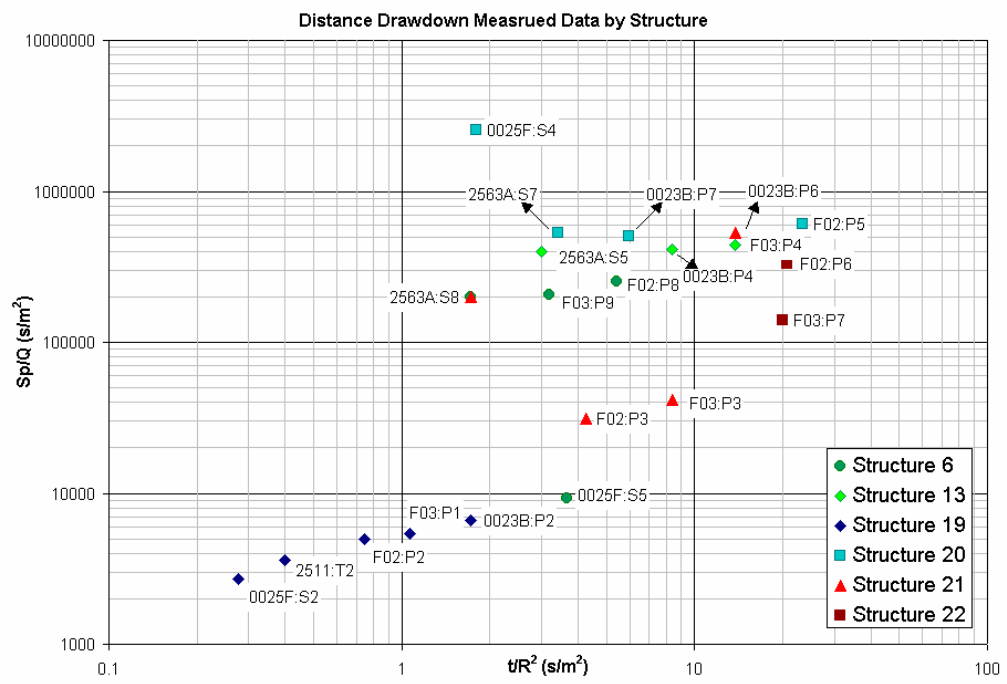

Figure 2-1 *Test A1: Measured Distance Drawdown Data.*

2.2 March 2000 Hydro-Structural Model

The first simulation of this study was carried out using the Hermanson and Doe (2000) hydro-structural model directly. The transmissivity, and geometric assumptions of this model are provided in Table 2-1 and Table 2-2 Transmissivity values of the deterministic structures are provided in Table 2-1. Table 2-2 lists the parameters of the background fractures. All features were assigned storativity according to the approximate relationship $S = 0.5\ T^{1/2}$ (Dershowitz et al., 2000).

Figure 2-2 presents a comparison of simulated and measured distance drawdown for Test A1 using the DFN model implementation of the Hermanson and Doe (2000) hydro-structural model including background fractures. This match is qualitatively fairly good, reproducing the types of behavior observed for Structures 19, 6, 20, and 13 fairly well. The hydraulic response of Structure 21 is not well modeled. While a distinctive distance drawdown is visible in the in-situ measurements, the simulation shows more of a compartmental response, with little distance dependence. On average, the simulated drawdowns are somewhat too low at small distances, and two high at larger distances. This indicates that the model is potentially more connected that the actual in-situ fracture system.

Figure 2-3presents the simulated drawdown of the Revised March 2000 Model without background fractures. The effects of lower connectivity are clearly visible in these results. The small response of structure 19 is matched much better than in the simulations including background fractures. However, the average drawdown closer to the pumping interval is still too high, and the distance dependence measured for Structure 21 is still not apparent in the simulations. This indicates a place for possible improvement to the hydro-structural model. Two types of improvements were considered – changes to transmissivity (Section 2.3) and changes to connectivity (Section 2.4).

Table 2-1 Structure Transmissivity in Revised March 2000 Hydro-structural Model (Hermanson and Doe, 2000).

Structure	Transmissivity (m^2/s)	Structure	Transmissivity (m^2/s)
1	$1.00*10^{-6}$	16	$1.00*10^{-11}$
2	$1.00*10^{-6}$	17	$2.00*10^{-11}$
3	$1.00*10^{-6}$	18	$1.00*10^{-11}$
4	$1.00*10^{-6}$	19	$1.80*10^{-6}$
5	$1.00*10^{-5}$	20	$9.60*10^{-7}$
6	$1.00*10^{-7}$	21	$8.10*10^{-7}$
7	$1.80*10^{-5}$	22	$3.70*10^{-7}$
8	$1.00*10^{-10}$	23	$6.78*10^{-9}$
9	$1.00*10^{-6}$	24	$2.89*10^{-8}$
10	$3.00*10^{-6}$	Z	$5.00*10^{-6}$
11	$1.00*10^{-6}$	EW-1	$1.20*10^{-5}$
12	$1.00*10^{-10}$	EW-3	$1.70*10^{-5}$
13	$1.70*10^{-7}$	NE-1	$2.20*10^{-4}$
14	$1.00*10^{-12}$	NE-2	$1.20*10^{-7}$
15	$2.00*10^{-11}$	NNW-7	$7.50*10^{-6}$

Table 2-2 Properties of Stochastic Background Fractures (Andersson et al., 2002a).

Parameter	Basis	Set #1	Set #2
Orientation Distribution	Two Fitted Sets to BIPS camera logs (NeurISIS)	Fisher Distribution, k = 9.4 Mean Pole (Trend, Plunge) = (211°, 0.6°)	Fisher Distribution, k = 3.8 Mean Pole (Trend, Plunge) = (250°, 54°)
Intensity P_{32}	Posiva Log Structures 0.29 m^2/m^3 total	0.16 m^2/m^3 (55.2% of fractures)	0.13 (44.8% of fractures)
Transmissivity	Posiva Log Structures, OxFilet Analysis of Packer Tests	Lognormal Distribution $\log_{10}$ mean = $-8.95\log_{10}$ m^2/s st.dev = $0.93\log_{10}$ m^2/s	Lognormal Distribution $\log_{10}$ mean = $-8.95\log_{10}$ m^2/s st.dev = $0.93\log_{10}$ m^2/s
Size Equivalent Radius	Hermanson et al. (1997)	Lognormal Distribution mean = 6 m st.dev. = 3 m.	Lognormal Distribution mean = 6 m st.dev. = 3 m.
Spatial Pattern	Fractal and Geostatistical Analyses	Baecher Model in TTS Region. Fractal (D≈2.6) for larger scale blocks.	Baecher Model in TTS Region. Fractal (D≈2.6) for larger scale blocks.

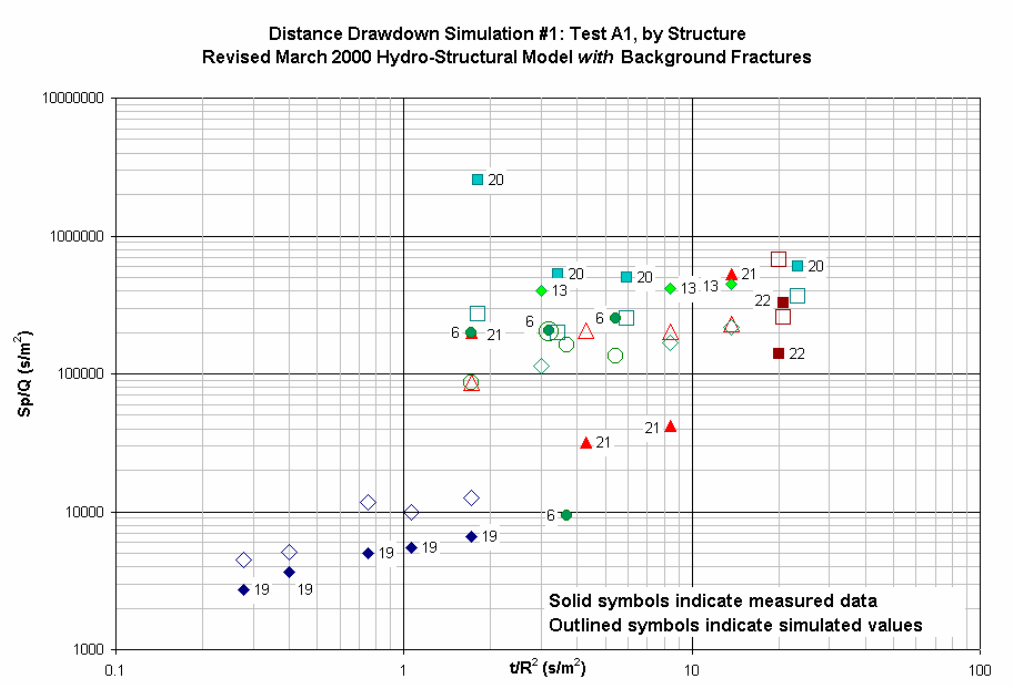

Figure 2-2 *Simulated Distance Drawdown March 2000 hydro-structural Model (Hermanson and Doe, 2000). Determination Structures and Background Fractures.*

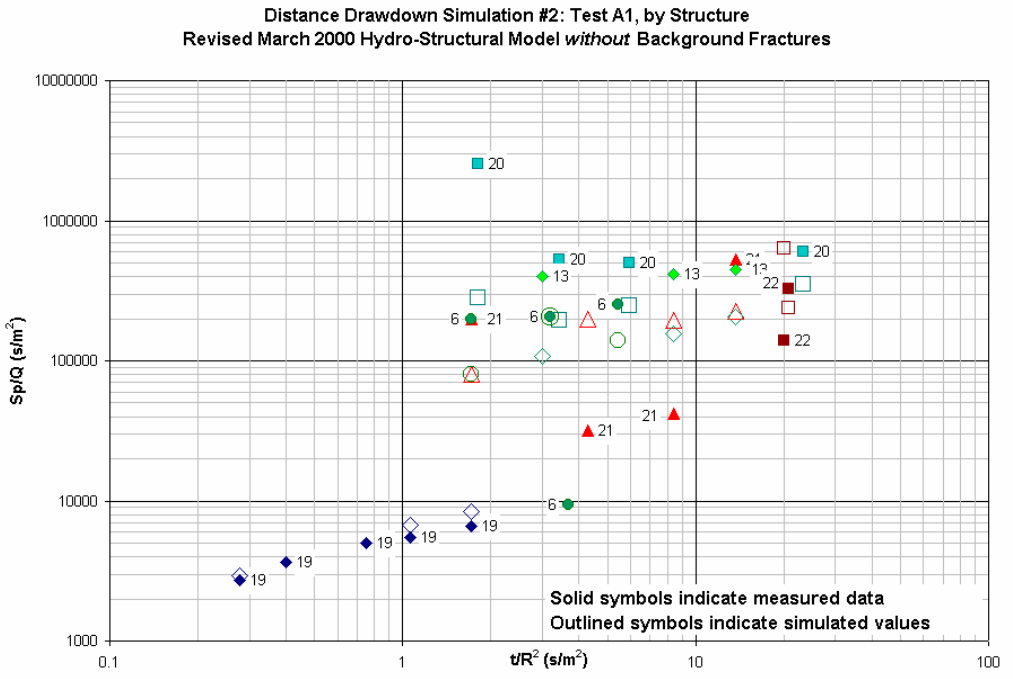

Figure 2-3 *Simulated Distance Drawdown of the March 2000 hydro-structural Model (Hermanson and Doe, 2000). Deterministic structures only.*

2.3 Modifications to Structure Transmissivity

Based on the results shown in the previous section, the hydro-structural model transmissivity and connectivity appear to be a fairly accurate representation of in situ conditions. The most direct place to look for improvements in the hydro-structural model is in the structure transmissivity, which can be scaled to adjust drawdowns.

A non-systematic study was carried out to determine which structure transmissivity could be adjusted to improve the match to measured drawdown. Given that the model without background fractures appeared to provide a better match than the model including background fractures, our efforts were focused on whether the same improvements could be achieved in the model including background fractures simply by changes feature transmissivity.

As a result of the study, it was determined that modifications to Structure 22 transmissivity affected the drawdown in Structures 6, 13, and 20. Modification to transmissivity of Structures 6, 13, and 20 have a large impact on Structure 22 drawdown. To improve the simulation results in order to better match the measured data, the connectivity of the model was modified.

Figure 2-3 illustrates the results of this study for a simulation in which the transmissivity of Structures 6, 13, 20, and 21 was lowered to reduce the hydraulic connectivity. The simulated drawdown in Structure 19 was decreased by increasing the assumed transmissivity of that structure, presumably providing a better connection to fixed head boundary conditions at the model boundaries. The modified transmissivities for this simulation are shown in Table 2-3.

Table 2-3 Modifications to Structure Transmissivity.

Structure	Original Transmissivity (m^2/s)	Modified Transmissivity (m^2/s)
6	$1.00*10^{-7}$	$4.00*10^{-9}$
13	$1.70*10^{-7}$	$6.70*10^{-8}$
19	$1.80*10^{-6}$	$8.00*10^{-6}$
20	$9.60*10^{-7}$	$4.80*10^{-7}$
21	$8.10*10^{-7}$	$1.30*10^{-9}$
22	$3.70*10^{-7}$	No change

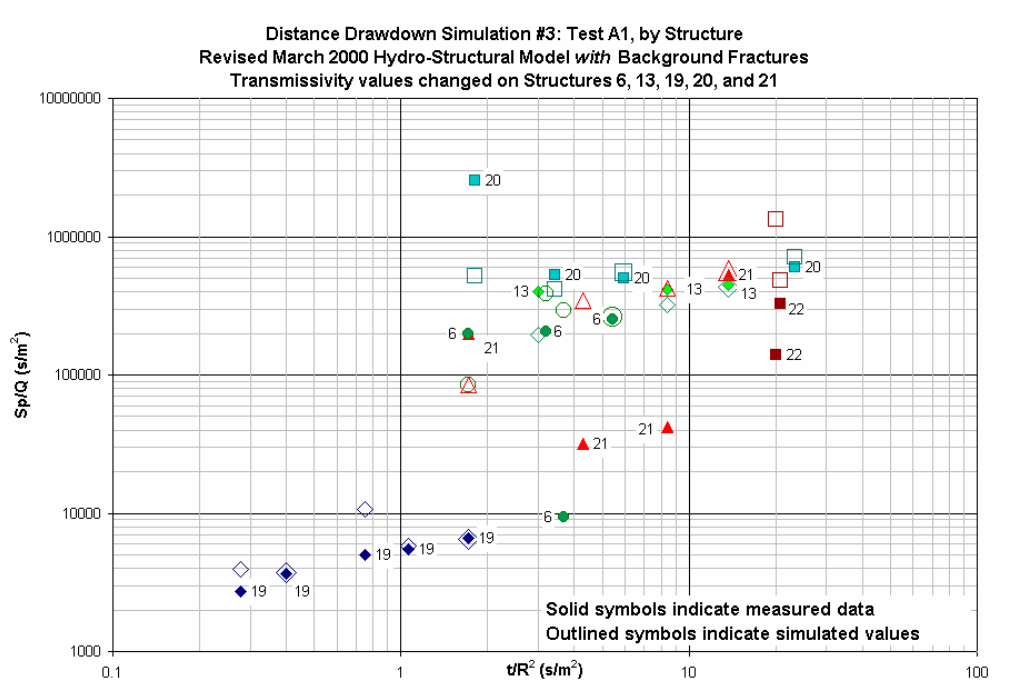

Figure 2-4 *Simulated Drawdown of the Revised March 2000 Hydro-structural Model (Hermanson and Doe, 2000). Modified Transmissivity of Structures 6, 13, 19, 20, and 21.*

2.4 Modifications to Structure Connectivity

Connectivity plays a large role in the hydraulic response of the model. It has already been seen that the connectivity of the model due to background fractures largely affects the drawdown, specifically in Structure 19. The method of adding anti-fractures, regions of decreased transmissivity at the fracture intersection, was used to alter the connectivity between fractures. The fracture intersection of interest in this study is the intersection of Structure 13 and 21. The anti-fracture in this study has a reduced transmissivity of 5 ordered of magnitude. An anti-fracture was added to the west side of Structure 21 along the 13/21 FIZ. This anti-fracture resulted in an improved Structure 21 drawdown response. Figure 2-5 and Figure 2.6 illustrates the results of the addition of an anti-fracture to the 13/21 FIZ.

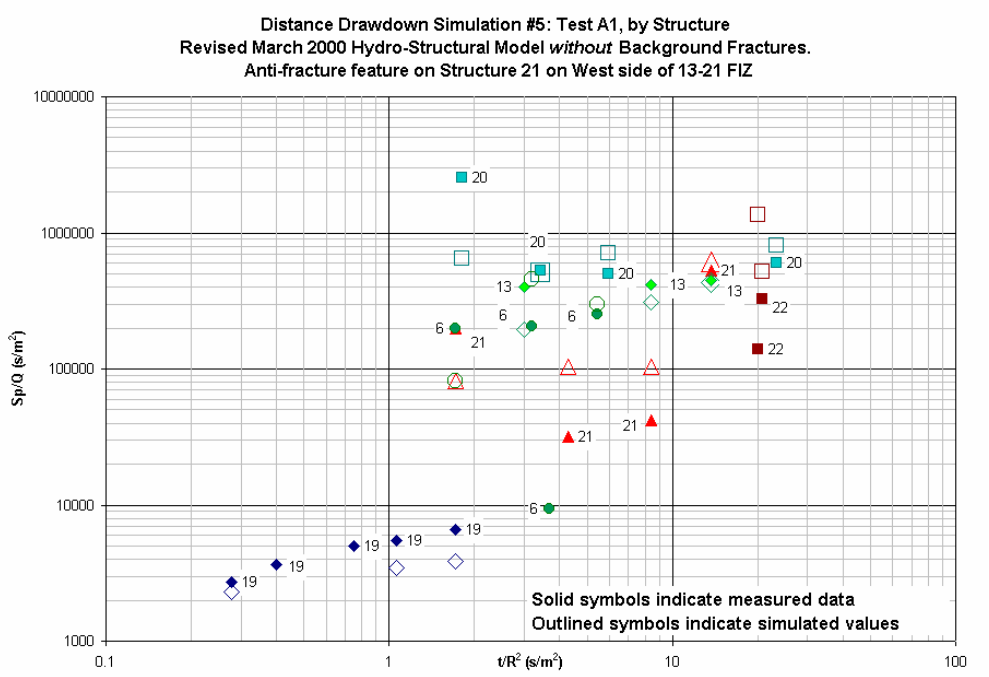

Figure 2-5 *Simulated Drawdown of the Revised March 2000 Hydro-structural Model (Hermanson and Doe, 2000) without Background Fractures. Anti Fracture added at 13-21 FIZ on West side of Structure 21.*

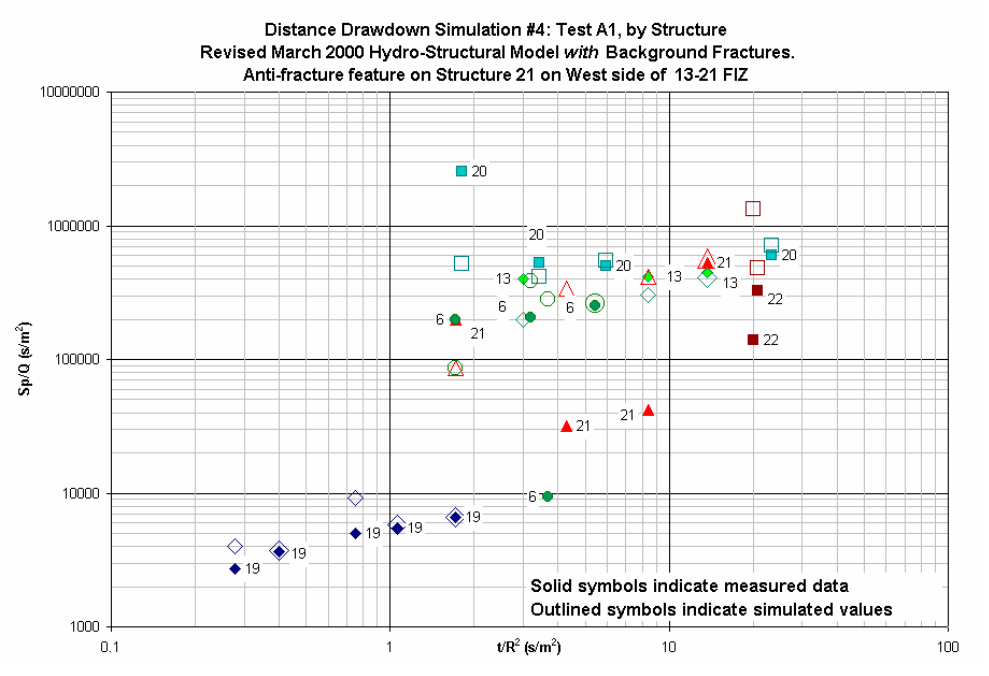

Figure 2-6 *Simulated Drawdown of the Revised March 2000 Hydro-structural Model (Hermanson and Doe, 2000). Anti Fracture added at 13-21 FIZ on West side of Structure 21.*

2.5 Discussion

By changing the transmissivity of a few of the structures, and adding an “anti-fracture” flow barrier to Structure 21, the hydro-structural model match to measured hydraulic interference of Test A1 was improved substantially. The fact that these improvements could be achieved without significant modification to the structural model increases confidence in the hydro-structural model.

Remaining monitoring intervals which could produce better matches to measured drawdown include Structure 6 in KI0025F:S5, Structure 20 in KI0025F:S4, and Structure 22 in KI0025F02:P7 and KI0025F03:P7. The low drawdown in KI0025F:S5 is suspected to be the effect of background fractures. KI0025F:S5 does not intersect Structure 6 in the March 2000 hydro-structural model. The high drawdown response in KI0025F:S4 was compared to Test A4 hydraulic response of the same interval. The drawdown data of Test A4 does not have the high drawdown at KI0025F:S4 and it is speculated to be measurement error or the effect of channelized flow which is not being modeled by the triangular elements. As discussed above, the Structure 22 drawdown is largely affected by the transmissivity values of Structures 6, 13 and 20. For this reason, the transmissivity of Structure 22 was not changed, instead the transmissivity values of 6, 13, and 20 were modified to obtain simulated values that best fit the remaining structures. The drawdown values in KI0025F03:P7 and KI0025F02:P6 differ by 9m. Structure 18 crosses Structure 22 between the two packer intervals. The difference in drawdown could be a result of unequal connectivity across Structure 22 at the 18-22 intersection.

Further study of interference tests could provide refinements to the hydro-structural model which address these issues. However, for the purposes of the present study, it was sufficient to demonstrate that improvements are possible within the context of minor adjustments to transmissivity and connectivity of the structures already defined in the hydro-structural model.

The fact that the model without background fractures consistently produces better interference results than the version with background fractures is significant. The presence of background fractures is confirmed by the density of flowing features detected by Posiva flow logs, and also by the lack of deterministic structures in some responding packer intervals. However, the observed hydraulic interference results indicate the possibility that the level of transmissivity or connectivity of the background fractures is significantly less that that of the deterministic structures. On the positive side, this suggests that DFN models potentially can be reasonably accurate when conductive background fractures are omitted, with increased computational efficiency as a result

3 Fracture Intersection Zone Evaluation

The TRUE Block Scale project focuses on improving the understanding of differences between solute transport in single fractures and fracture networks. One of the major project hypotheses (Hypothesis #2) is therefore focused on determining whether fracture intersection zones (FIZ) can have significant effect on transport pathways.

Based on previous studies (Winberg et al., 2000) it does not appear that the tracer tests conducted can distinguish effects of fracture intersection zones on pathway transport parameters. However, it may be possible to distinguish FIZ effects in terms of mass lost to alternative sinks along FIZ related pathways. This section presents an evaluation of this possibility based on a compilation of the conservative tracer experiments carried out in the TRUE Block Scale rock block. The effect of FIZ on mass recovery in breakthrough curves will be studied in greater detail in the next chapter.

3.1 Mass Loss During Tracer Tests

Mass loss during tracer tests can be due to one or more of the following processes:

- pathways connecting to alternative sink locations,
- experimental error, and
- solute retention at time scales significantly greater than the experimental measurements

The possibility that fracture intersection zones (FIZ) provides pathways to alternative sink locations can be addressed by first eliminating mass loss due to the second and third processes, and then determining whether there is a correlation between those experiments with the lowest projected ultimate mass recovery and the presence of hypothetical FIZ features along those pathways.

The effect of solute retention processes is partly eliminated by focuses on experiments using conservative tracers. There were 20 experiments (or rather tracer injections) using conservative tracers. Measurements relative to the evaluation of the FIZ hypothesis are summarized in Table 3-1. Projected ultimate recoveries provided in this table are based on visual extrapolation of experimental breakthrough curves.

The first task was to distinguish cases where mass loss could also be a function of experimental error. Injected mass is calculated using two methods: integration and weighing. The recovered mass for both methods is computed through integration. Mass recovery based on integration was consistently higher than the recovery calculated through weighing. Integrated recovery often is calculated to over 100%. This is explained by the large volume of injection as compared to the maximum withdrawal rate. The increased pressure causes tracer to be pushed into fractures and therefore not accounted in the injection integration, resulting in underestimated injected mass. The maximum amount of error in mass recovery due to this experimental error is estimated at approximately 32%, the maximum difference between the possible mass recovery (100%) and the reported experimental mass recovery (132%). For this level of

experimental error, projected ultimate recoveries of 76% and greater could reflect experimental error rather than actual mass loss. These levels of mass loss can therefore not be considered definitive indication of mass loss related to for example fracture intersection zones (FIZ).

On the other hand, error in projected ultimate recovery is greatest for those tests, which have measured breakthrough for the smallest portion of the tracer recovery period. For example, for tracer test B2c, where the measured recovery is 3.4%, only a small portion of the recovery was measured, and the projection to ultimate recovery has higher uncertainty. Other tests that have a small portion of the recovery measured include: A4a, A4b, A5a, A5d, B1b, B1c, B2a, B2e, and C3. For these tests, some of the mass loss indicated by the projected ultimate mass recovery may be due to the limitations of visual extrapolation of the breakthrough curves.

The pathways for tracer tests A4a, A5c, B1a, B2g, and C1 do not cross identified fracture intersection zones (FIZ), although there is a possibility that other FIZ may occur on these pathways, possibly created in conjunction with background fractures. The remaining 15 tracer test pathways do cross fracture intersection zones. Table 3-2 compares the ultimate projected recovery statistics between these two populations of tracer tests, those that cross a FIZ and those that do not. The pathways related fracture intersection zones have significantly lower mean recovery than those for the pathways which do not. This provides at least a statistical indication that mass loss (i.e., branching pathways) is more likely for pathways which cross fracture intersection zones than for pathways contained within single structures. However, the mean path length for the pathways which cross a FIZ is also greater, such that other connections to sinks such as tunnels for they also need to be considered.

Table 3-1 Head values at the source and sink location and surrounding region and measured and projected ultimate recovery for Phase A, B, and C Tests.

Test	Source Head (masl)	Sink Head (masl)	Local Head Value Range	Measured Recovery	Projected Ultimate Recovery
A4a	402.2	220.7	287.3 - 405.1	37.9%	70%
A4b	418.6	220.7	287.3 - 422.8	50.8%	90%
A4c	410.4	220.7	287.3 - 422.8	Below background levels	
A5a	285.2	150.1	304.90 - 399.1	64.3%	72%
A5b	412.5	150.1	155.5 - 399.1	Below background levels	
A5c	394.7	150.1	285.2 - 399.1	132.2%	Na
A5d	408.4	150.1	285.2 - 399.1	43.2%	60%
A5e	346.4	150.1	285.2 - 399.1	94.9%	100%
B1a	401.4	237.4	286.9 - 404.1	99.2%	100%
B1b	419.1	237.4	286.9 - 415.5	45.4%	65%
B1c	401.1	237.4	286.9 - 404.1	36.4%	38%
B2a	416.1	231.7	285.7 - 409.9	48.8%	60%
B2b	420.0	231.7	402.1 - 420.4	81.9%	85%
B2c	308.5	231.7	289.7 - 423.1	3.4%	10%
B2d	407.1	231.7	285.7 - 409.9	75.9%	80%
B2e	420.4	231.7	402.1 - 420.0	32.1%	36%
B2g	400.1	231.7	285.7-402.9	97.0%	99%
C1	399.8	236.6	284.6 - 401.9	111.2%	Na
C2	411.4	236.6	284.6 - 414.8	80.4%	100%
C3	418.5	236.6	400.9 - 418.4	73.1%	80%

Table 3-2 Projected Ultimate Recovery for Pathways Involving FIZ.

	5 Pathways NOT Involving FIZ	15 Pathways Involving FIZ
Average	94%	58%
St. Dev	13%	34%
Min	70%	0%
Max	100%	100%

3.2 Visualization of Conservative Tracer Pathways

Having established that there is at least a statistical relationship between mass recovery and the occurrence of fracture intersection zones, the next step is to visualize those pathways. Figure 3-1 thorough Figure 3-20 present visualizations of the transport pathways along the deterministic structures of the Revised March 2000 Hydro-structural Model (Hermanson and Doe, 2000. Head values, breakthrough statistics, and recovery data are reported based on experimental results. In addition, the simulated pathway properties indicated by the studies in Chapter 4 are provided for reference.

From these visualizations, the following are apparent:

- The only pathways which could not involve FIZ pipes are A4a, A5c, B1a, B2g, and C1. These pathways have the highest projected ultimate recoveries, in the upper 90 percents, except for A4a, which has an ultimate projected recovery of only 70%. However, since only 37% of mass was recovered during A4a, higher ultimate recovery could be possible.
- The pathways with the lowest recovery (i.e., below background level) are A4c, which crosses the 20/21, 20/22, and 22/23 fracture intersections, and A5b, which crosses the 20/21 fracture intersection. High projected ultimate recovery was only achieved on one of the pathways crossing three fracture intersection zones (A4b).
- All pathways reflect measured head lower than the injection interval along pathways other than the direct channel to the sink. This indicates that there are also possibilities for pathways not related to FIZ diverting mass from the experiments.
- Simulations for pathways crossing multiple fracture intersection zones lost mass fairly equally distributed between FIZ crossed.

The tracer test source, sink, Cartesian distance, DFN path length, structures, FIZ statistics, and numbering system according to Andersson et al. (2002b) is outlined in Table 3-3.

Table 3-3 Phase A, B, and C Tracer Tests: Sink-Source Pairs and Flow Pathway.

Test	Source	Sink	Cartesian Distance	DFN Path Length	Structures Traveled	Possible FIZ	DFN Path Length with FIZ	Distance to FIZ	Pathway *
A4a	F03:P5	23B:P6	12.8	17.9	20	Na	Na	Na	I
A4b	F03:P6	23B:P6	14.9	51.2	22, 20, 21	20/21	52.7	47.3	IV
A4c	F03:P7	23B:P6	17.7	66.0	23, 22, 20,	20/21	68.6	62.2	II
A5a	2563A:S4	F03:P5	30.6	30.6	20	20/21	38.4	15.3	A5
A5b	F02:P3	F03:P5	29.3	55.9	21, 20	20/21	63.3	34.4	A5
A5c	F02:P5	F03:P5	12.9	12.9	20	Na	Na	Na	A5
A5d	F02:P6	F03:P5	10.4	34.4	22, 20	Na	Na	Na	A5
A5e	F03:P6	F03:P5	7.0	35.0	22, 20	Na	Na	Na	A5
B1a	F03:P5	23B:P6	12.8	17.9	20	Na	Na	Na	I
B1b	F03:P6	23B:P6	14.9	51.2	22, 20, 21	20/21	52.7	47.3	IV
B1c	F02:P5	23B:P6	19.5	19.5	20	20/21	33.8	19.1	VI
B2a	F03:P6	23B:P6	14.9	51.2	22, 20, 21	20/21	52.7	47.3	IV
B2b	F02:P3	23B:P6	32.5	32.5	21	13/21	46.5	5.0	III
B2c	2365S:S1	23B:P6	55.0	169.2	19, 13, 21	13/21	186.9	145.6	VIII
B2d	F03:P7	23B:P6	17.7	66.0	23, 22, 20,	20/21	68.6	62.2	II
B2e	F03:P3	23B:P6	25.3	25.3	21	13/21	35.4	5.3	V
B2g	F03:P5	23B:P6	12.8	17.9	20	Na	Na	Na	I
C1	F03:P5	23B:P6	12.8	17.9	20	Na	Na	Na	I
C2	F03:P7	23B:P6	17.7	66.0	23, 22, 20,	20/21	68.6	62.2	II
C3	F02:P3	23B:P6	32.5	32.5	21	13/21	46.5	5.0	III
*According to the numbering system of Andersson et al., 2002b									

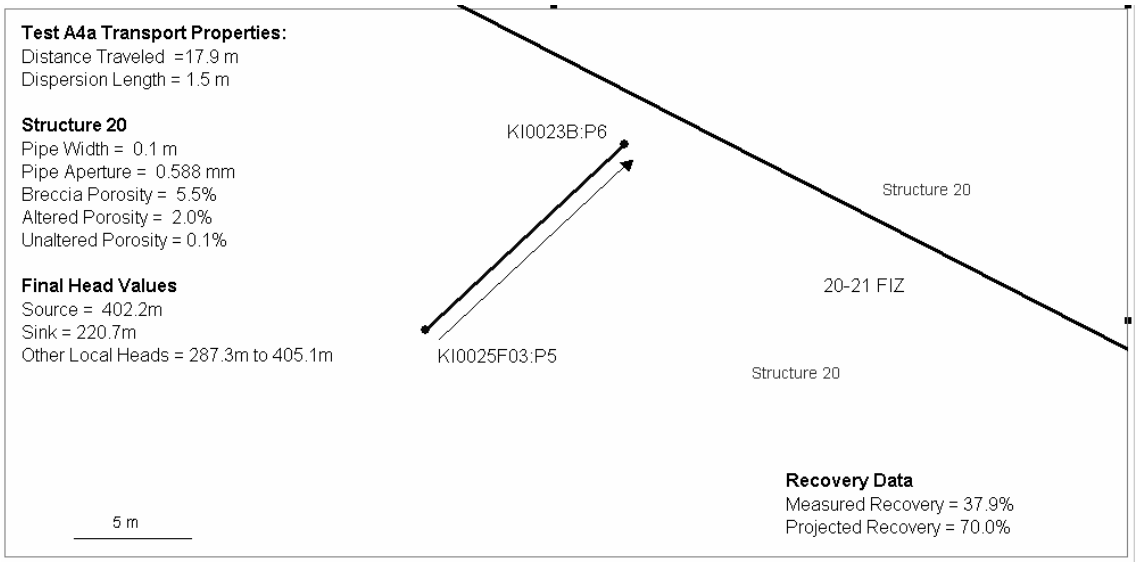

Figure 3-1 *Tracer Test A4a, Pathway I: Transport, Path Transport Parameters, Head Values, and Recovery Data.*

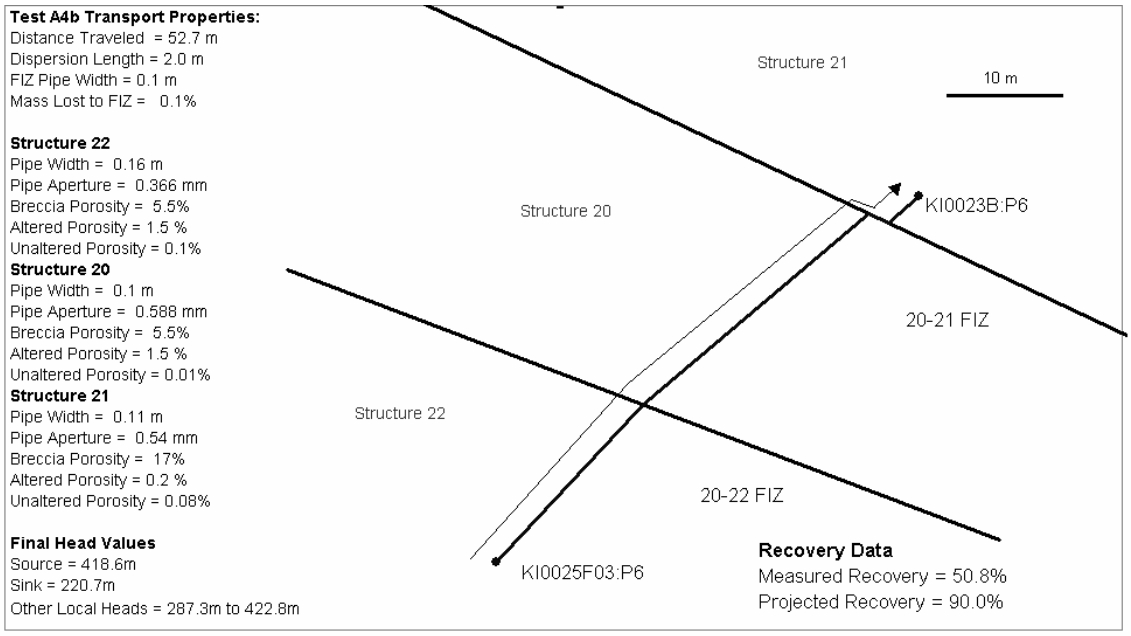

Figure 3-2 *Tracer Test A4b, Pathway IV: Transport Path, Transport Parameters, Head Values, and Recovery Data.*

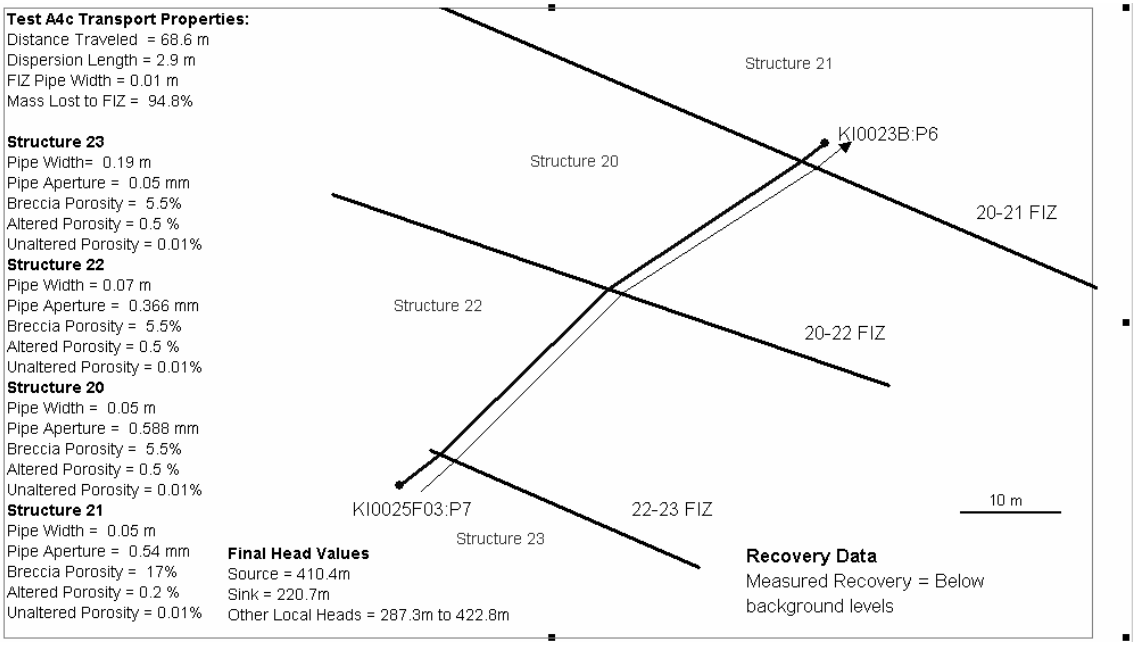

Figure 3-3 *Tracer Test A4c, Pathway II: Transport Path, Transport Parameters, Head Values, and Recovery Data.*

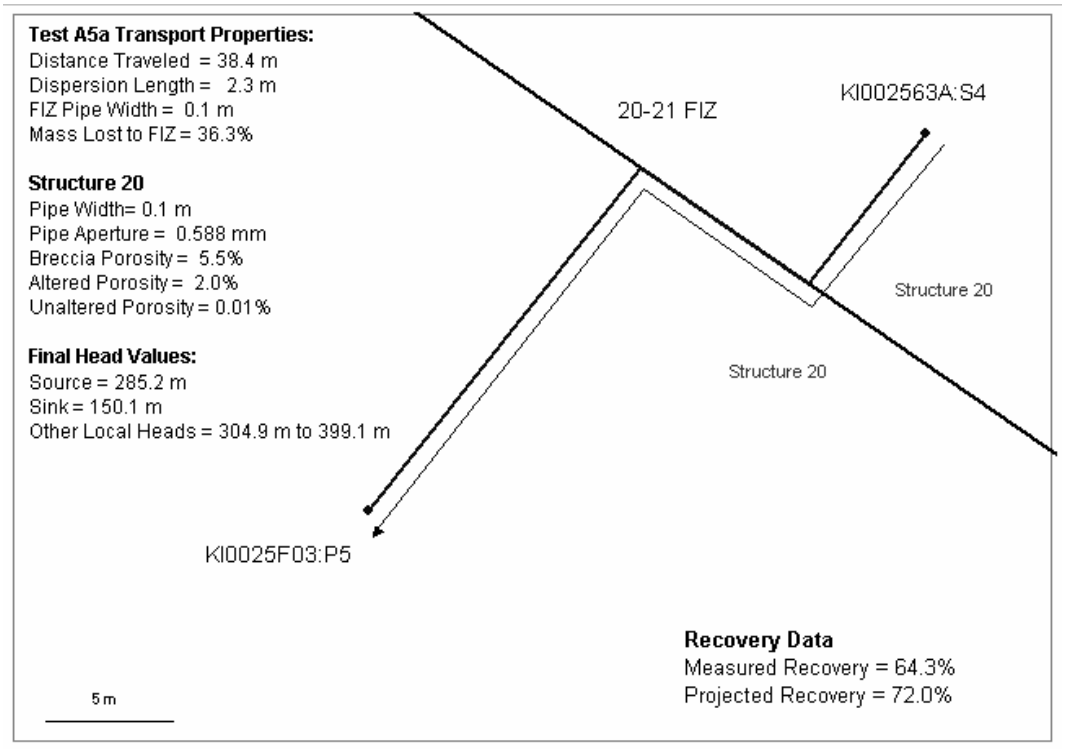

Figure 3-4 *Tracer Test A5a: Transport Path, Transport Parameters, Head Values, and Recovery Data.*

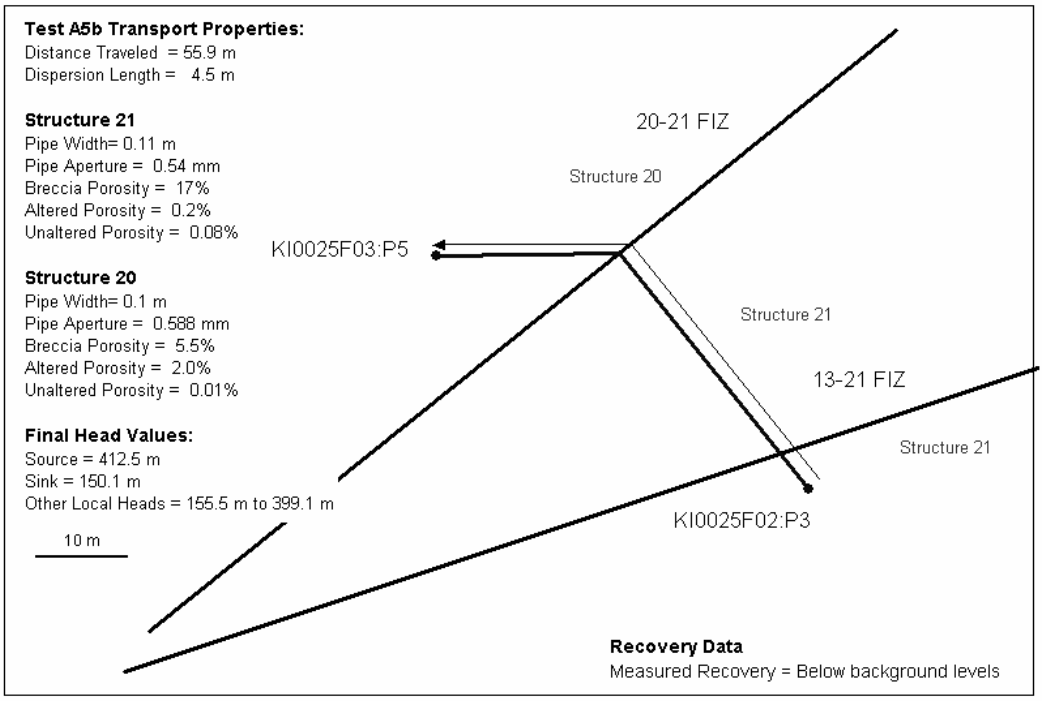

Figure 3-5 *Tracer Test A5b: Transport Path, Transport Parameters, Head Values, and Recovery Data.*

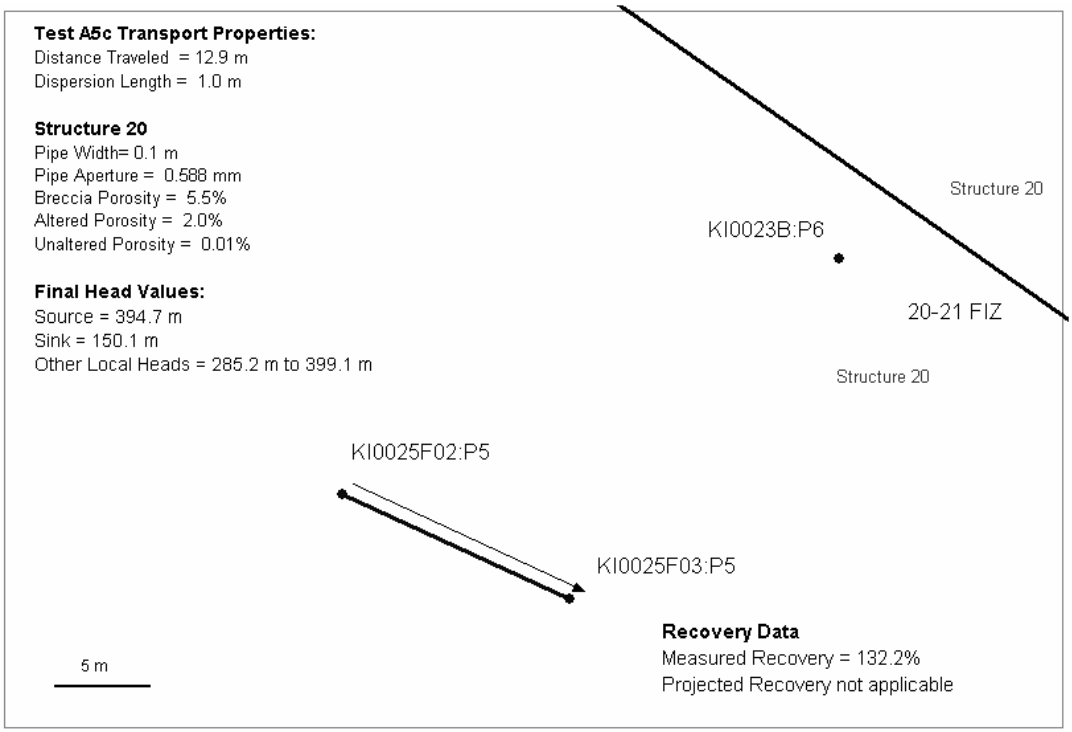

Figure 3-6 *Tracer Test A5c: Transport Path, Transport Parameters, Head Values, and Recovery Data.*

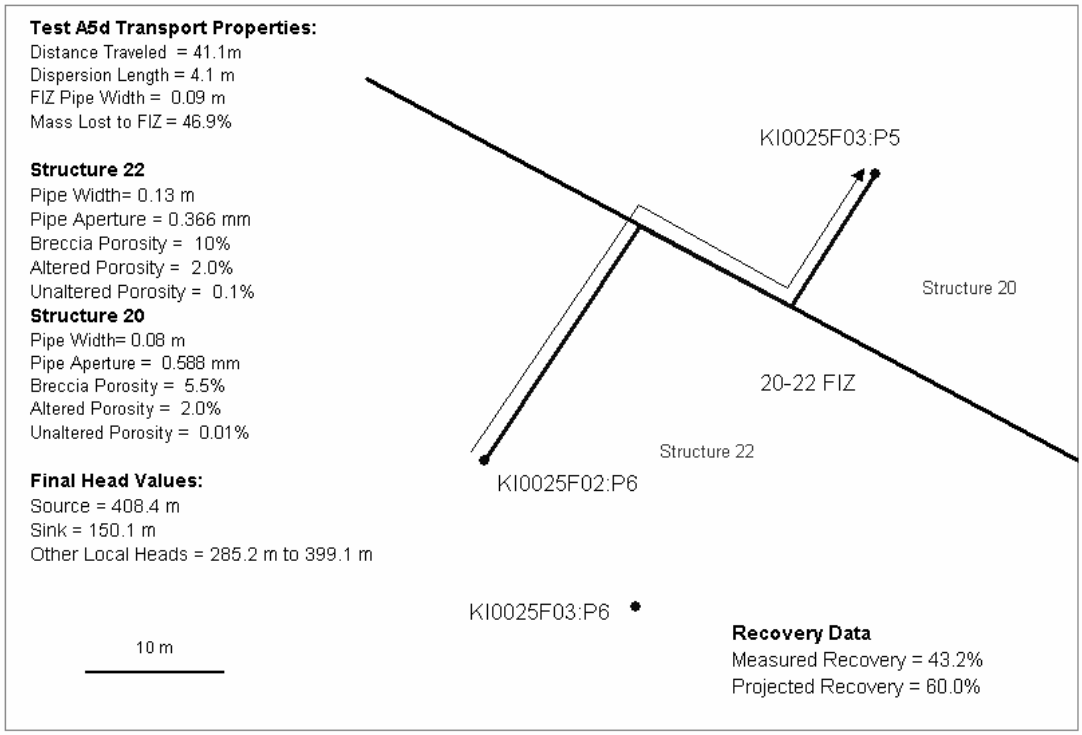

Figure 3-7 *Tracer Test A5d: Transport Path, Transport Parameters, Head Values, and Recovery Data.*

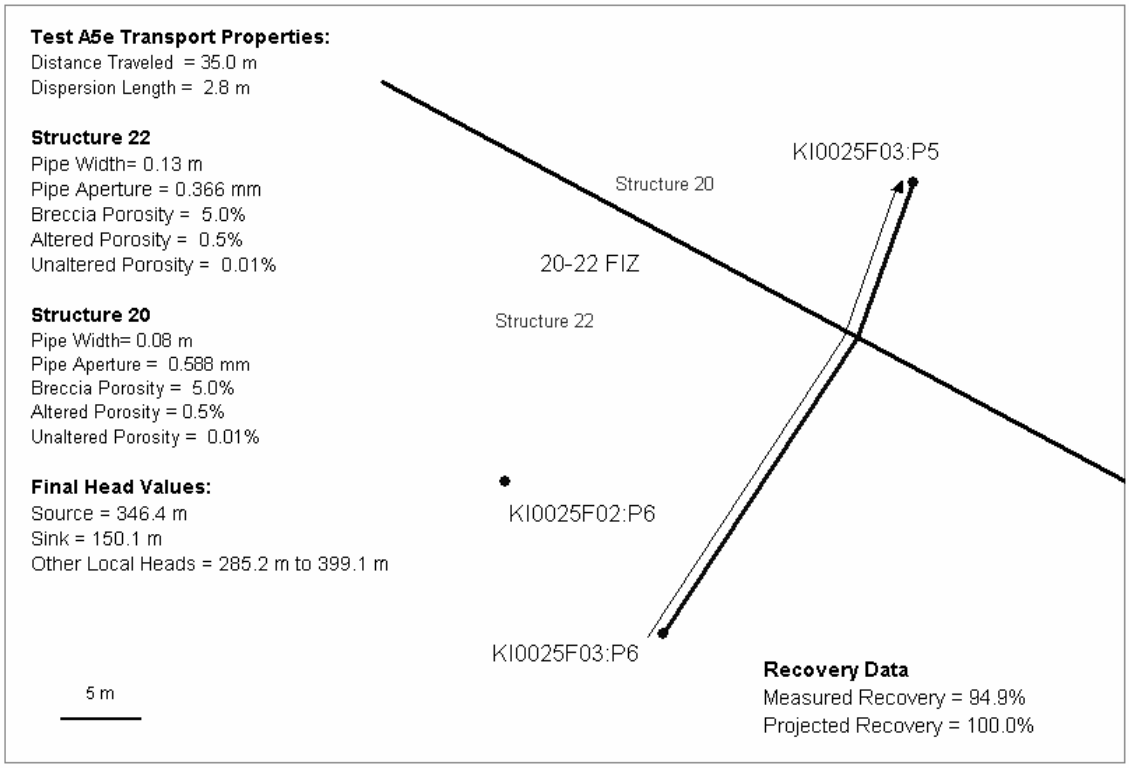

Figure 3-8 *Tracer Test A5e: Transport Path, Transport Parameters, Head Values, and Recovery Data.*

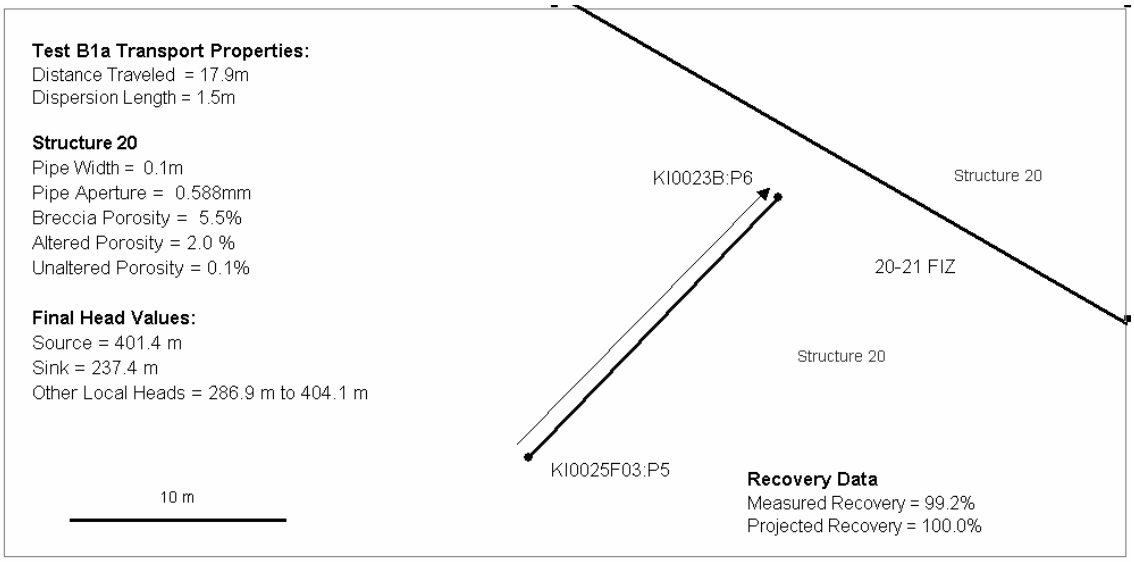

Figure 3-9 *Tracer Test B1a, Pathway I: Transport Path, Transport Parameters, Head Values, and Recovery Data.*

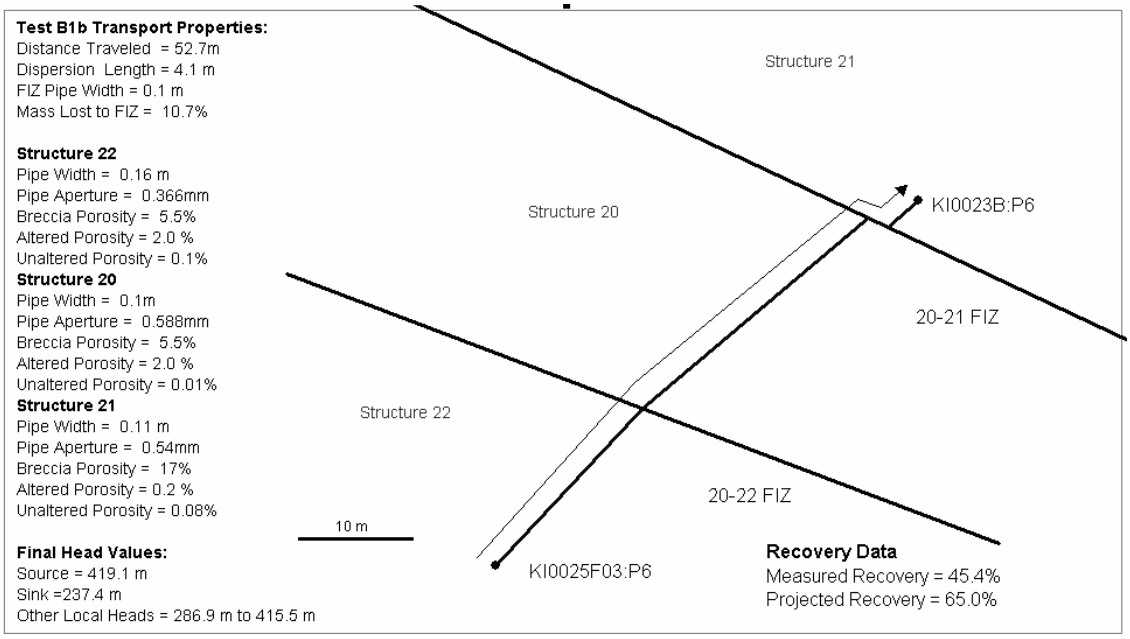

Figure 3-10 *Tracer Test B1b, Pathway IV: Transport Path, Transport Parameters, Head Values, and Recovery Data.*

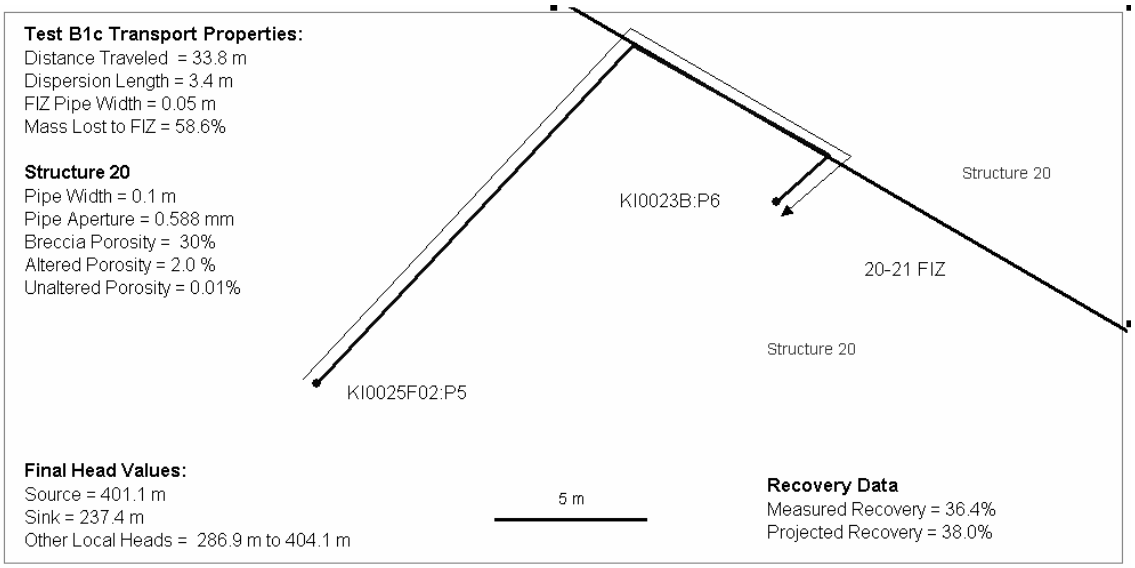

Figure 3-11 *Tracer Test B1c, Pathway VI: Transport Path, Transport Parameters, Head Values, and Recovery Data.*

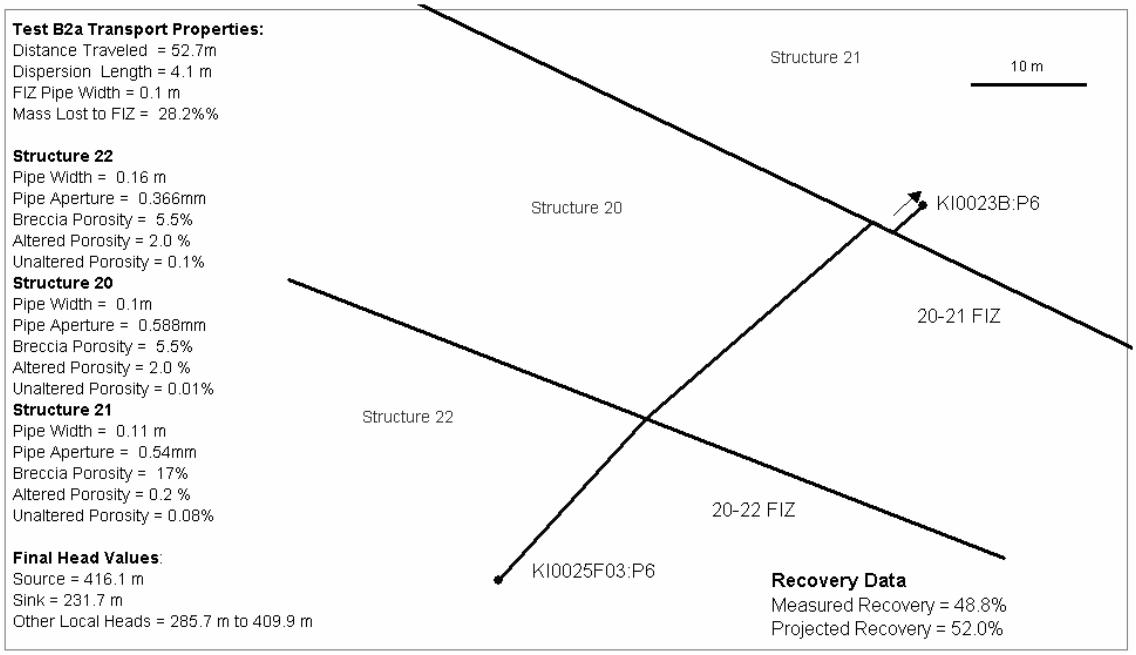

Figure 3-12 *Tracer Test B2a, Pathway IV: Transport Path, Transport Parameters, Head Values, and Recovery Data.*

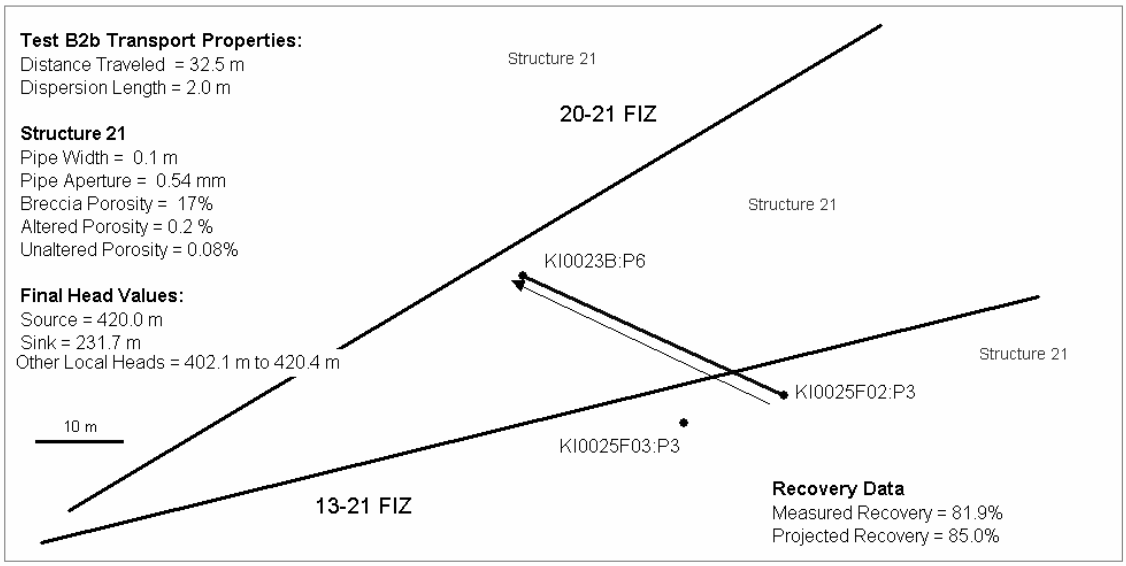

Figure 3-13 *Tracer Test B2b, Pathway III: Transport Path, Transport Parameters, Head Values, and Recovery Data.*

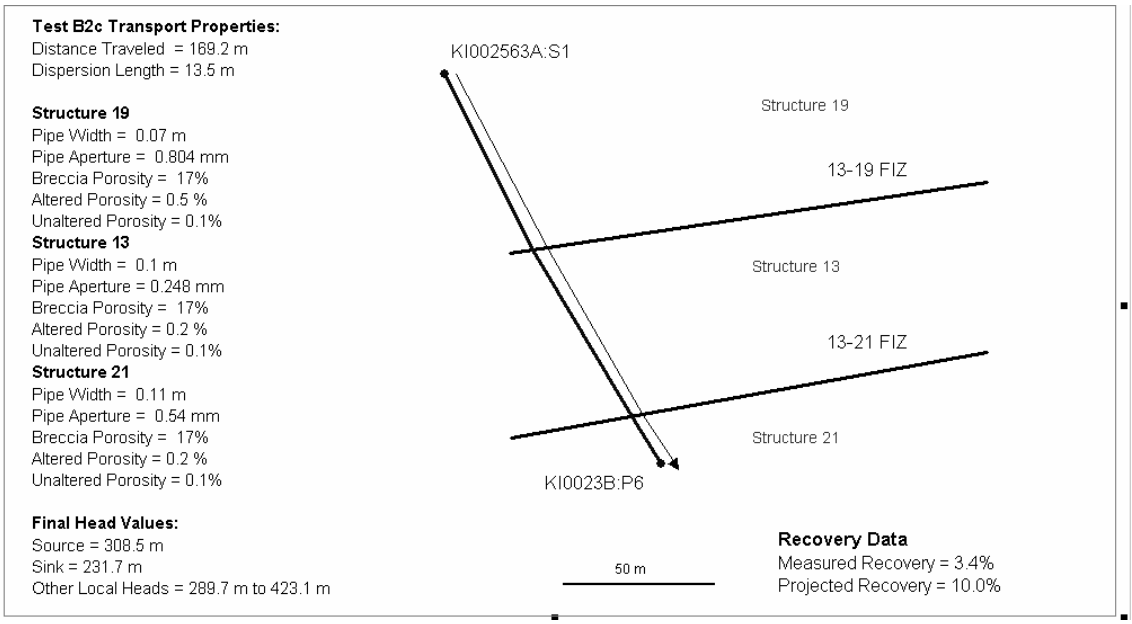

Figure 3-14 *Tracer Test B2c, Pathway VIII: Transport Path, Transport Parameters, Head Values, and Recovery Data.*

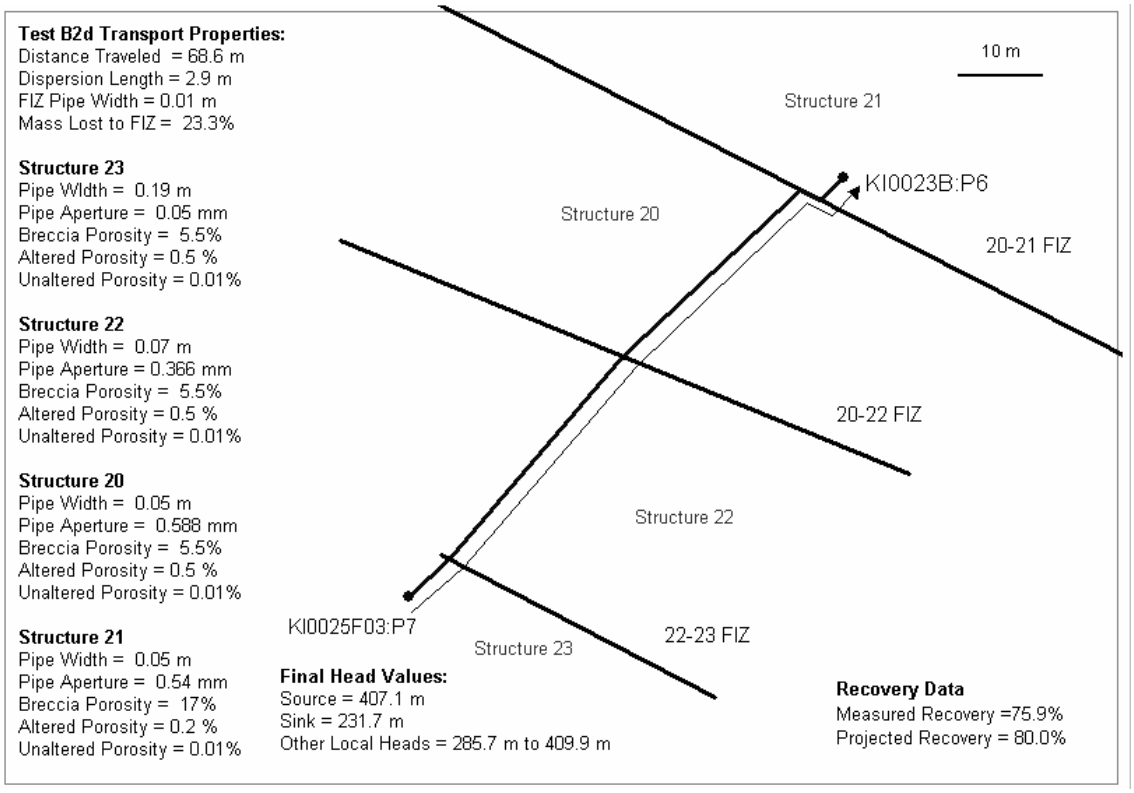

Figure 3-15 *Tracer Test B2d, Pathway II: Transport Path, Transport Parameters, Head Values, and Recovery Data.*

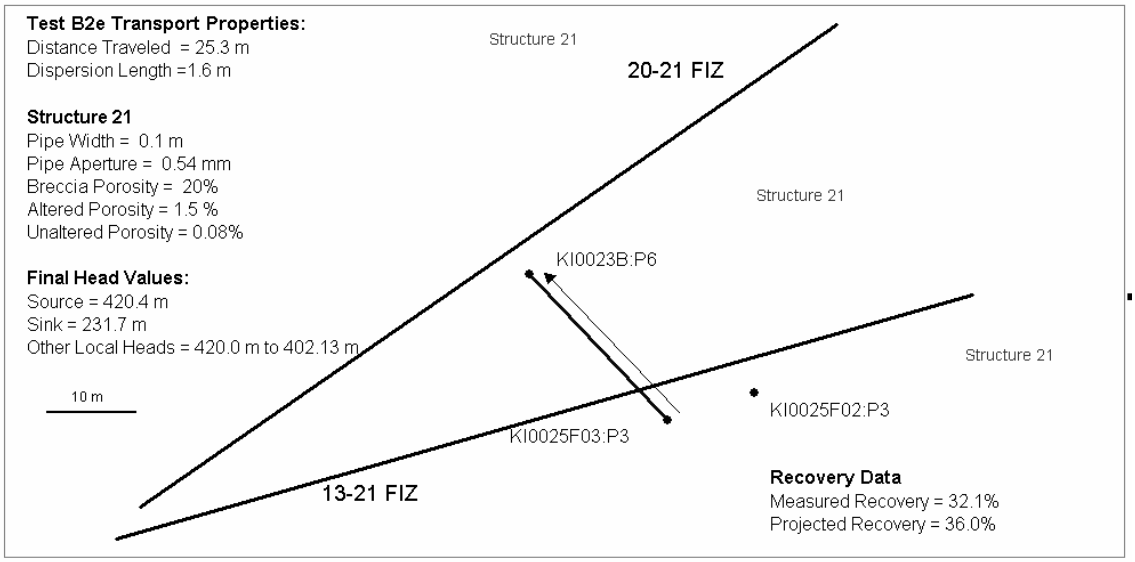

Figure 3-16 *Tracer Test B2e, Pathway V: Transport Path, Transport Parameters, Head Values, and Recovery Data.*

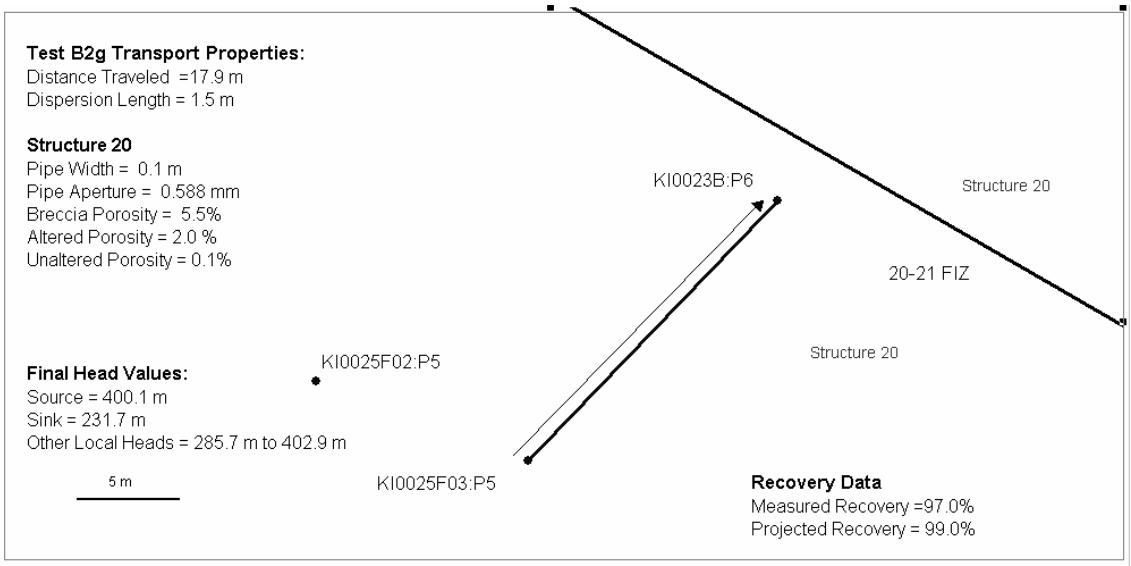

Figure 3-17 *Tracer Test B2g, Pathway I: Transport Path, Transport Parameters, Head Values, and Recovery Data.*

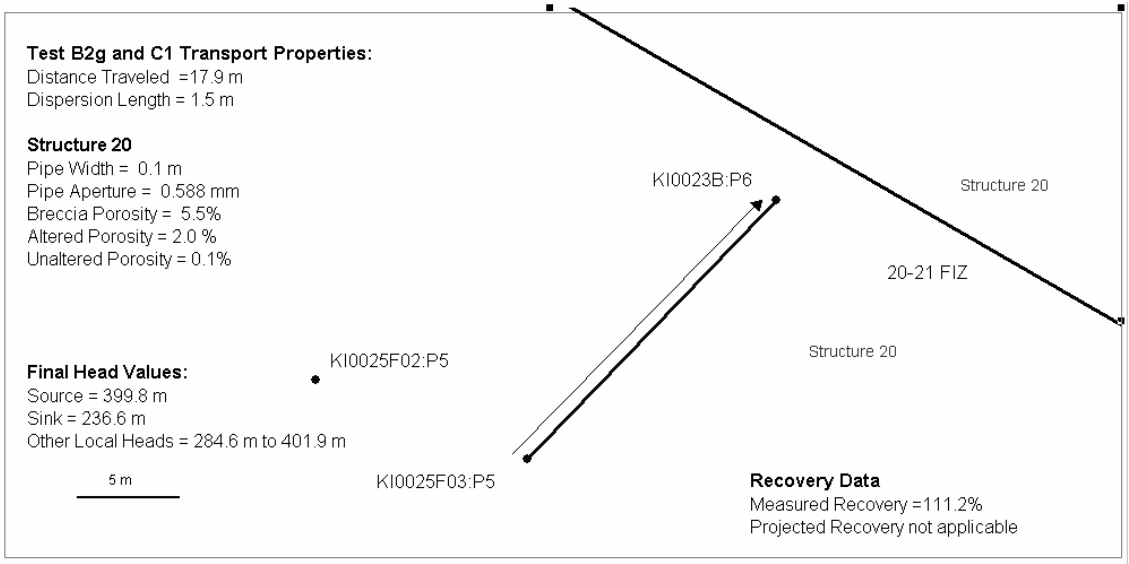

Figure 3-18 *Tracer Test C1, Pathway I: Transport Path, Transport Parameters, Head Values, and Recovery Data.*

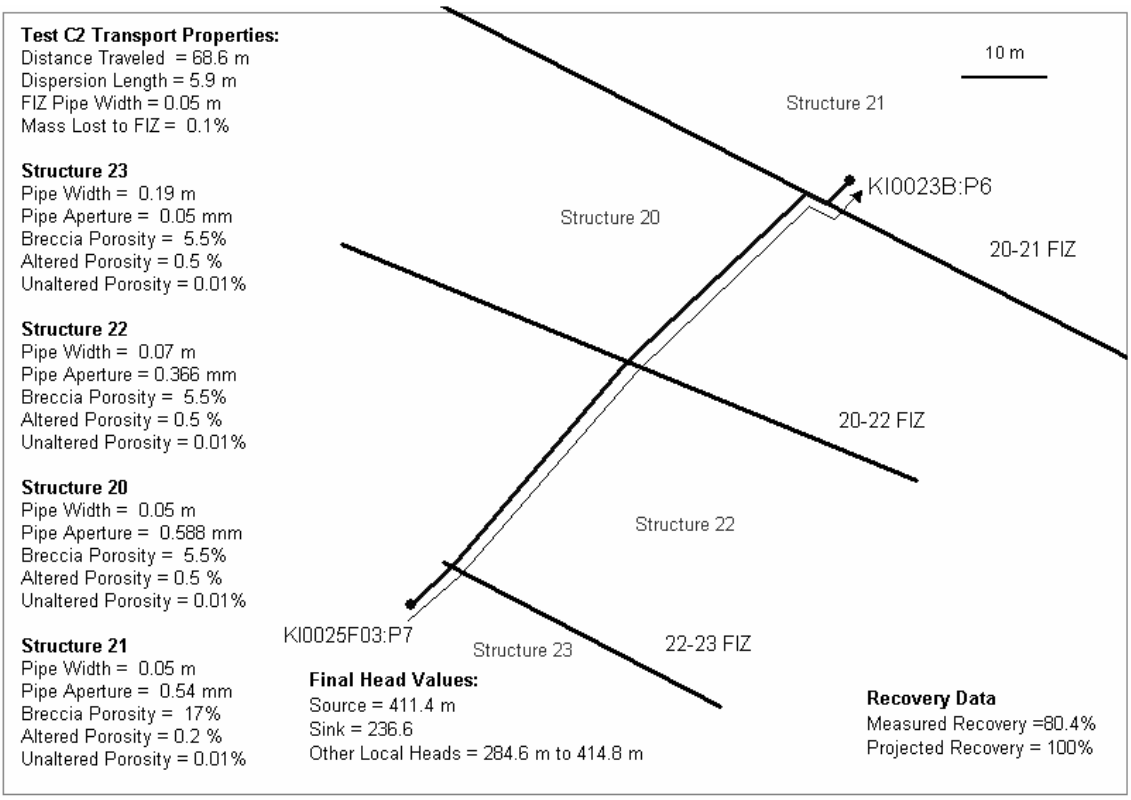

Figure 3-19 *Tracer Test C2, Pathway II: Transport Path, Transport Parameters, Head Values, and Recovery Data.*

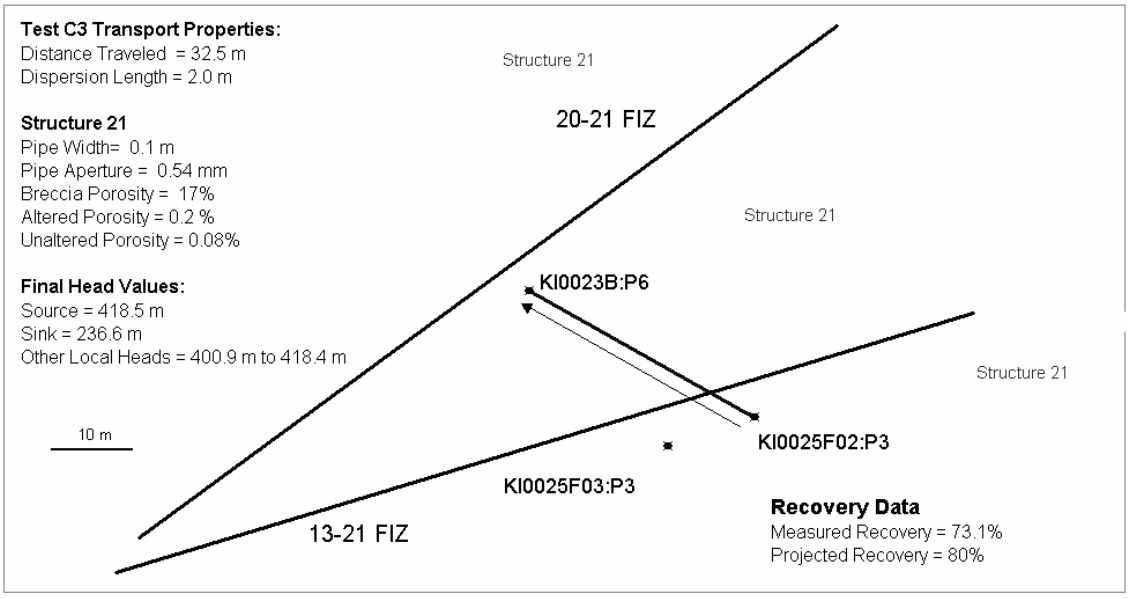

Figure 3-20 *Tracer Test C3, Pathway III: Transport Path, Transport Parameters, Head Values, and Recovery Data.*

4 Transport process evaluation

4.1 Introduction

Throughout the TRUE Block Scale project, the JNC/Golder team has carried out studies based on the use of complex channel network models intended to represent the geometry and properties of pathways through the fracture network as realistically as possible. In this study, transport pathway properties were studied in greater detail by focusing on the individual pathways, independent of the more complex fracture network or channel network containing the pathways. This made it possible to focus on a) effective dispersion along pathways, b) immobile zone (diffusion) properties, and c) effective sorption properties.

The simplified pipe network for this study is shown in Figure 4-1. This pipe network includes pipes directly from source to sink, and the possibility of pipes from the source to alternative sinks via a fracture intersection zone (FIZ) connection. The model also includes immobile zones for a) fracture infilling (fault gouge) b) altered rock, and c) intact wall rock (Äspö diorite), based on the microstructural conceptual model of Figure 4-2 shows the Winberg et al. (2000) microstructural model as implemented for this study. Solute transport is solved using the same Advection-Dispersion-Diffusion solution used for the DFN/CN modeling studies of Dershowitz et al (2000).

The tracer tests studied with the simplified pipe channel model are listed in Table 3-3. These 20 tests have pathways through the fracture network from 13 to 169 meters, and include between one and four deterministic structures. Most include the possibility of flow along fracture intersection zones (FIZ). Of the 20 tracer tests listed in Table 3-3, several travel along the same paths. Between tracer tests that share travel paths, the same diffusion parameters are used. Table 4-1 lists the tracer tests that share travel paths.

For conservative tracer experiments, diffusion rates were assumed to be equal to the free water diffusion and are not considered to be a calibration parameter. Free water diffusion values are given in Andersson et al. (2002b).

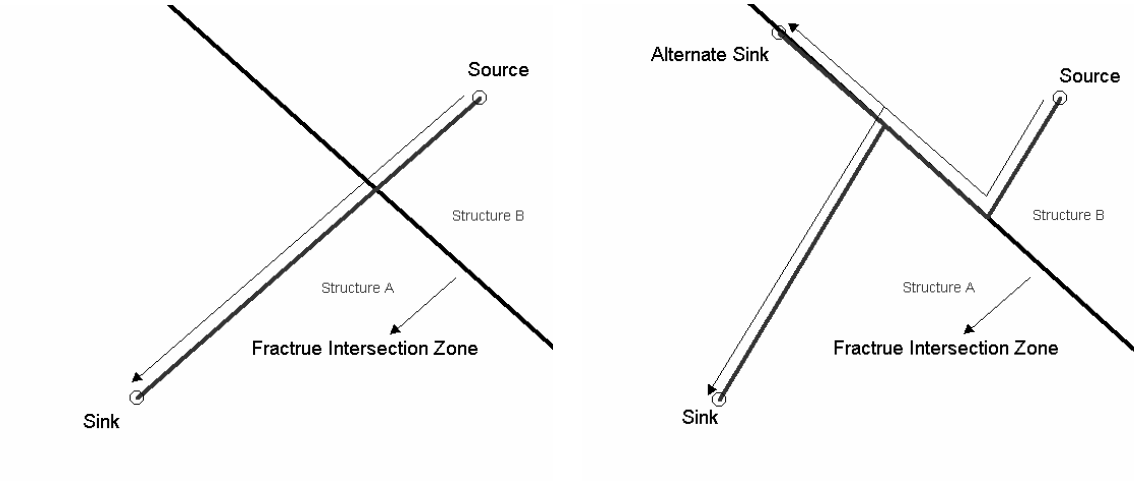

Figure 4-1 *Simplified Pipe Channel Transport Pathways.*

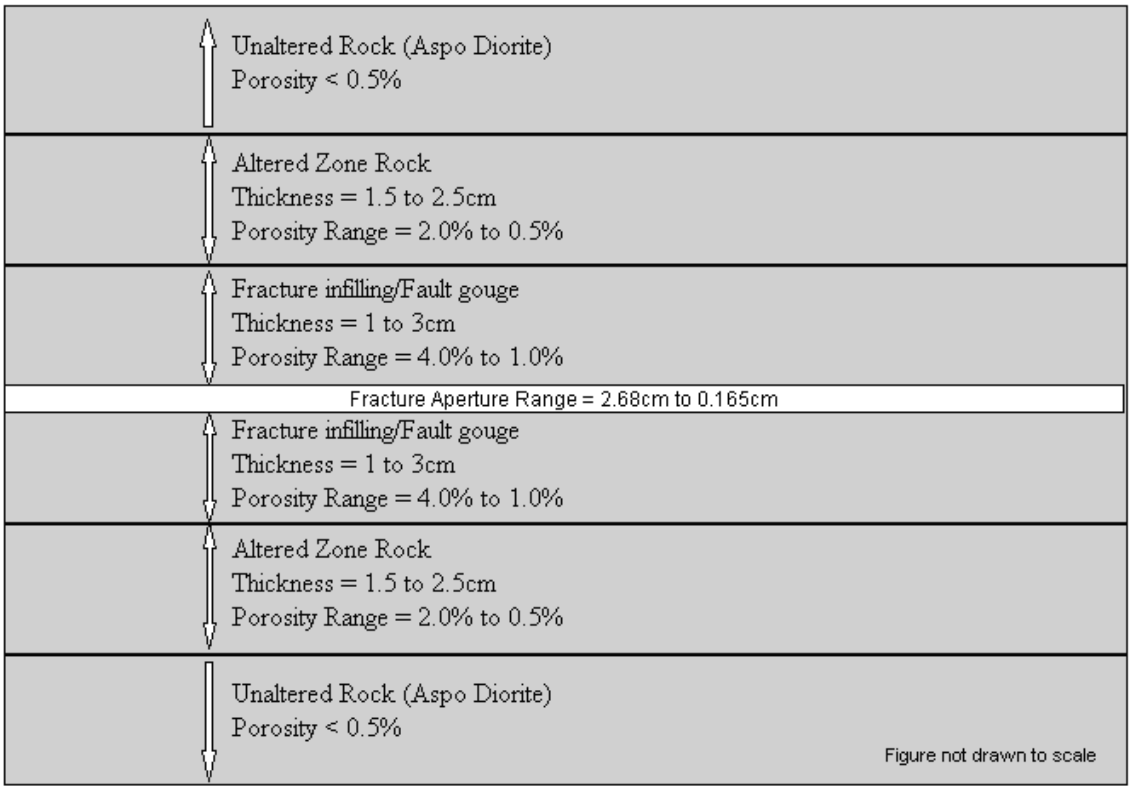

Figure 4-2 *Microstructural Model based on Winberg et al. (2000).*

Table 4-1 Tracer Tests sharing Travel paths.

Source	Sink	Structures Traveled	Tracer Tests
KI00F03:P5	KI0023B:P6	20	A4a, B1a, B2g, C1
KI00F02:P3	KI0023B:P6	21	B2b, C3
KI00F03:P6	KI0023B:P6	22, 20, 21	A4b, B1b, B2a
KI00F03:P7	KI0023B:P6	23, 22, 20, 21	A4c, B2d, C2

By using simplified pipe geometry, it was hoped to obtain more information on the possible in-situ values for transport properties along pathways. The transport pathway properties studied were as follows:

- advective velocity (expressed as transport aperture)
- path (pipe) width (perpendicular to the direction of flow)
- porosity and thickness for each immobile porosity

Three immobile zones were considered for modeling diffusive processes: the fracture infilling zone, closest to the pipe, followed by the altered rock zone, and finally the unaltered rock zone. Note that in the model the fracture infill zone is made up of a combination of:

- fine grained fault gauge (n > 10%?)
- mylonite (n = 0.3 to 0.6%)
- breccia fragments (n = 1 to 3%)
- very porous coatings (n > 10%)
- breccia pieces (n = 0.5 to 2%)
- cataclastic/altered wall rock (n = 0.5 to 2%)

The total thickness of all these zones together is up to 25 mm. In the present study, all of these porosities are combined as a single fracture infilling/fault gouge zone. Unaltered rock zone porosity is set to 0.1% for the following simulations.

The effect of the immobile zones on tracer breakthrough is shown in Figure 4-3. Simulations for this figure assumed a pipe channel path length 33m. The aperture is equal to 1.8 mm and the width is 0.1 m. Dispersion is 3.3m. The five simulations are in order of decreasing matrix porosity for each diffusion zone. The fracture infilling, altered rock , and unaltered rock zone porosities for simulations 1 through 5 are set equal to 20.0%/2.0%/0.1%, 15.0%/1.5%/0.075%, 10.0%/1.0%/0.05%, 5.0%/0.5%/0.025%, and the final simulation has no diffusion into the matrix. Increasing immobile zone porosity a) decreases peak breakthrough, b) increases the relative strength of the tail of the breakthrough curve, increases the apparent time to 50% recovery t_{50}, and c) reduces the total recovery achieved during the limited experimental time.

The effect of dispersion on the breakthrough and recovery solution is shown in Figure 4-4. Simulations use the same pipe model as used in the comparison of diffusion. Fracture infilling porosity is held constant at 10.0%, altered rock zone porosity at 1%, and unaltered rock zone porosity at 0.05%. Simulations are in order of decreasing dispersion length α_L. Simulations 1 through 5 have dispersion lengths of 3.25m, 2.44m,

1.63m, 0.81m, and 0.08m respectively. Decreased dispersion increases the peak breakthrough, and delays the early breakthrough (t_5). It has less effect on the later arrivals than changes in diffusion parameters.

Flow aperture is assumed correlated to fracture transmissivity according to a power-law relationship (Equation 1). The values of A and B were initially based on Dershowitz et al (2000). Flow aperture parameters are assigned as A = 2 and B = 0.5. Transport aperture is defined as a percentage of the flow aperture.

In the following simulations the transport aperture is set to 30% of the flow aperture.

$$Flow\ Aperture = A*T^B \qquad \textbf{Equation 1}$$

Where A = 2 and B = 0.5

Transport Aperture = 30% of the Flow Aperture

Simulation of transport pathways were carried out both with and without fracture intersection zones (FIZ). For DFN paths modified to include travel along the FIZ, the FIZ was assigned a transport aperture assumed as 10 times the larger of the apertures of the structures making up the intersection. The FIZ is extended along the wide fracture intersection to allow for a loss of mass and further dilution of the tracer at the sink. Immobile zone parameters within the FIZ pipe have an average fracture infilling zone porosity of 13%, an average altered rock zone porosity of 1.6% and an average unaltered rock porosity of 0.05%. The thickness of the fracture infilling zone within the FIZ pipe is set to 3mm, the altered zone is set to 2cm and the unaltered zone is set at 10m.

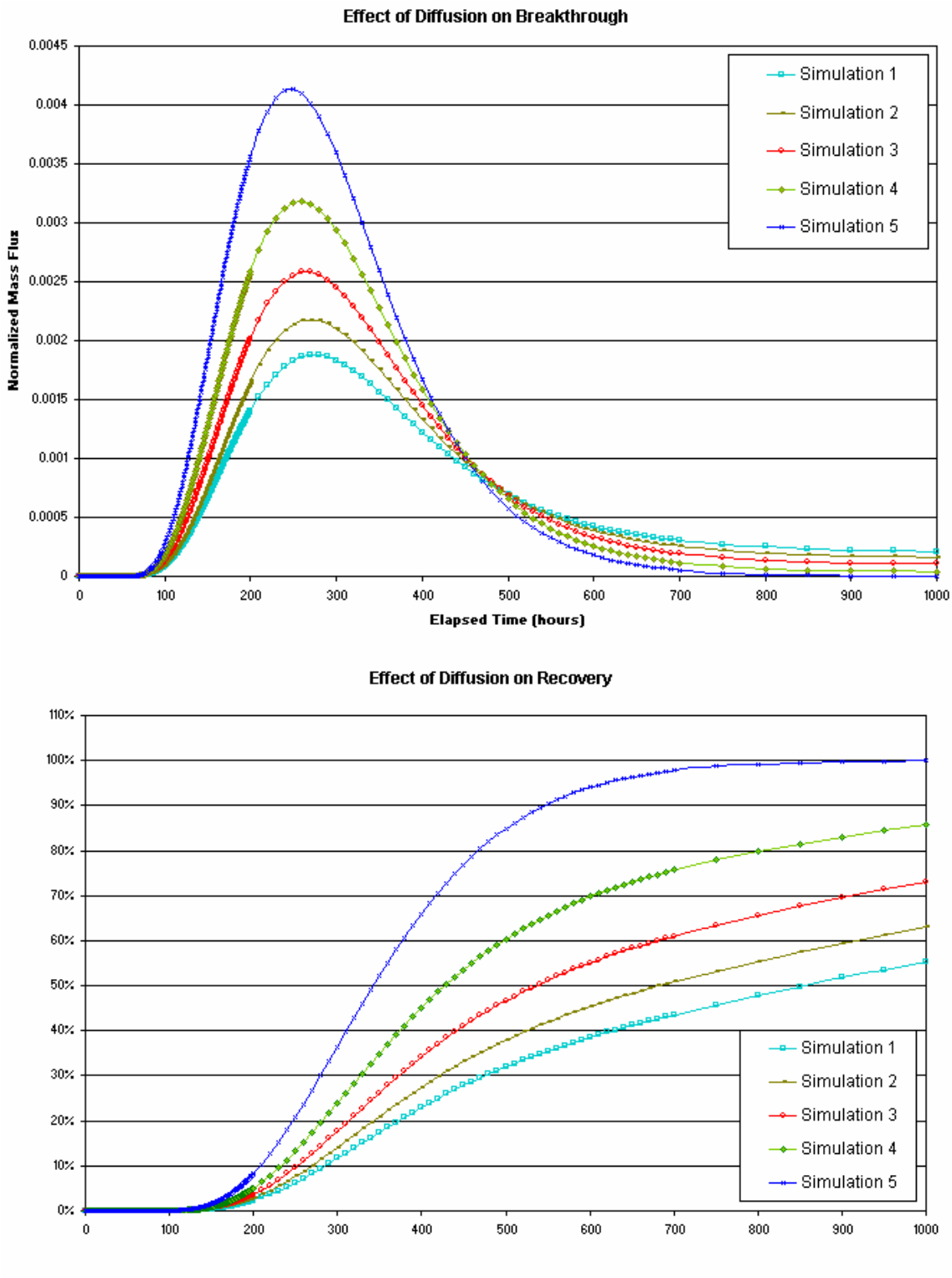

Figure 4-3 *Effect of Diffusion on Breakthrough and Recovery. Simulations 1 through 5 are in order of decreasing matrix diffusion.*

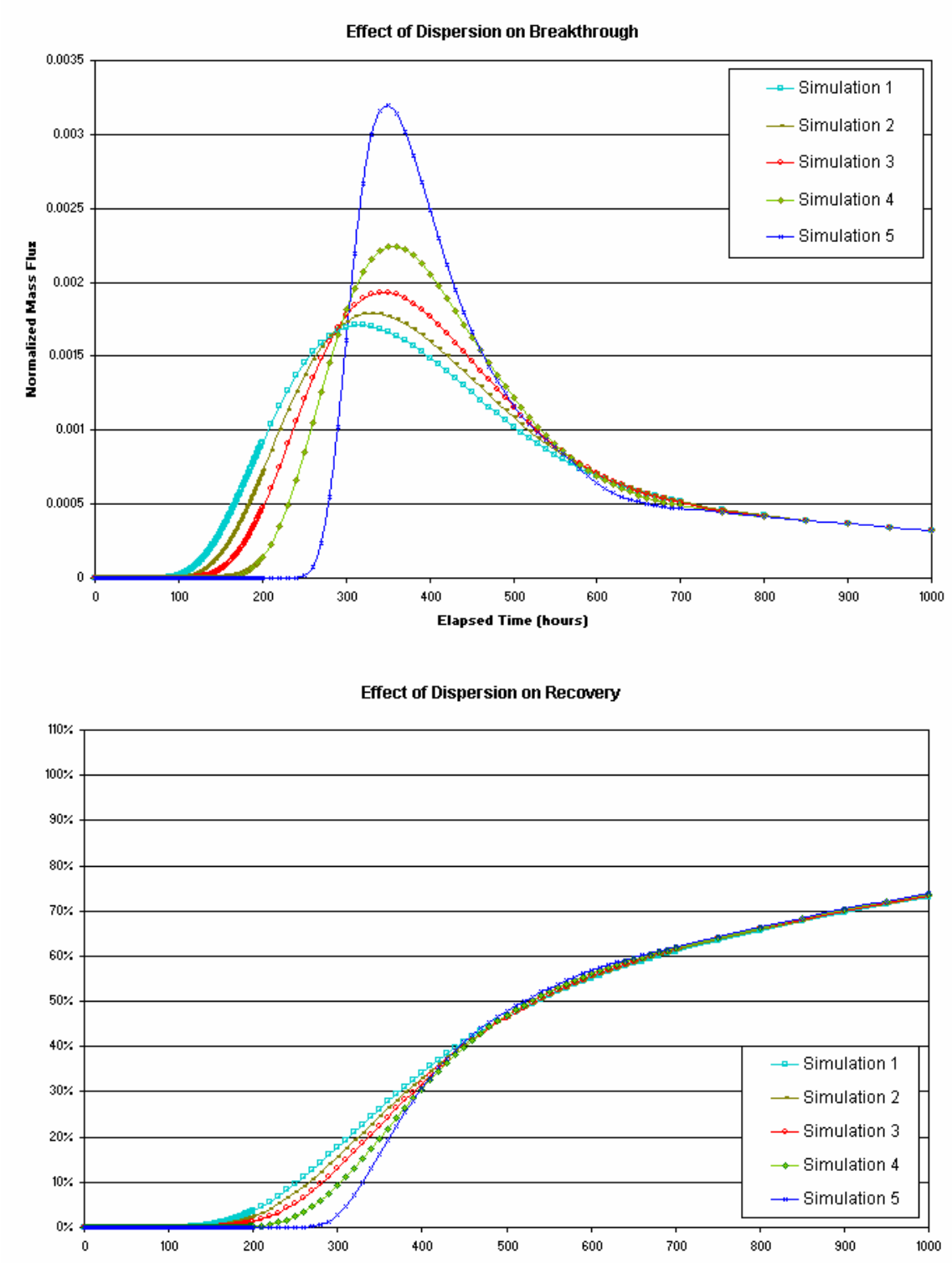

Figure 4-4 *Effect of Dispersion on Breakthrough and Recovery. Simulations 1 through 5 are in order of decreasing dispersion length.*

4.2 Transport Properties by Pathway

The following sections present studies to evaluate the effective pathway transport parameters using the simple pipe model. For each pathway, the study varied transport aperture and path width, dispersion length, and immobile zone porosities and thicknesses.

For each pathway, the range of immobile zone properties based on the fracture microstructural model shown in Figure 4-2 were investigated to determine the range of transport parameters consistent with the measured breakthrough curves. Simulations are organized according to pathways. Simulations are visually compared to measured breakthrough, and in terms of the breakthrough statistics t_5, t_{50}, t_{95}, and simulated ultimate mass recovery.

4.2.1 Pathway I: Tracer Tests B2g, C1, B1a, A4a

Tracer tests B2g, C1, B1a, and A4a share the travel path from KI0025F03:P5 to KI0023B:P6 (Pathway I). The tracer tests run along Structure 20 and do not cross a FIZ. Transport parameters found through simulations of tracer test B2g were used to model tracer transport of tests C1, B1a, and A4a. Simulation 1 of Test B2g was run with advective velocity, a width of 0.1m and no diffusion into the matrix. Test B2g is best fit by the parameters of Simulation 5. The parameters from this simulation are used in Simulation 5 for Test C1 and B1a. A better match to Test B1a is obtained by increasing the transport velocity since Test B1a is pumped at a different rate then Test C1 and B2g. The velocity was likewise modified to best-fit Test A4a (Simulation 6).

Table 4-2 lists the range of parameters studied in these simulations. Table 4-3 lists the t_5, t_{50}, t_{95}, and percent recovery of all simulations carried out for the group of tracer tests. Figure 4-5 through Figure 4-8 illustrates the simulations of Tests B2g, C1, B1a, and A4a respectively.

Table 4-2 Pathway I (Tests B2g, C1, B1a, A4a) Tracer Tests Transport Parameters. Immobile Zone parameters reported as porosity, n, and thickness, t (m).

Test B2g	Simulation 1	Simulation 2	Simulation 3	Simulation 4	Simulation 5
Transport Aperture (m)	0.3*0.00196	0.3*0.00196	0.3*0.00196	0.3*0.00196	0.3*0.00196
Pipe Width (m)	0.1	0.1	0.1	0.1	0.1
Velocity (m/s)	$2.37*10^{-4}$	$3.80*10^{-4}$	$3.80*10^{-4}$	$5.70*10^{-4}$	$5.70*10^{-4}$
Infilling Zone n, t (m)	0%, 0	0%, 0	15%, 0.001	20%, 0.001	5.5%, 0.003
Altered Zone n, t (m)	0%, 0	0%, 0	0.5%, 0.01	1%, 0.01	2%, 0.02
Unaltered Zone n, t (m)	0%, 0	0%, 0	0.1%, 10	0.1%, 10	0.1%, 10
Dispersion Length (m)	1.79	1.79	1.79	1.5	1.5

Test C1	Simulation 5
Transport Aperture (m)	0.3*0.00196
Pipe Width (m)	0.1
Velocity (m/s)	$5.70*10^{-4}$
Infilling Zone n, t (m)	5.5%, 0.003
Altered Zone n, t (m)	2%, 0.02
Unaltered Zone n, t (m)	0.1%, 10
Dispersion Length (m)	1.5

Test B1a	Simulation 5	Simulation 6
Transport Aperture (m)	0.3*0.00196	0.3*0.00196
Pipe Width (m)	0.1	0.1
Velocity (m/s)	$5.70*10^{-4}$	$3.42*10^{-4}$
Infilling Zone n, t (m)	5.5%, 0.003	5.5%, 0.003
Altered Zone n, t (m)	2%, 0.02	2%, 0.02
Unaltered Zone n, t (m)	0.1%, 10	0.1%, 10
Dispersion Length (m)	1.5	1.5

Test A4a	Simulation 5	Simulation 6
Transport Aperture (m)	0.3*0.00196	0.3*0.00196
Pipe Width (m)	0.1	0.1
Velocity (m/s)	$5.70*10^{-4}$	$6.18*10^{-5}$
Infilling Zone n, t (m)	5.5%, 0.003	5.5%, 0.003
Altered Zone n, t (m)	2%, 0.02	2%, 0.02
Unaltered Zone n, t (m)	0.1%, 10	0.1%, 10
Dispersion Length (m)	1.5	1.5

Table 4-3 Pathway I (Tests B2g, C1, B1a, A4a) Simulated and Measured t5, t50, t95, and Percent Recovery.

Test B2g	t_5 (hours)	t_{50} (hours)	t_{95} (hours)	Recovery %
Measured Data	9.1	20.8	166.4	100%
Simulation 1	14	25	45	100%
Simulation 2	10	17	32	100%
Simulation 3	12	24	550	98%
Simulation 4	10	20	550	98%
Simulation 5	9	20	165	100%

Test C1	t_5 (hours)	t_{50} (hours)	t_{95} (hours)	Recovery %
Measured Data	9.3	21.1	49.0	115%
Simulation 5	9	23	167	100%

Test B1a	t_5 (hours)	t_{50} (hours)	t_{95} (hours)	Recovery %
Measured Data	16.0	44.0	176.2	100%
Simulation 5	9	25	200	100%
Simulation 6	15	40	290	100%

Test A4a	t_5 (hours)	t_{50} (hours)	t_{95} (hours)	Recovery %
Measured Data	51.2	Na	Na	90%
Simulation 5	10	35	200	100%
Simulation 6	55	220	Na	95%

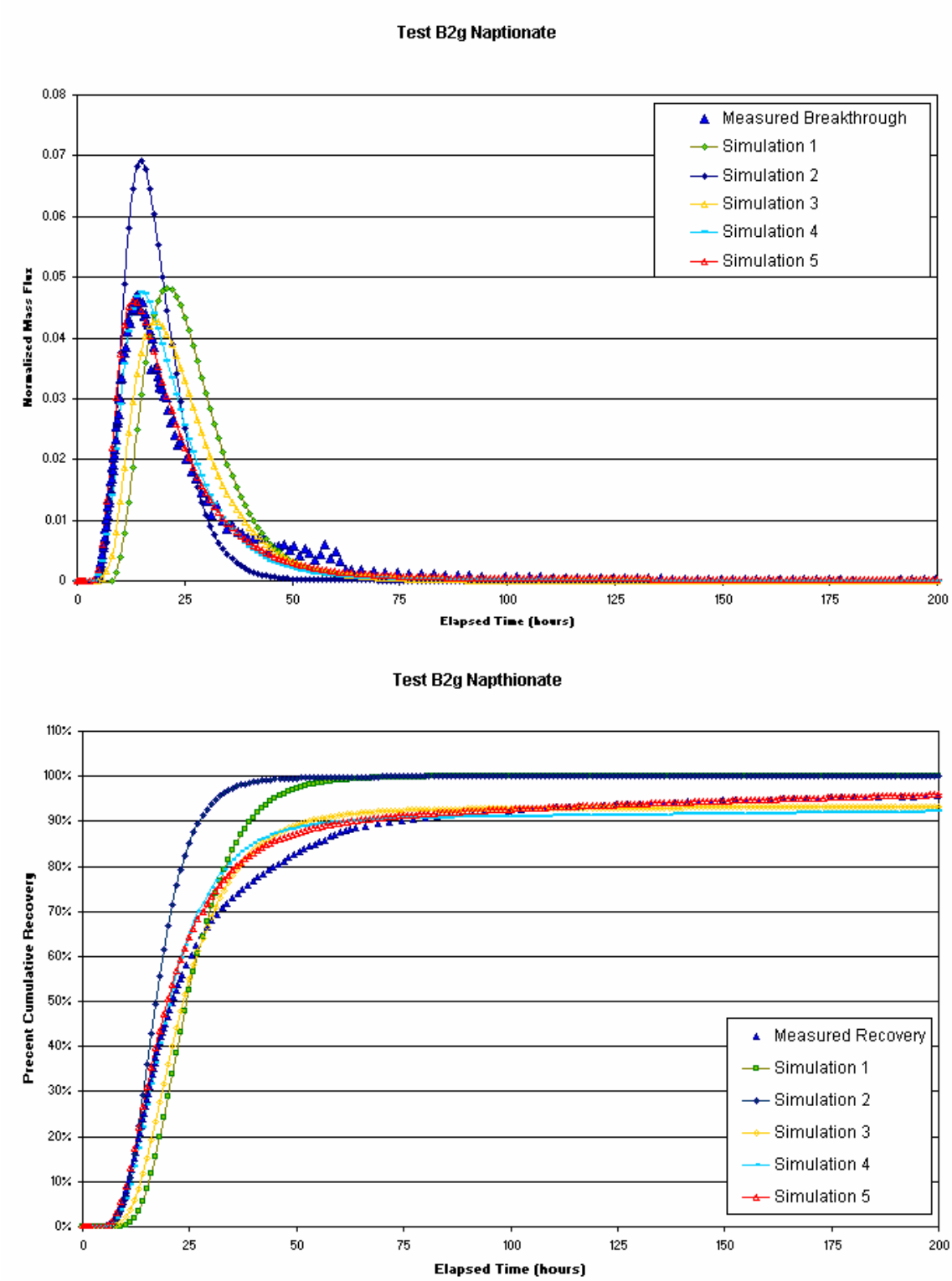

Figure 4-5 *Tracer Test B2g: Simulations and Measured Data.*

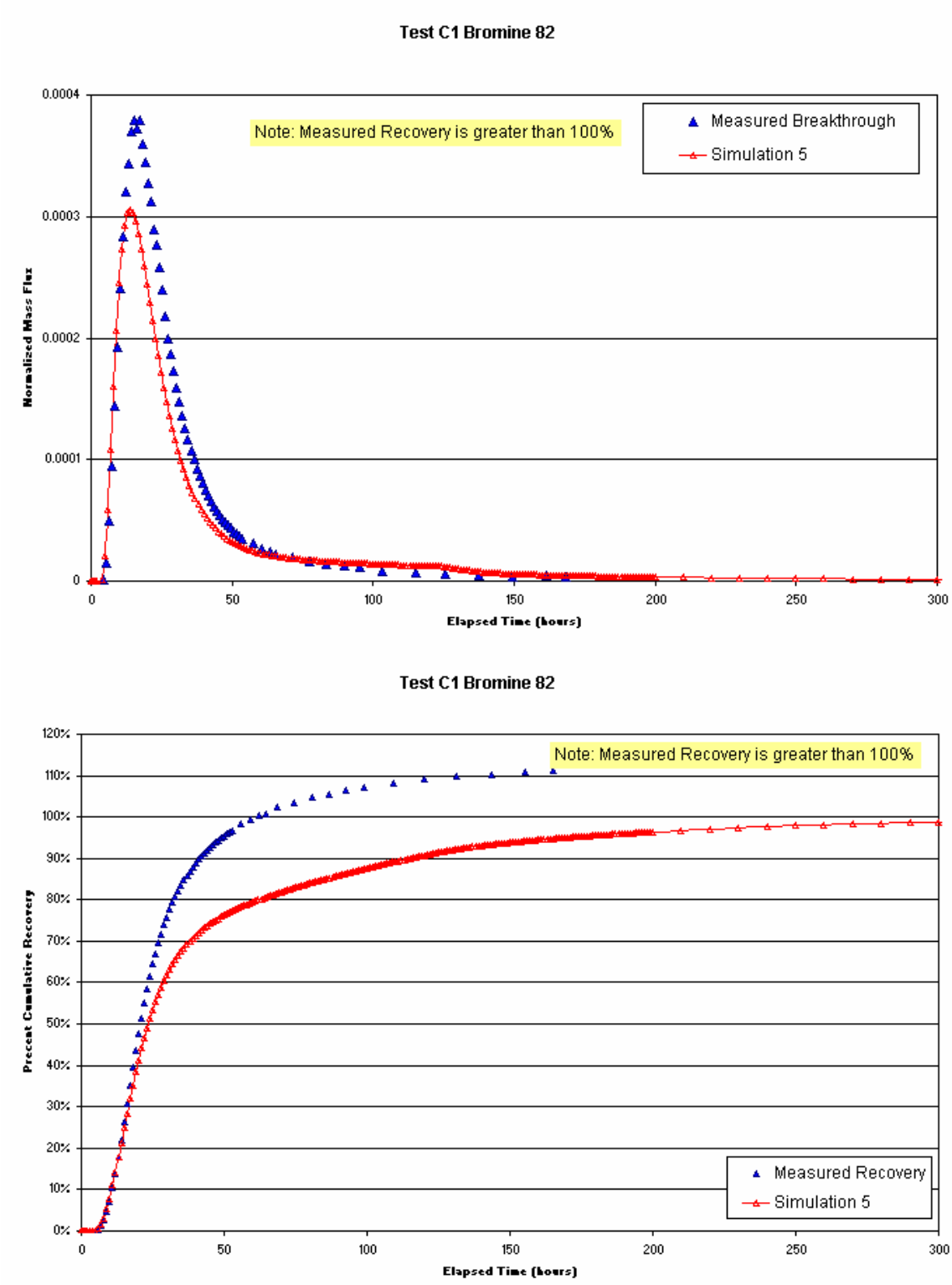

Figure 4-6 *Tracer Test C1: Simulations and Measured Data.*

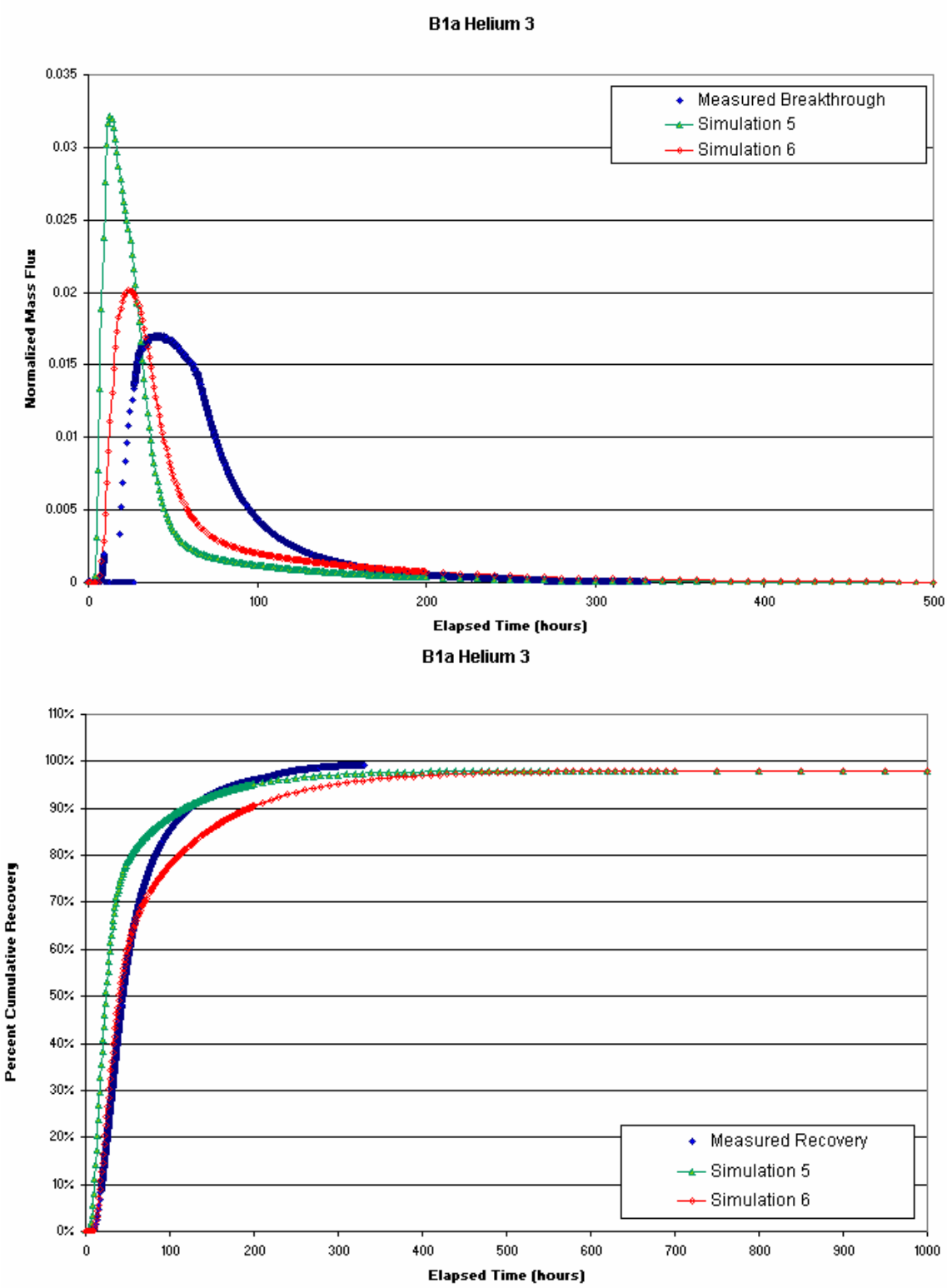

Figure 4-7 *Tracer Test B1a: Simulations and Measured Data.*

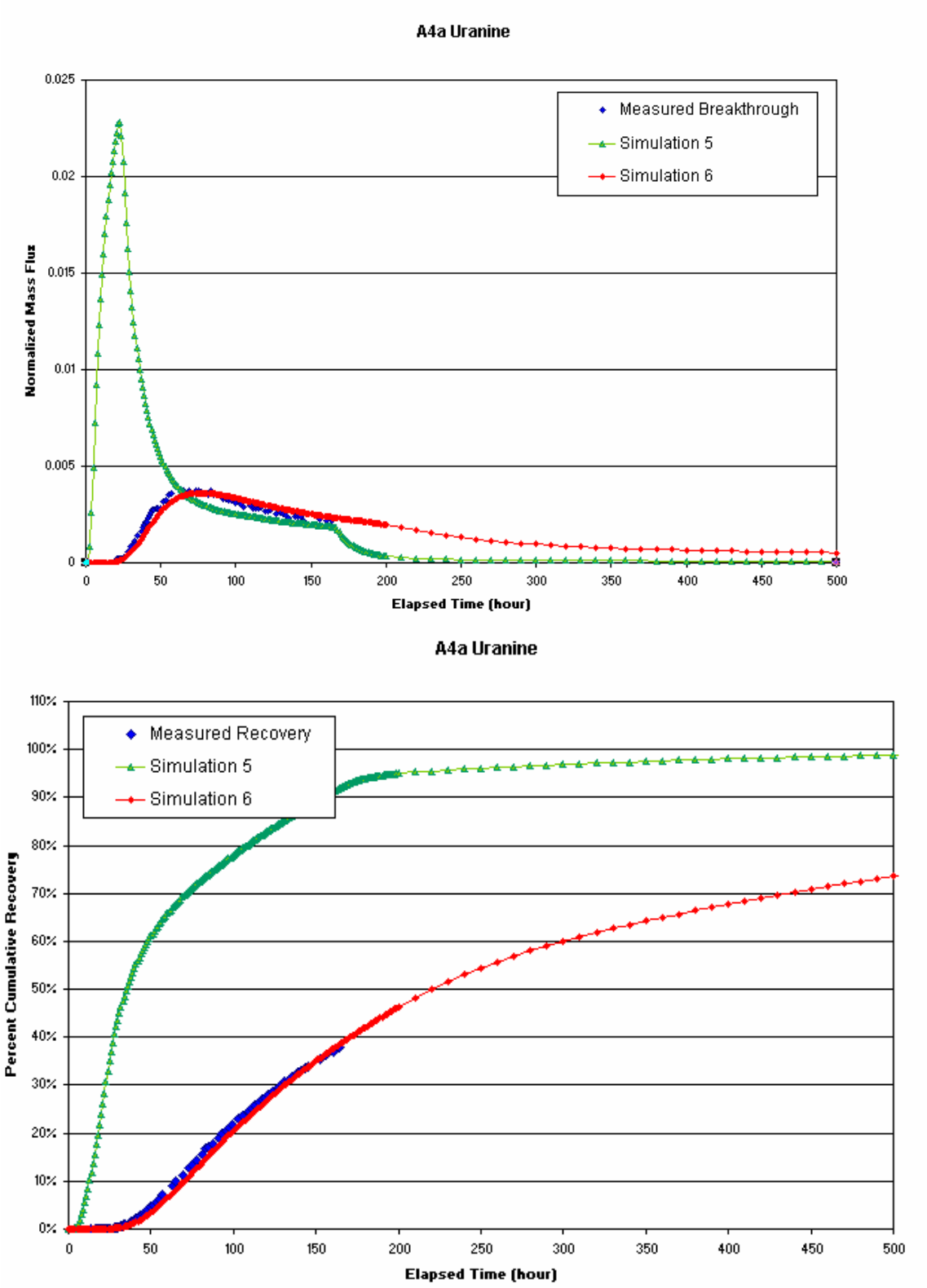

Figure 4-8 *Tracer Test A4a: Simulations and Measured Data.*

4.2.2 Pathway VI: Tracer Test B1c

Tracer test B1c involves transport from KI0025F02:P5 to KI0023B:P6 along the same structure as the above 4 tracer tests (B2g, C1, B1a, and A4a) however, the cumulative recovery is significantly smaller. This implies that, for the boundary conditions applied during B1c, the travel path includes a connection to an alternative sink. For this reason the travel path was altered to include travel along the 20/21 FIZ. This increased the total travel length from 19.5m to 33.8m. FIZ properties were added to the model. Table 4-4 lists the transport parameters studied for this pathway including the FIZ pipes. Simulation 1 uses the same parameters as found through the simulations for B2g, C1, B1a, and A4a. Simulations 2 and 3 modify the advective velocity. Simulations 4 through 6 use the modified path length and include FIZ properties. Table 4-5 lists the t_5, t_{50}, t_{95} and percent recovery of all simulations carried out for tracer test B1c. Figure 4-9 displays the simulations of Test B1c. Simulation 6 is the best fit to the measured data.

Table 4-4 Pathway VI (Test B1c) Tracer Test Transport Parameters. Immobile Zone parameters reported as porosity, n, and thickness, t (m).

Test B1c	Simulation 1	Simulation 2	Simulation 3	Simulation 4	Simulation 5	Simulation 6
Transport Aperture (m)	0.3*0.00196	0.3*0.00196	0.1*0.00196	0.3*0.00196	0.3*0.00196	0.3*0.00196
Pipe Width (m)	0.1	0.1	0.1	0.1	0.1	0.1
Velocity (m/s)	$3.42*10^{-4}$	$3.42*10^{-4}$	$3.42*10^{-4}$	$3.42*10^{-4}$	$3.42*10^{-4}$	$3.42*10^{-4}$
Infilling Zone n, t (m)	5.5%, 0.003	40%, 0.003	40%, 0.003	5.5%, 0.003	15%, 0.003	30%, 0.003
Altered Zone n, t (m)	2%, 0.02	2%, 0.02	2%, 0.02	2%, 0.02	2%, 0.02	2%, 0.02
Unaltered Zone n, t (m)	0.1%, 10	0%, 0	0.1%, 10	0.1%, 10	0.01%, 10	0.01%, 10
Dispersion Length (m)	1.63	1.63	1.63	2.84	3.38	3.38
FIZ Pipe Width (m)	Na	Na	Na	0.1	0.05	0.05
Mass lost to FIZ	Na	Na	Na	42.2%	61.1%	58.6%

Table 4-5 Pathway VI (Test B1c) Simulated and Measured t5, t50, t95, and Percent Recovery.

Test B1c	t_5 (hours)	t_{50} (hours)	t_{95} (hours)	Recovery %
Measured Data	82.5	Na	Na	38%
Simulation 1	17	43	Na	100%
Simulation 2	25	91	Na	100%
Simulation 3	37	250	Na	85%
Simulation 4	77	Na	Na	50%
Simulation 5	77	Na	Na	39%
Simulation 6	85	Na	Na	42%

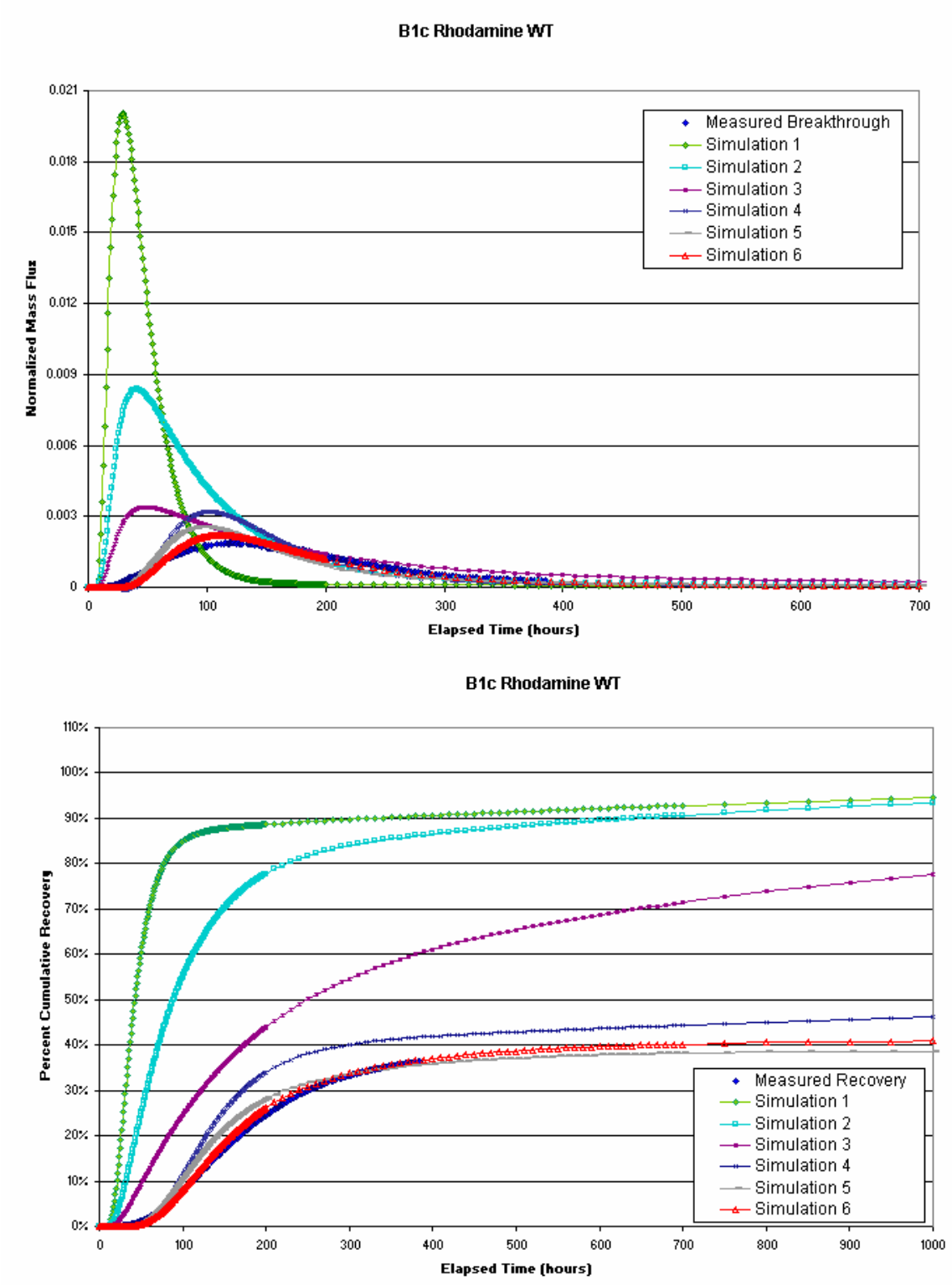

Figure 4-9 *Tracer Test B1c: Simulations and Measured Data.*

4.2.3 Pathway III: Tracer Tests C3, B2b

Tracer tests C3 and B2b were conducted from KI0025F02:P3 to KI0023B:P6 along Structure 21. The two tests have different pumping rates and therefore have different velocities. Test C3 was best matched by Simulation 5. The corresponding parameters were assumed also for tracer test B2b. Simulation 6 provides an acceptable match to Test B2b while using the same diffusion parameters as in Test C3. Table 4-6 lists the transport parameters used in simulating tracer tests C3 and B2b. Table 4-7 contains t_5, t_{50}, t_{95}, and percent recovery values for all simulations of Tests C3 and B2b. Figure 4-10 and Figure 4-11 illustrate the simulations of Tests C3 and B2b.

Table 4-6 Pathway III (Tests C3, B2b) Tracer Test Transport Parameters. Immobile Zone parameters reported as porosity, n, and thickness, t (m).

Test C3	Simulation 1	Simulation 2	Simulation 3	Simulation 4	Simulation 5
Transport Aperture (m)	0.3*0.0018	0.3*0.0018	0.3*0.0018	0.3*0.0018	0.3*0.0018
Pipe Width (m)	0.1	0.1	0.1	0.1	0.1
Velocity (m/s)	$1.13*10^{-5}$	$4.12*10^{-5}$	$4.12*10^{-5}$	$4.12*10^{-5}$	$4.39*10^{-5}$
Infilling Zone n, t (m)	0%, 0	20%, 0.002	1%, 0.001	20%, 0.002	17%, 0.003
Altered Zone n, t (m)	0%, 0	1%, 0.01	1%, 0.01	0.25%, 0.01	0.2%, 0.02
Unaltered Zone n, t (m)	0%, 0	0.1%, 10	0.1%, 10	0.1%, 10	0.08%, 10
Dispersion Length (m)	2	2	2	2	2

Test B2b	Simulation 5	Simulation 6
Transport Aperture (m)	0.3*0.0018	0.3*0.0018
Pipe Width (m)	0.1	0.1
Velocity (m/s)	$4.39*10^{-5}$	$6.02*10^{-5}$
Infilling Zone n, t (m)	17%, 0.003	17%, 0.003
Altered Zone n, t (m)	0.2%, 0.02	0.2%, 0.02
Unaltered Zone n, t (m)	0.08%, 10	0.08%, 10
Dispersion Length (m)	2	2

Table 4-7 Pathway III (Tests C3, B2b) Simulated and Measured t5, t50, t95, and Percent Recovery.

Test C3	t_5 (hours)	t_{50} (hours)	t_{95} (hours)	Recovery %
Measured Data	227.3	831.8	Na	80%
Simulation 1	510	853	1700	98%
Simulation 2	340	2200	Na	80%
Simulation 3	210	1700	Na	85%
Simulation 4	260	1700	Na	80%
Simulation 5	240	750	Na	85%

Test B2b	t_5 (hours)	t_{50} (hours)	t_{95} (hours)	Recovery %
Measured Data	188.5	472.9	Na	85%
Simulation 5	230	600	Na	77%
Simulation 6	180	450	Na	85%

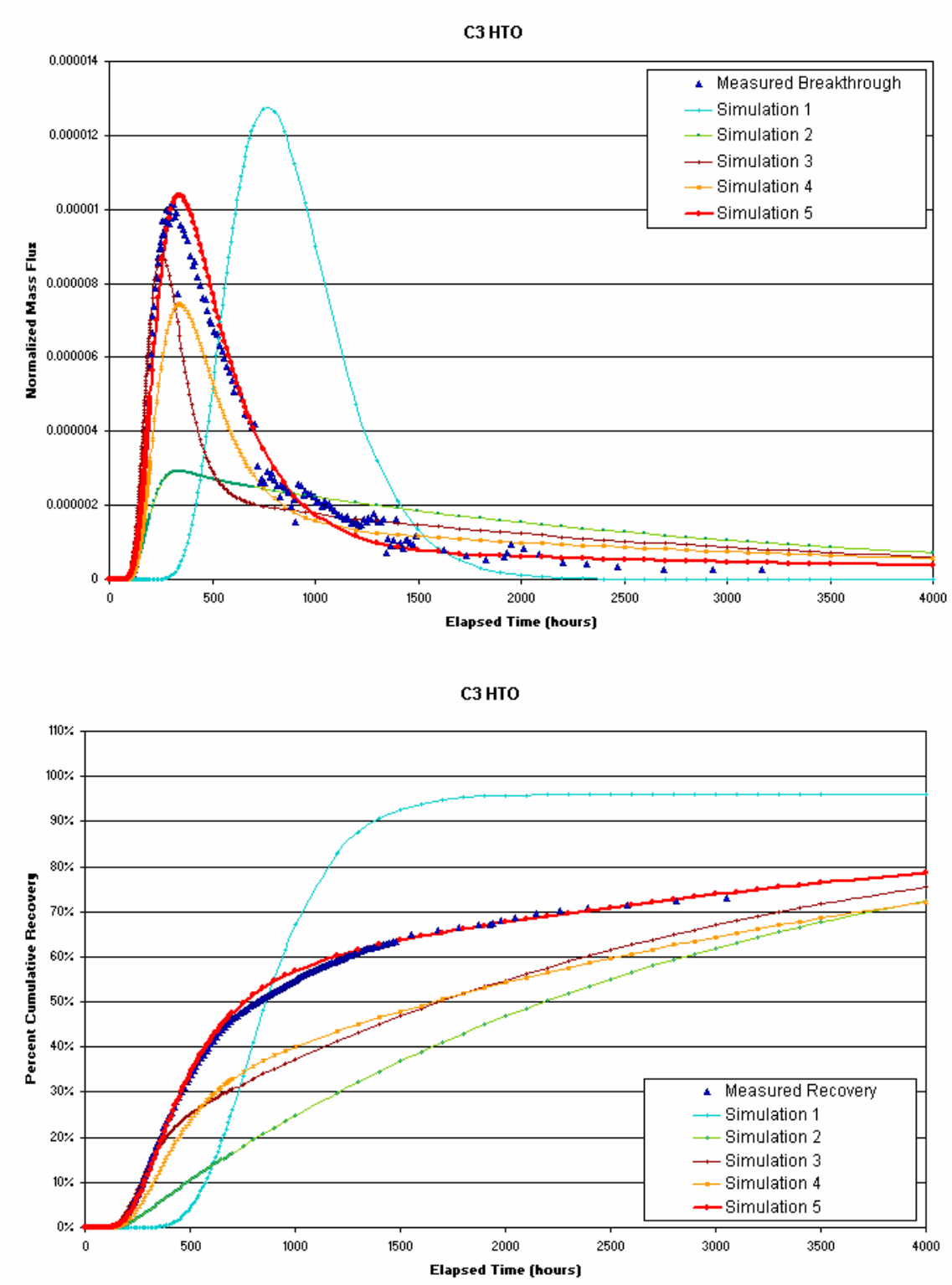

Figure 4-10 *Tracer Test C3: Simulations and Measured Data.*

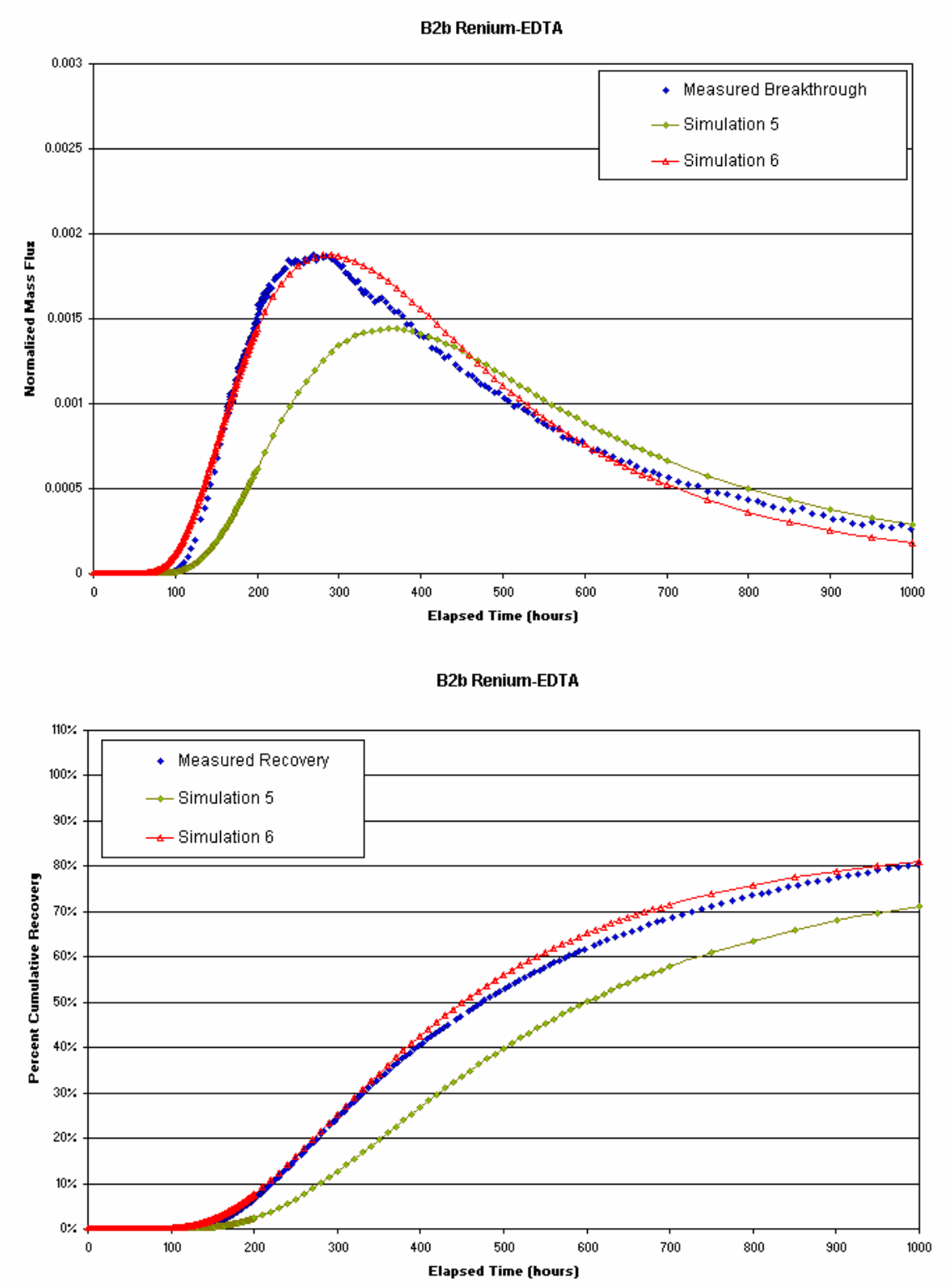

Figure 4-11 *Tracer Test B2b: Simulations and Measured Data.*

4.2.4 Pathway V: Tracer Test B2e

Tracer test B2e was conducted from KI0025F03:P3 to KI0023B:P6 along Structure 21. The initial transport parameters for this pathway were based on the simulation of tracer tests C3 and B2b because of the similar travel path. The travel parameters used in Simulation 1 are equivalent to the transport parameters of Test C3. These transport parameters result in greater recovery than measured recovery data. Immobile zone porosities are increased in Simulation 2 and the velocity is decreased to provide a better fit to the situ measurements. Table 4-8 lists transport parameters for Test B2e. Table 4-9 contains t_5, t_{50}, t_{95}, and percent recovery for all simulations of Test B2e. The simulations of Test B2e are displayed in Figure 4-12.

Table 4-8 Pathway V (Table B2e) Tracer Test Transport Parameters. Immobile Zone parameters reported as porosity, n, and thickness, t (m).

Test B2e	Simulation 1	Simulation 2
Transport Aperture (m)	0.3*0.0018	0.3*0.0018
Pipe Width (m)	0.1	0.1
Velocity (m/s)	$4.39*10^{-5}$	$2.22*10^{-5}$
Infilling Zone n, t (m)	17%, 0.003	20%, 0.003
Altered Zone n, t (m)	0.2%, 0.02	1.5%, 0.02
Unaltered Zone n, t (m)	0.08%, 10	0.08%, 10
Dispersion Length (m)	1.6	1.6

Table 4-9 Pathway V (Table B2e) Simulated and Measured t5, t50, t95, and Percent Recovery.

Test B2e	t_5 (hours)	t_{50} (hours)	t_{95} (hours)	Recovery %
Measured Data	330.4	Na	Na	36%
Simulation 1	160	420	Na	85%
Simulation 2	340	Na	Na	35%

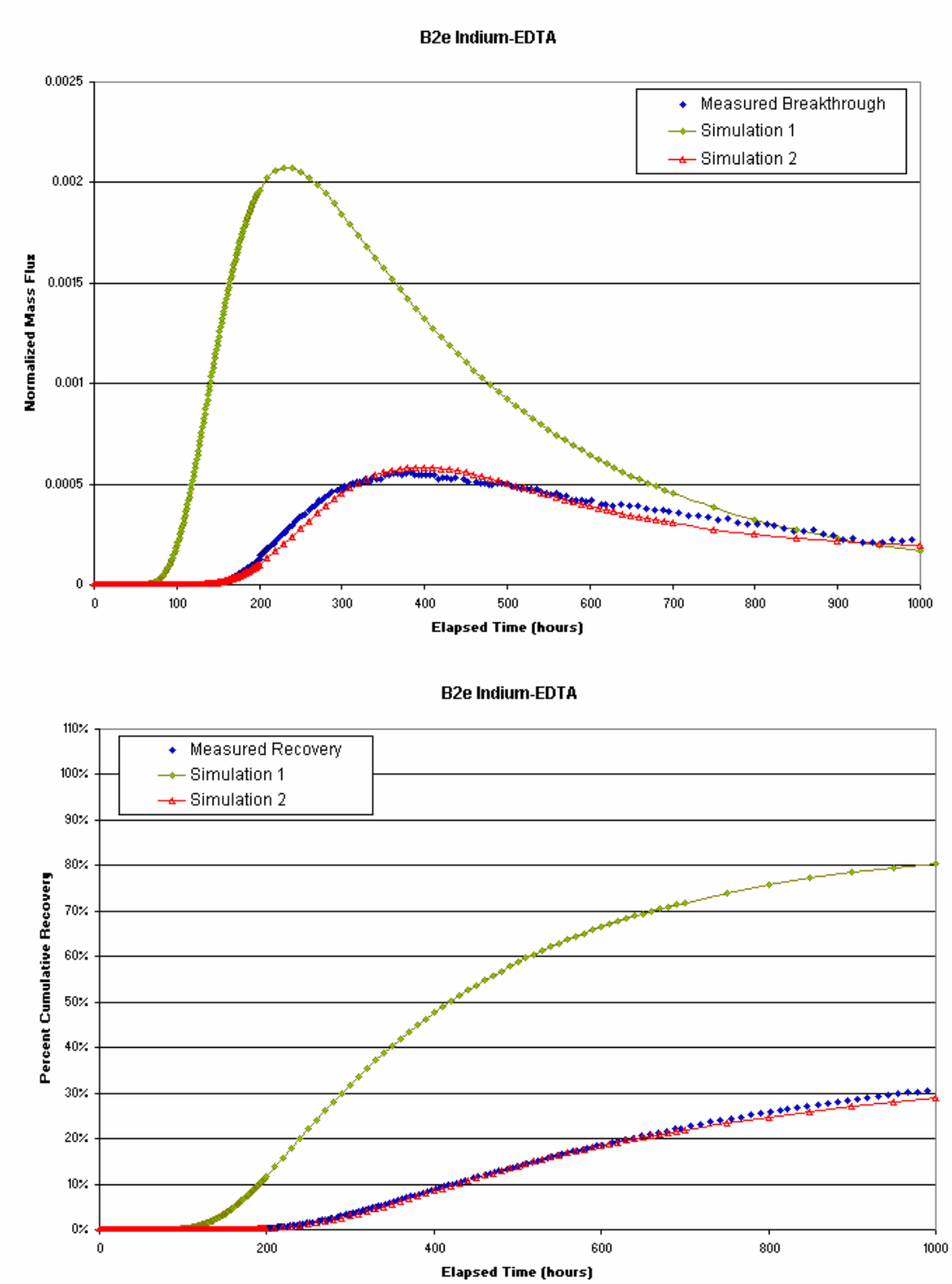

Figure 4-12 *Tracer Test B2e: Simulations and Measured Data.*

4.2.5 Pathway IV: Tracer Tests B2a, B1b, A4b

The pathway of tracer tests B2a, B1b, and A4b travel from KI0025F03:P6 to KI0023B:P6 passes through Structures 22, 20, and 21. All three tracer tests along this pathway have different pumping rates and therefore are simulated with different velocities. B2a was initially matched with no FIZ (Simulation 3). The resulting parameters were used in simulations for Test B1b and A4b. The parameters result in poor matches due to the different pumping rate and ultimate recovery. Parameters were modified to best fit Test B1b and A4b (Simulation 5 in both tests). For Test B1b the velocity was decreased and the immobile zone parameters used to fit previous tests traveling on structure 20 and 21 were used. For Test A4b the velocity was increased and the immobile zone parameters of previous tests were used with the exception of the altered zone with was given a porosity of half the prescribed value. The dispersion length is also reduced by half in Test A4b to produce the best fit.

Both sets of parameters used to fit B1b and A4b were run with the B2a test (with scaled velocity). The results show that B2a has a significantly lower recovery than B1b and A4b when using the same parameters. For this reason, a FIZ pipe was added to the B2a simulation. Results of the B1b and A4b parameters with the addition of a FIZ pipe are featured in Simulation 6. Results of the B1b Test provide a good match. Test A4b is best match with Simulation 7, which has the same parameters as the Simulation 6 with the exception that the altered zone porosity of Structures 22 and 20 have half the porosity as Simulation 6 and the dispersion is also reduced by half.

Table 4-10 lists the transport parameters studied for tests B2a, B1b, and A4b.

Table 4-11 presents t_5, t_{50}, t_{95}, and percent recovery values for simulations of Tests B2a, B1b, and A4b. Figure 4-13 through Figure 4-15 illustrates the sensitivity studies for tests B2a, B1b, and A4b respectively.

Table 4-10 Pathway IV (Tests B1b, B2a and A4b) Tracer Test Transport Parameters. Immobile Zone parameters reported as porosity, n, and thickness, t (m).

Test B2a	Structure	Simulation 1	Simulation 2	Simulation 3	Simulation 6
Transport Aperture (m)	22	0.3*0.00122	0.3*0.00122	0.3*0.00122	0.3*0.00122
	20	0.3*0.00196	0.3*0.00196	0.3*0.00196	0.3*0.00196
	21	0.3*0.0018	0.3*0.0018	0.3*0.0018	0.3*0.0018
Pipe Width (m)	22	0.16	0.16	0.16	0.16
	20	0.1	0.1	0.1	0.1
	21	0.11	0.11	0.11	0.11
Velocity (m/s)	All	$3.09*10^{-5}$	$1.9*10^{-4}$	$1.9*10^{-4}$	$2.54*10^{-4}$
Infilling Zone n, t (m)	22	0%, 0	5.5%, 0.003	5.5%, 0.003	5.5%, 0.003
	20	0%, 0	5.5%, 0.003	5.5%, 0.003	5.5%, 0.003
	21	0%, 0	17%, 0.003	17%, 0.003	17%, 0.003
Altered Zone n, t (m)	22	0%, 0	2%, 0.02	2%, 0.02	2%, 0.02
	20	0%, 0	2%, 0.02	2%, 0.02	2%, 0.02
	21	0%, 0	0.2%, 0.02	2%, 0.02	0.2%, 0.02
Unaltered Zone n, t (m)	22	0%, 0	0.1%, 10	0.1%, 10	0.1%, 10
	20	0%, 0	0.01%, 10	0.1%, 10	0.01%, 10
	21	0%, 0	0.08%, 10	0.1%, 10	0.08%, 10
Dispersion Length (m)	All	4.1	4.1	4.1	4.1
FIZ Pipe Width (m)	FIZ Pipe	Na	Na	Na	0.1
Mass lost to FIZ		Na	Na	Na	28.2%

Test B1b	Structure	Simulation 3	Simulation 4	Simulation 5	Simulation 6
Transport Aperture (m)	22	0.3*0.00122	0.3*0.00122	0.3*0.00122	0.3*0.00122
	20	0.3*0.00196	0.3*0.00196	0.3*0.00196	0.3*0.00196
	21	0.3*0.0018	0.3*0.0018	0.3*0.0018	0.3*0.0018
Pipe Width (m)	22	0.16	0.16	0.16	0.16
	20	0.1	0.1	0.1	0.1
	21	0.11	0.11	0.11	0.11
Velocity (m/s)	All	$1.9*10^{-4}$	$1.11*10^{-4}$	$1.58*10^{-4}$	$1.84*10^{-4}$
Infilling Zone n, t (m)	22	5.5%, 0.003	5.5%, 0.003	5.5%, 0.003	5.5%, 0.003
	20	5.5%, 0.003	5.5%, 0.003	5.5%, 0.003	5.5%, 0.003
	21	17%, 0.003	17%, 0.003	17%, 0.003	17%, 0.003
Altered Zone n, t (m)	22	2%, 0.02	2%, 0.02	2%, 0.02	2%, 0.02
	20	2%, 0.02	2%, 0.02	2%, 0.02	2%, 0.02
	21	2%, 0.02	2%, 0.02	0.2%, 0.02	0.2%, 0.02
Unaltered Zone n, t (m)	22	0.1%, 10	0.1%, 10	0.1%, 10	0.1%, 10
	20	0.1%, 10	0.1%, 10	0.01%, 10	0.01%, 10
	21	0.1%, 10	0.1%, 10	0.08%, 10	0.08%, 10
Dispersion Length (m)	All	4.1	4.1	4.1	4.1
FIZ Pipe Width (m)	FIZ Pipe	Na	Na	Na	0.1
Mass lost to FIZ		Na	Na	Na	10.7%

Table 4-10 (continued) Pathway IV (Tests B1b, B2a and A4b) Tracer Test Transport Parameters. Immobile Zone parameters reported as porosity, n, and thickness, t (m).

Test A4b	Structure	Simulation 3	Simulation 4	Simulation 5	Simulation 6	Simulation 7
Transport Aperture (m)	22	0.3*0.00122	0.3*0.00122	0.3*0.00122	0.3*0.00122	0.3*0.00122
	20	0.3*0.00196	0.3*0.00196	0.3*0.00196	0.3*0.00196	0.3*0.00196
	21	0.3*0.0018	0.3*0.0018	0.3*0.0018	0.3*0.0018	0.3*0.0018
Pipe Width (m)	22	0.16	0.16	0.16	0.16	0.16
	20	0.1	0.1	0.1	0.1	0.1
	21	0.11	0.11	0.11	0.11	0.11
Velocity (m/s)	All	$1.9*10^{-4}$	$2.12*10^{-4}$	$2.12*10^{-4}$	$2.85*10^{-4}$	$2.85*10^{-4}$
Infilling Zone	22	5.5%, 0.003	5.5%, 0.003	5.5%, 0.003	5.5%, 0.003	5.5%, 0.003
n, t (m)	20	5.5%, 0.003	5.5%, 0.003	5.5%, 0.003	5.5%, 0.003	5.5%, 0.003
	21	17%, 0.003	17%, 0.003	5%, 0.003	17%, 0.003	17%, 0.003
Altered Zone	22	2%, 0.02	2%, 0.02	1%, 0.02	2%, 0.02	1.5%, 0.02
n, t (m)	20	2%, 0.02	2%, 0.02	1%, 0.02	2%, 0.02	1.5%, 0.02
	21	2%, 0.02	2%, 0.02	0.2%, 0.02	0.2%, 0.02	0.2%, 0.02
Unaltered Zone	22	0.1%, 10	0.1%, 10	0.1%, 10	0.1%, 10	0.1%, 10
n, t (m)	20	0.1%, 10	0.1%, 10	0.01%, 10	0.01%, 10	0.01%, 10
	21	0.1%, 10	0.1%, 10	0.08%, 10	0.08%, 10	0.08%, 10
Dispersion Length (m)	All	4.1	4.1	2.0	4.1	2.0
FIZ Pipe Width (m)	FIZ Pipe	Na	Na	Na	0.1	0.1
Mass lost to FIZ		Na	Na	Na	0.1%	0.1%

Table 4-11 Pathway IV (Tests B1b, B2a and A4b) Simulated and Measured t5, t50, t95, and Percent Recovery.

Test B2a	t_5 (hours)	t_{50} (hours)	t_{95} (hours)	Recovery %
Measured Data	96.5	460.7	Na	65%
Simulation 1	240	430	700	100%
Simulation 2	97	420	Na	70%
Simulation 3	83	470	Na	67%
Simulation 5 (B1b)	80	180	Na	95%
Simulation 5 (A4b)	58	163	Na	95%
Simulation 6	78	460	Na	65%

Test B1b	t_5 (hours)	t_{50} (hours)	t_{95} (hours)	Recovery %
Measured Data	88.5	Na	Na	65%
Simulation 3	59	220	Na	95%
Simulation 4	143	Na	Na	55%
Simulation 5	93	480	Na	80%
Simulation 6	100	480	Na	70%

Test A4b	t_5 (hours)	t_{50} (hours)	t_{95} (hours)	Recovery %
Measured Data	75.5	163.5	Na	90%
Simulation 3	85	590	Na	70%
Simulation 4	76	490	Na	80%
Simulation 5	74	166	Na	90%
Simulation 6	68	189	Na	90%
Simulation 7	74	166	Na	90%

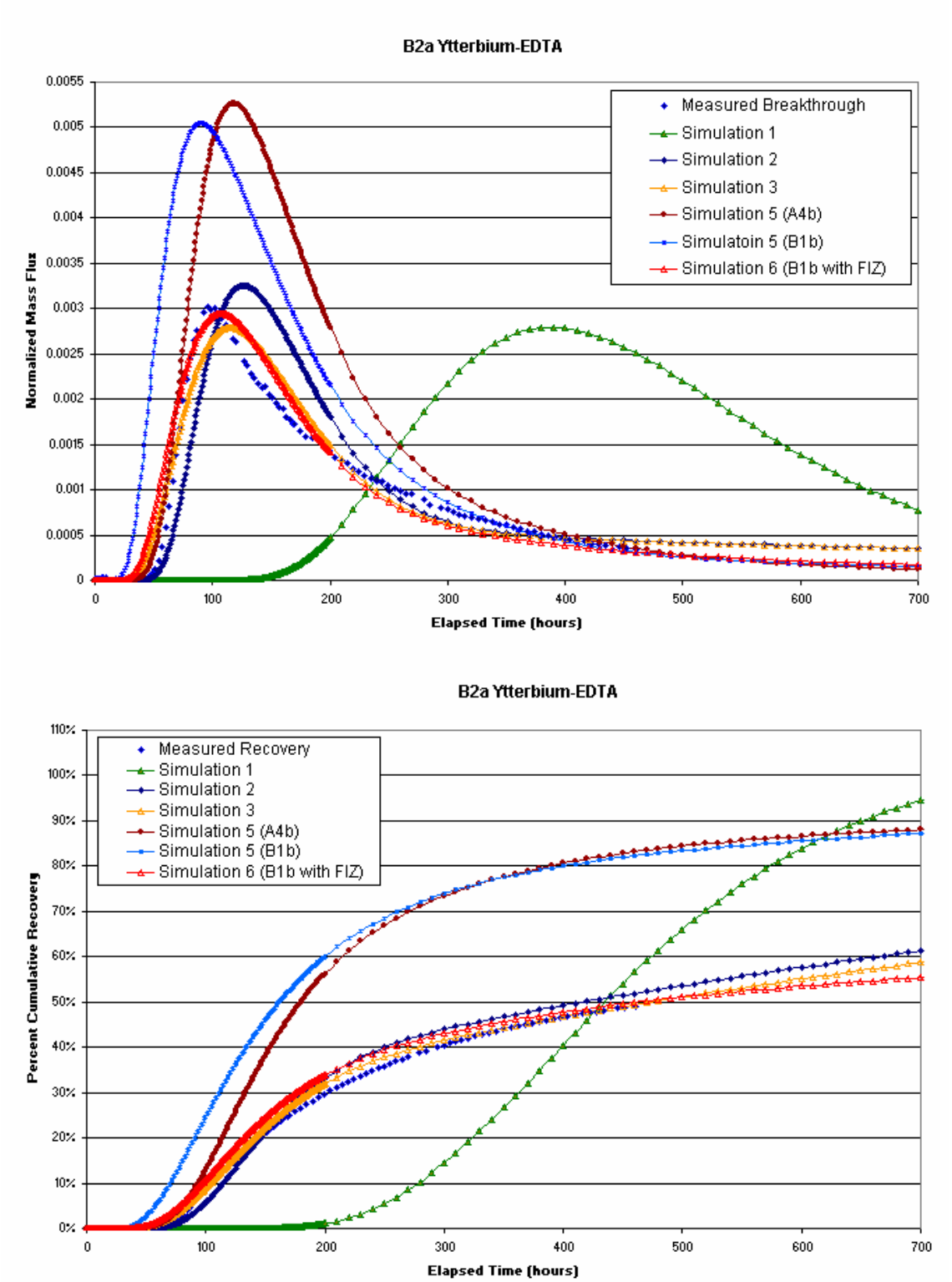

Figure 4-13 *Tracer Test B2a (Amino G): Simulations and Measured Data.*

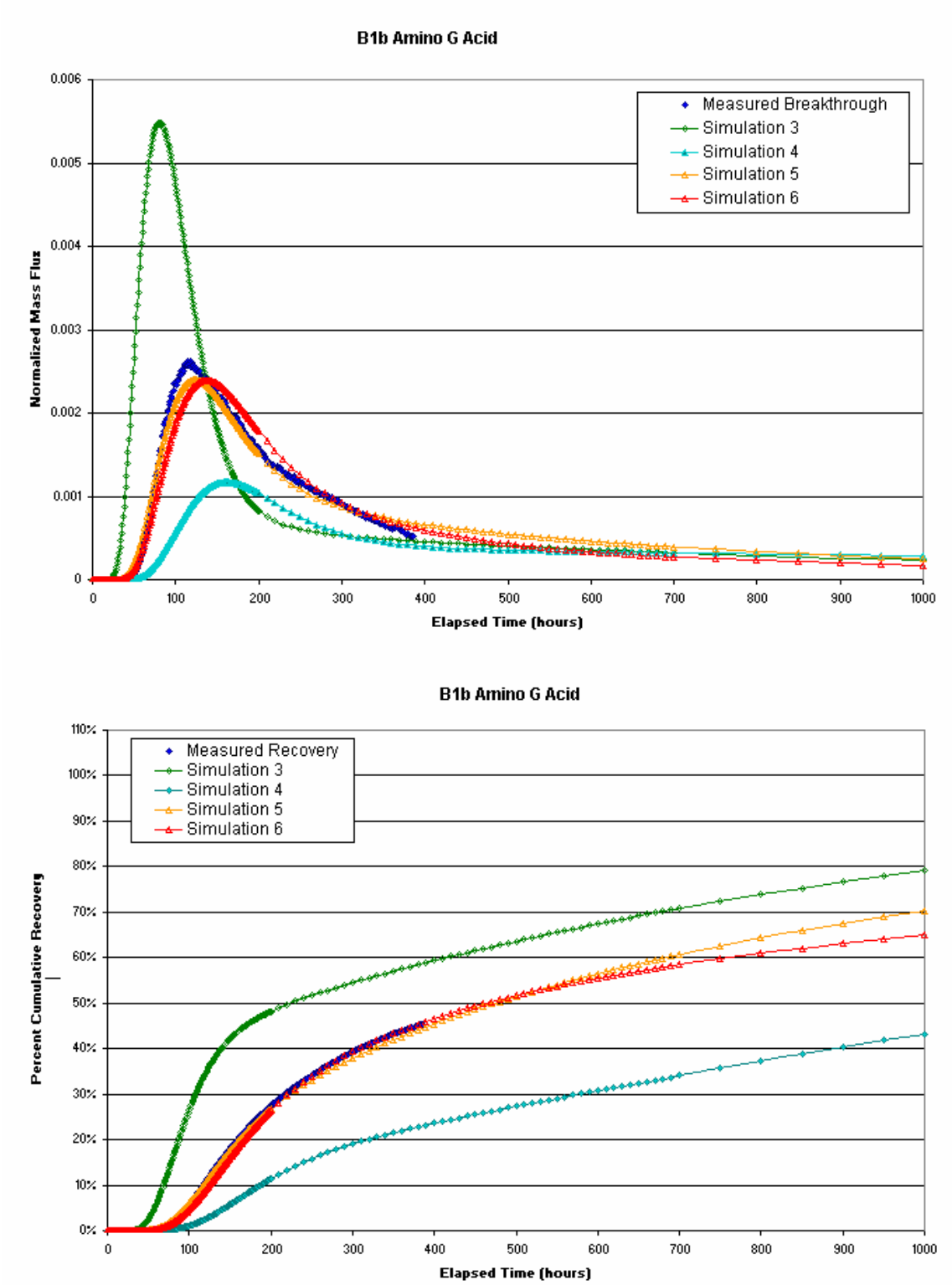

Figure 4-14 *Tracer Test B1b (Ytterblum-EDTA): Simulations and Measured Data.*

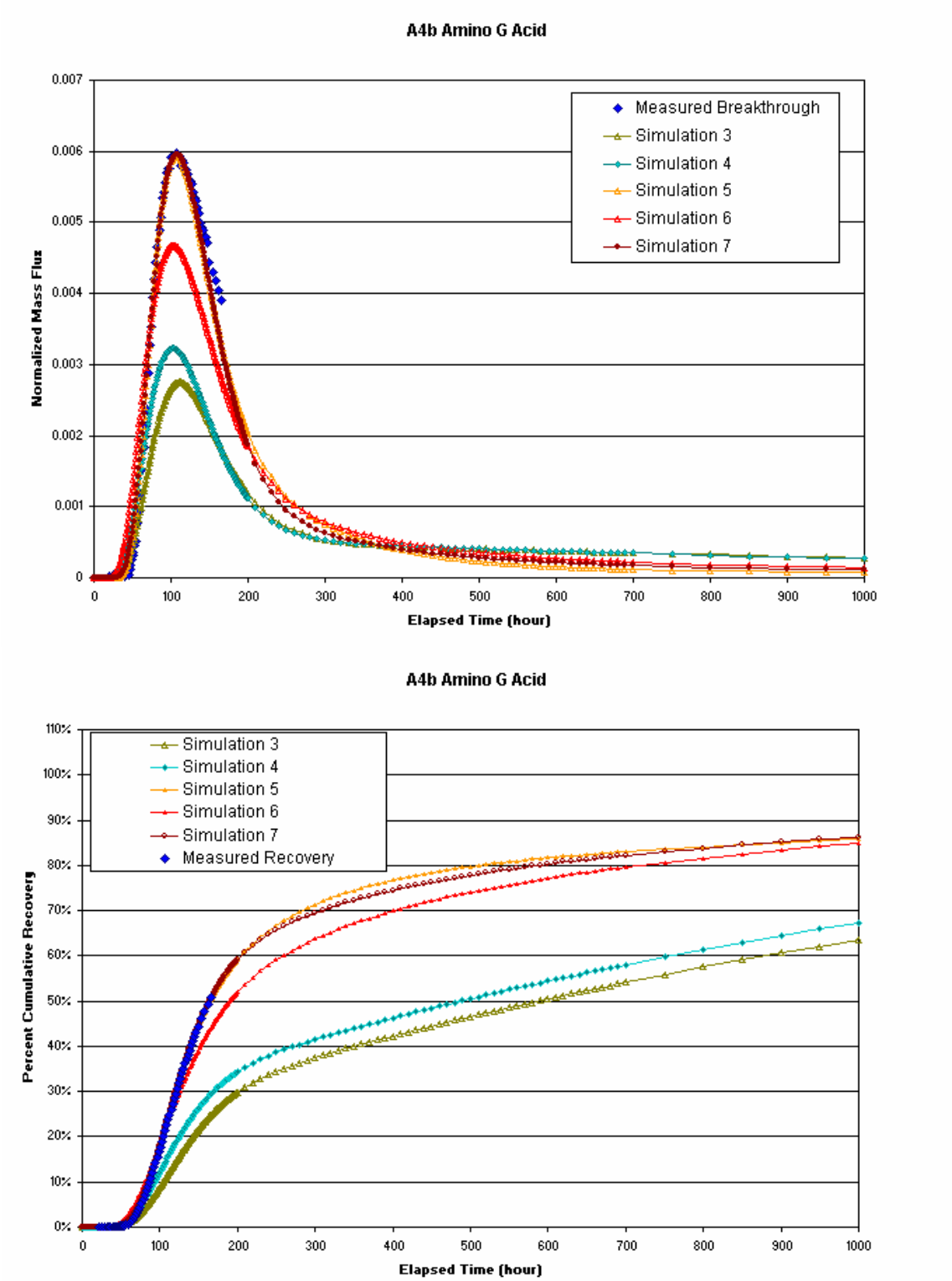

Figure 4-15 *Tracer Test A4b (Amino G): Simulations and Measured Data.*

4.2.6 Pathway II: Tracer Tests C2, B2d, A4c

Tracer tests C2, B2d, and A4c includes transport from KI0025F03:P7 to KI0023B:P6 along a pathway through Structures 23, 22, 20, and 21. Simulations were carried out for this pathway both with and without FIZ pipes. The transport parameters simulated are provided in Table 4-12. Test C2 was initially matched with the use of a FIZ pipe due to the large difference in recovered mass between Test C2 (100% ultimate recovery), B2d (80% ultimate recovery), and A4c (ultimate recovery is below background levels). All three tests are matched with the same travel paths but different percent mass lost to the FIZ. Test C2 is best matched by Simulation 5. The same parameters are used to match B2d and A4c. B2d was best matched by Simulation 7, which differs from Simulation 5 by the dispersion and the percent mass lost to FIZ. Since Test A4c measured data is below background levels, both sets of parameters are shown (Simulation 5 and Simulation 7). Simulation 8 of Test A4c has a percent mass loss such that less than 6% of the mass is recovered after 1000 hours.

Table 4-12 lists the transport parameters studied for tests C2, B2d, and A4c. Table 4-13 provides t_5, t_{50}, t_{95}, and percent recovery for simulations along this pathway. Figure 4-16 through Figure 4-18 illustrates the sensitivity studies carried out for this pathway.

Table 4-12 Path II (Test C2, B2d, A4c) Tracer Tests Transport Parameters. Immobile Zone parameters reported as porosity, n, and thickness, t (m).

Test C2	Structure	Simulation 1	Simulation 2	Simulation 3	Simulation 4	Simulation 5
Transport Aperture (m)	23	0.3*0.000165	0.3*0.000165	0.3*0.000165	0.3*0.000165	0.3*0.000165
	22	0.3*0.00122	0.3*0.00122	0.3*0.00122	0.3*0.00122	0.3*0.00122
	20	0.3*0.00196	0.3*0.00196	0.3*0.00196	0.3*0.00196	0.3*0.00196
	21	0.3*0.0018	0.3*0.0018	0.3*0.0018	0.3*0.0018	0.3*0.0018
Pipe Width (m)	23	0.5	0.5	0.5	0.11	0.19
	22	0.07	0.07	0.07	0.07	0.07
	20	0.05	0.05	0.05	0.05	0.05
	21	0.05	0.05	0.05	0.05	0.05
Velocity (m/s)	23	$7.17*10^{-5}$	$3.17*10^{-4}$	$3.17*10^{-4}$	$1.58*10^{-3}$	$8.87*10^{-4}$
	22	$7.17*10^{-5}$	$3.17*10^{-4}$	$3.17*10^{-4}$	$3.17*10^{-4}$	$3.17*10^{-4}$
	20	$7.17*10^{-5}$	$3.17*10^{-4}$	$3.17*10^{-4}$	$3.17*10^{-4}$	$3.17*10^{-4}$
	21	$7.17*10^{-5}$	$3.17*10^{-4}$	$3.17*10^{-4}$	$2.54*10^{-4}$	$2.54*10^{-4}$
Infilling Zone n, t (m)	23	0%, 0	5.5%, 0.003	5.5%, 0.003	5.5%, 0.003	5.5%, 0.003
	22	0%, 0	5.5%, 0.003	5.5%, 0.003	5.5%, 0.003	5.5%, 0.003
	20	0%, 0	5.5%, 0.003	5.5%, 0.003	5.5%, 0.003	5.5%, 0.003
	21	0%, 0	17%, 0.003	17%, 0.003	17%, 0.003	17%, 0.003
Altered Zone n, t (m)	23	0%, 0	2%, 0.02	2%, 0.02	0.5%, 0.02	0.5%, 0.02
	22	0%, 0	2%, 0.02	2%, 0.02	1%, 0.02	0.5%, 0.02
	20	0%, 0	2%, 0.02	2%, 0.02	2%, 0.02	0.5%, 0.01
	21	0%, 0	0.2%, 0.02	0.2%, 0.02	0.2%, 0.02	0.2%, 0.02
Unaltered Zone n, t (m)	23	0%, 0	0.1%, 10	0.1%, 10	0.1%, 10	0.01%, 10
	22	0%, 0	0.1%, 10	0.1%, 10	0.1%, 10	0.01%, 10
	20	0%, 0	0.01%, 10	0.01%, 10	0.01%, 10	0.01%, 10
	21	0%, 0	0.08%, 10	0.08%, 10	0.08%, 10	0.01%, 10
Dispersion Length (m)	All	5.4	5.4	5.9	5.9	5.9
FIZ Pipe Width (m)	FIZ Pipe	Na	Na	0.05	0.05	0.05
Mass lost to FIZ		Na	Na	0.1%	0.1%	0.1%

Table 4-12 (continued) Path II (Test C2, B2d, A4c) Tracer Tests Transport Parameters. Immobile Zone parameters reported as porosity, n, and thickness, t (m).

Test B2d	Structure	Simulation 5	Simulation 6	Simulation 7
Transport Aperture (m)	23	0.3*0.000165	0.3*0.000165	0.3*0.000165
	22	0.3*0.00122	0.3*0.00122	0.3*0.00122
	20	0.3*0.00196	0.3*0.00196	0.3*0.00196
	21	0.3*0.0018	0.3*0.0018	0.3*0.0018
Pipe Width (m)	23	0.19	0.19	0.19
	22	0.07	0.07	0.07
	20	0.05	0.05	0.05
	21	0.05	0.05	0.05
Velocity (m/s)	23	$8.87*10^{-4}$	$8.87*10^{-4}$	$8.87*10^{-4}$
	22	$3.17*10^{-4}$	$3.17*10^{-4}$	$3.17*10^{-4}$
	20	$3.17*10^{-4}$	$3.17*10^{-4}$	$3.17*10^{-4}$
	21	$2.54*10^{-4}$	$2.54*10^{-4}$	$2.54*10^{-4}$
Infilling Zone n, t (m)	23	5.5%, 0.003	5.5%, 0.003	5.5%, 0.003
	22	5.5%, 0.003	5.5%, 0.003	5.5%, 0.003
	20	5.5%, 0.003	5.5%, 0.003	5.5%, 0.003
	21	17%, 0.003	17%, 0.003	17%, 0.003
Altered Zone n, t (m)	23	0.5%, 0.02	0.5%, 0.02	0.5%, 0.02
	22	0.5%, 0.02	0.5%, 0.02	0.5%, 0.02
	20	0.5%, 0.01	0.5%, 0.01	0.5%, 0.01
	21	0.2%, 0.02	0.2%, 0.02	0.2%, 0.02
Unaltered Zone n, t (m)	23	0.01%, 10	0.01%, 10	0.01%, 10
	22	0.01%, 10	0.01%, 10	0.01%, 10
	20	0.01%, 10	0.01%, 10	0.01%, 10
	21	0.01%, 10	0.01%, 10	0.01%, 10
Dispersion Length (m)	All	5.9	5.9	2.9
FIZ Pipe Width (m)	FIZ Pipe	0.05	0.05	0.01
Mass lost to FIZ		0%	22.5%	23.3%

Test A4c	Structure	Simulation 5	Simulation 7	Simulation 8
Transport Aperture (m)	23	0.3*0.000165	0.3*0.000165	0.3*0.000165
	22	0.3*0.00122	0.3*0.00122	0.3*0.00122
	20	0.3*0.00196	0.3*0.00196	0.3*0.00196
	21	0.3*0.0018	0.3*0.0018	0.3*0.0018
Pipe Width (m)	23	0.19	0.19	0.19
	22	0.07	0.07	0.07
	20	0.05	0.05	0.05
	21	0.05	0.05	0.05
Velocity (m/s)	23	$8.87*10^{-4}$	$9.93*10^{-4}$	$9.93*10^{-4}$
	22	$3.17*10^{-4}$	$3.55*10^{-4}$	$3.55*10^{-4}$
	20	$3.17*10^{-4}$	$3.55*10^{-4}$	$3.55*10^{-4}$
	21	$2.54*10^{-4}$	$2.84*10^{-4}$	$2.84*10^{-4}$
Infilling Zone n, t (m)	23	5.5%, 0.003	5.5%, 0.003	5.5%, 0.003
	22	5.5%, 0.003	5.5%, 0.003	5.5%, 0.003
	20	5.5%, 0.003	5.5%, 0.003	5.5%, 0.003
	21	17%, 0.003	17%, 0.003	17%, 0.003
Altered Zone n, t (m)	23	0.5%, 0.02	0.5%, 0.02	0.5%, 0.02
	22	0.5%, 0.02	0.5%, 0.02	0.5%, 0.02
	20	0.5%, 0.01	0.5%, 0.01	0.5%, 0.01
	21	0.2%, 0.02	0.2%, 0.02	0.2%, 0.02
Unaltered Zone n, t (m)	23	0.01%, 10	0.01%, 10	0.01%, 10
	22	0.01%, 10	0.01%, 10	0.01%, 10
	20	0.01%, 10	0.01%, 10	0.01%, 10
	21	0.01%, 10	0.01%, 10	0.01%, 10
Dispersion Length (m)	All	5.9	5.9	2.9
FIZ Pipe Width (m)	FIZ Pipe	0.05	0.05	0.01
Mass lost to FIZ		0%	23.6%	94.8%

Table 4-13 Path II (Test C2, B2d, A4c) Simulated and Measured t5, t50, t95, and Percent Recovery.

Test C2	t_5 (hours)	t_{50} (hours)	t_{95} (hours)	Recovery %
Measured Data	92.8	255.2	Na	100%
Simulation 1	141	260	460	100%
Simulation 2	121	Na	Na	45%
Simulation 3	150	Na	Na	45%
Simulation 4	88	220	Na	85%
Simulation 5	95	260	900	100%

Test B2d	t_5 (hours)	t_{50} (hours)	t_{95} (hours)	Recovery %
Measured Data	80.7	280.0	Na	80%
Simulation 5	93	240	750	100%
Simulation 6	94	240	Na	80%
Simulation 7	88	260	Na	80%

Test A4c	t_5 (hours)	t_{50} (hours)	t_{95} (hours)	Recovery %
Measured Data	Na	Na	Na	Below background levels
Simulation 5	98	230	590	100%
Simulation 7	116	310	Na	80%
Simulation 8	680	Na	Na	10%

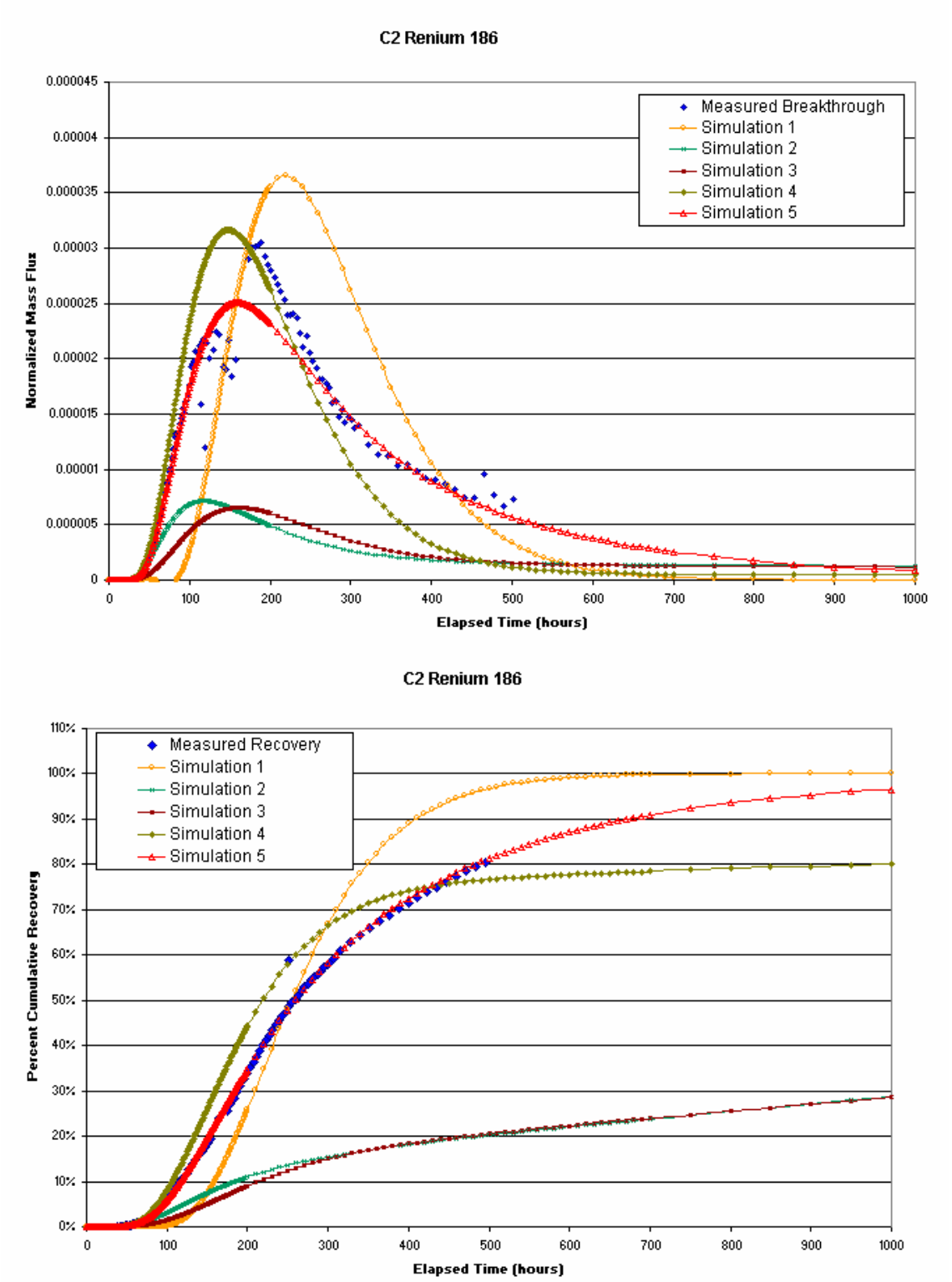

Figure 4-16 *Tracer Test C2 (Renium 186): Simulations and Measured Data.*

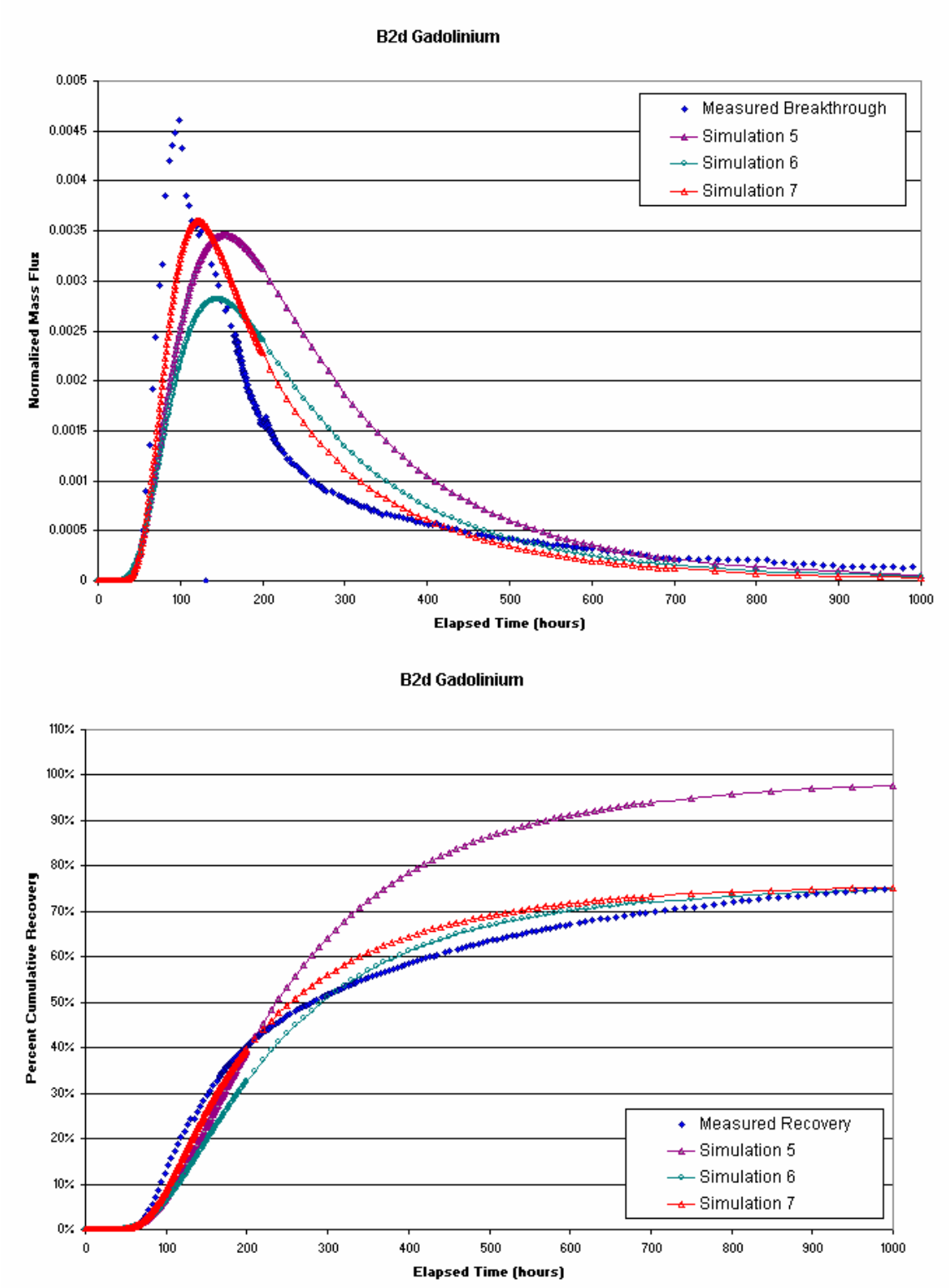

Figure 4-17 *Tracer Test B2d (Gadolinium): Simulations and Measured Data.*

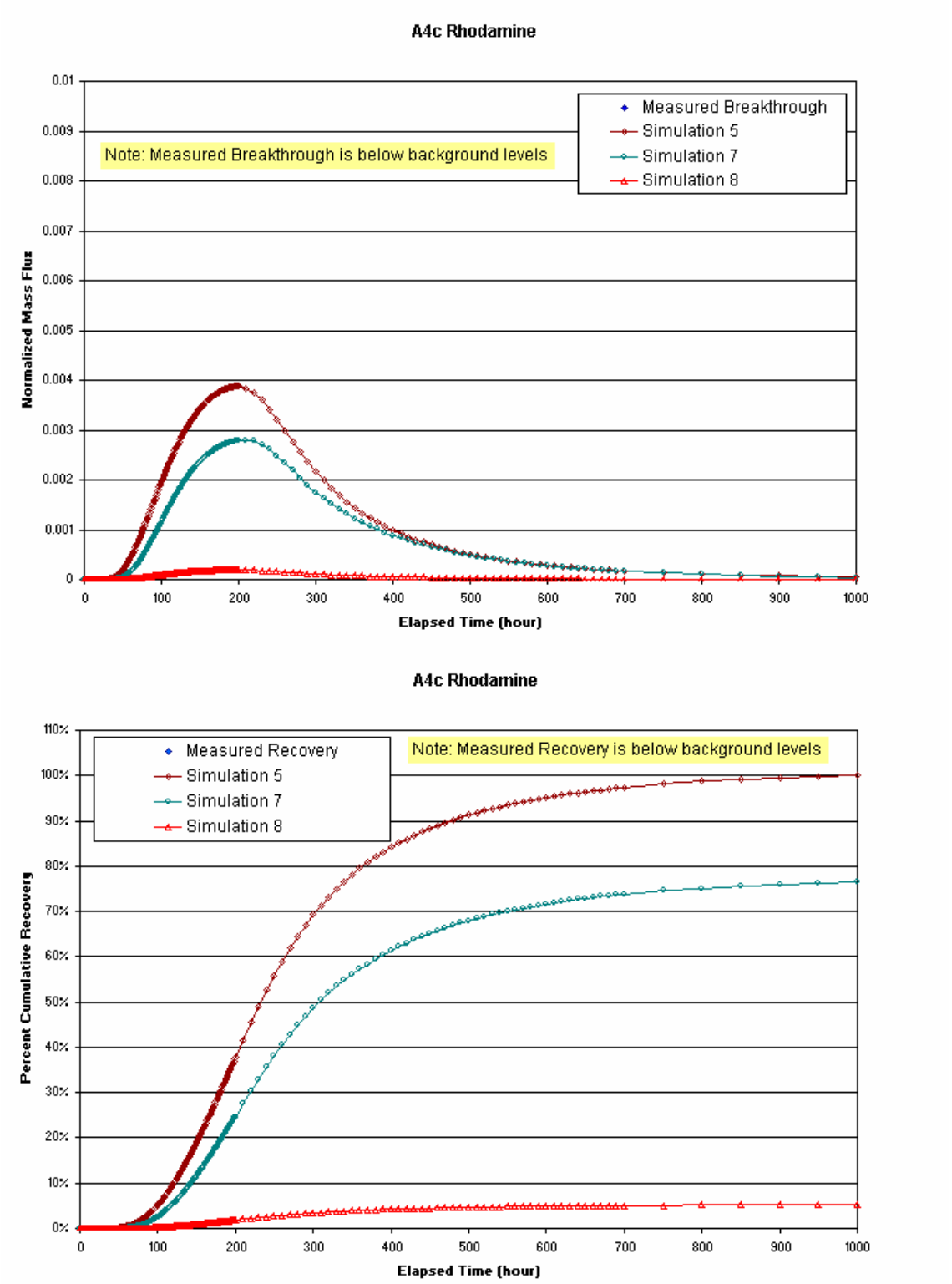

Figure 4-18 *Tracer Test A4c (Rhodamine): Simulations and Measured Data.*

4.2.7 Pathway VIII: Tracer Test B2c

Structures 19, 13, and 21 form the pathway for tracer test B2c from KI002563A:S1 to KI0023B:P6. The travel distance of 169.2m is among the longer distances tested, and had low recovery, projected to be around 10%. This low recovery may be due to FIZ pipes along the pathway. However, for this pathway, FIZ pipes were not simulated because the low measured recovery could be adequately explained simply in terms of the diffusive processes occurring along the pathway, together with the low advective velocity. Simulation 2 immobile zone parameters are equal to those used in previous simulations for tracer traveling along structure 21. The best-fit simulation for this test slightly modifies those parameters (Simulation 3).

Table 4-14 provides the transport parameters studied for tracer test B2c. Table 4-15 contains t_5, t_{50}, t_{95}, and percent recovery for the simulations. Figure 4-19 illustrates the simulations of Test B2c.

Table 4-14 Pathway VIII (Test B2c) Tracer Test Transport Parameters. Immobile Zone parameters reported as porosity, n, and thickness, t (m).

Test B2c	Structure	Simulation 1	Simulation 2	Simulation 3
Transport Aperture (m)	19	0.3*0.00268	0.3*0.00268	0.3*0.00268
	13	0.3*0.00082	0.3*0.00082	0.3*0.00082
	21	0.3*0.0018	0.3*0.0018	0.3*0.0018
Pipe Width (m)	19	0.07	0.07	0.07
	13	0.22	0.22	0.22
	21	0.1	0.1	0.1
Velocity (m/s)	All	$6.34*10^{-5}$	$6.65*10^{-5}$	$6.65*10^{-5}$
Infilling Zone n, t (m)	19	0%, 0	17%, 0.003	17%, 0.003
	13	0%, 0	17%, 0.003	17%, 0.003
	21	0%, 0	17%, 0.003	17%, 0.003
Altered Zone n, t (m)	19	0%, 0	0.2%, 0.02	0.5, 0.02
	13	0%, 0	0.2%, 0.02	0.2%, 0.02
	21	0%, 0	0.2%, 0.02	0.2%, 0.02
Unaltered Zone n, t (m)	19	0%, 0	0.08%, 10	0.1%, 10
	13	0%, 0	0.08%, 10	0.1%, 10
	21	0%, 0	0.08%, 10	0.1%, 10
Dispersion Length (m)	All	13.5	13.5	13.5

Table 4-15 Pathway VIII (Test B2c) Simulated and Measured t5, t50, t95, and Percent Recovery.

Test B2c	t_5 (hours)	t_{50} (hours)	t_{95} (hours)	Recovery %
Measured Data	Na	Na	Na	10%
Simulation 1	500	900	Na	100%
Simulation 2	Na	Na	Na	10%
Simulation 3	Na	Na	Na	10%

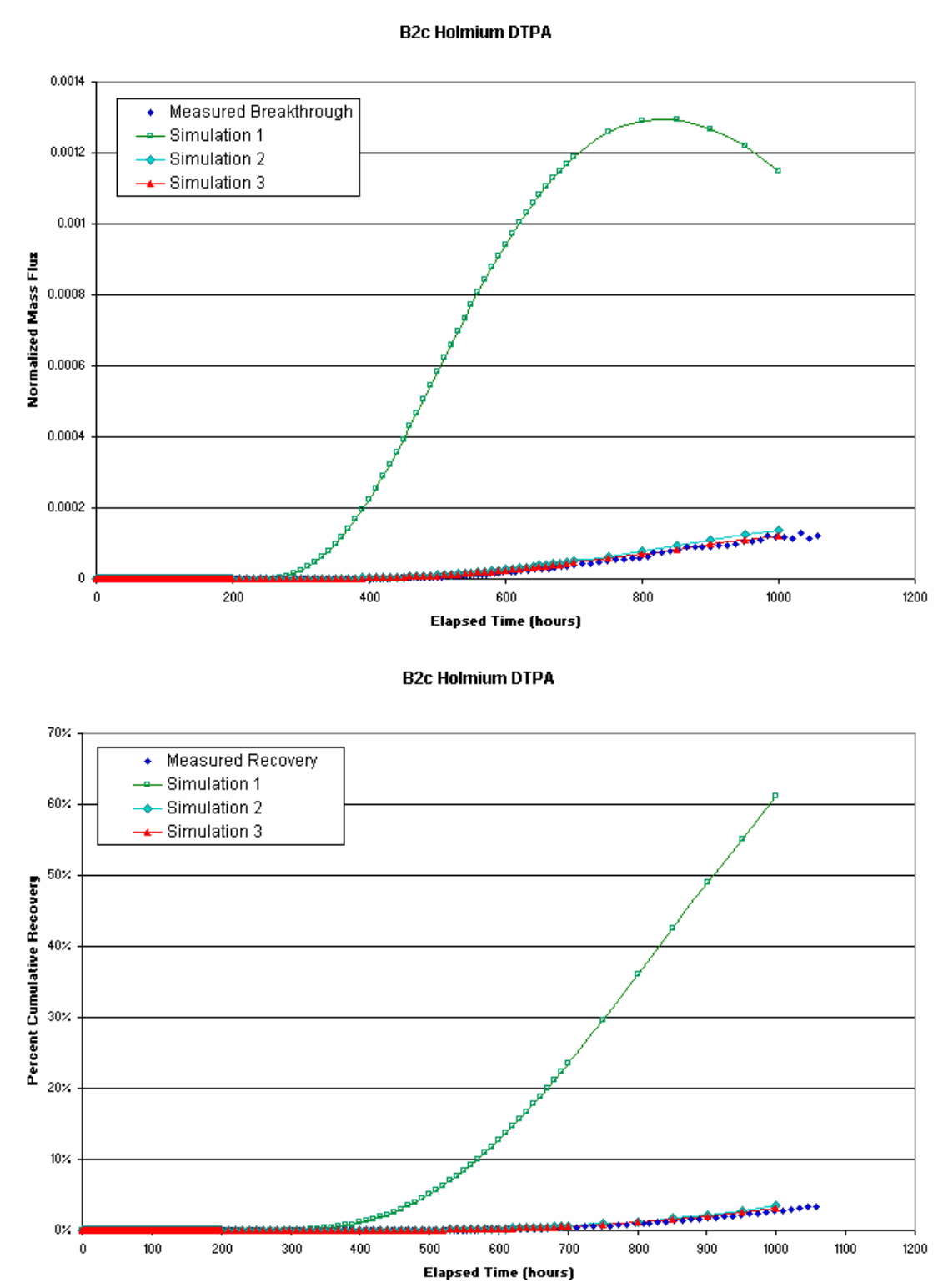

Figure 4-19 *Tracer Test B2c (Holmium DTPA): Simulations and Measured Data.*

4.2.8 Tracer Tests Pathways with sink location KI0025F03:P5: Tracer Tests A5a, A5b, A5c, A5d, and A5e

The final set of tracer tests studied in this evaluation are tracer tests that have the sink location KI0025F03:P5. These tests include all tracers injected in Test A5. Tracer test A5a, traveling from KI002563A:S4 along Structures 21 and 20, was best simulated by Simulation 4. The low recovery of the measured data was best matched with a path along the 20/21 FIZ. Measured data for Test A5b is below background levels. Test A5b source location is at KI0025F02:P3 and with transport from Structure 21 to 20. Two simulation were carried out for this test with the second having Structure 20 and 21 immobile zone parameters as found in previous simulations. Test B2c, with transport from KI0025F02:P5 to KI0025F03:P5 along structure 20, was best fit through Simulation 2. Tracer test A5d goes from KI0025F02:P6 on Structure 22 to the sink location on Structure 20. Although 22/20 FIZ has not been previously studied in this evaluation, the low recovery of the tracer could not be matched with reasonable parameters without having an alternate sink location. Test A5d goes along the 20/22 FIZ to establish an alternate sink for the loss of mass. Test A5e also goes from Structure 22 to 20. The source location for A5e is KI0025F03:P6. The test is best match through Simulation 4 and does not include the 20/22 FIZ.

Table 4-16 provides the transport parameters studied for Test A5 tracer tests. Table 4-17 contains t_5, t_{50}, t_{95}, and percent recovery for the simulations. Figure 4-20 through Figure 4-24 illustrate the simulations of Test A5.

Table 4-16 Sink Location KI0025F03:P5 Path (Test A5a, A5b, A5c, A5d, A5e) Transport Parameters. Immobile Zone parameters reported as porosity, n, and thickness, t (m).

Test A5a	Simulation 1	Simulation 2	Simulation 3	Simulation 4
Transport Aperture (m)	0.3*0.00196	0.3*0.00196	0.3*0.00196	0.3*0.00196
Pipe Width (m)	0.1	0.1	0.1	0.1
Velocity (m/s)	$1.01*10^{-4}$	$5.39*10^{-4}$	$5.39*10^{-4}$	$8.87*10^{-4}$
Infilling Zone n, t (m)	0%, 0	5.5%, 0.003	20%, 0.003	5.5%, 0.003
Altered Zone n, t (m)	0%, 0	2%, 0.02	2%, 0.02	2%, 0.02
Unaltered Zone n, t (m)	0%, 0	0.01%, 10	0.1%, 10	0.01%, 10
Dispersion Length (m)	2.4	2.4	2.4	2.3
FIZ Pipe Width (m)	Na	Na	Na	0.1
Mass lost to FIZ	Na	Na	Na	36.3%

Table 4-16 (continued) Sink Location KI0025F03:P5 Path (Test A5a, A5b, A5c, A5d, A5e) Transport Parameters. Immobile Zone parameters reported as porosity, n, and thickness, t (m).

Test A5b	Structure	Simulation 1	Simulation 2
Transport Aperture (m)	21 20	0.3*0.0018 0.3*0.00196	0.3*0.0018 0.3*0.00196
Pipe Width (m)	21 20	0.11 0.1	0.11 0.1
Velocity (m/s)	All	$1.55*10^{-5}$	$1.55*10^{-5}$
Infilling Zone n, t (m)	21 20	0%, 0	17%, 0.003 5.5%, 0.003
Altered Zone n, t (m)	21 20	0%, 0	0.2%, 0.02 2%, 0.02
Unaltered Zone n, t (m)	21 20	0%, 0	0.08%, 10 0.01%, 10
Dispersion Length (m)	All	4.5	4.5

Test A5c	Simulation 1	Simulation 2
Transport Aperture (m)	0.3*0.00196	0.3*0.00196
Pipe Width (m)	0.1	0.1
Velocity (m/s)	$4.62*10^{-4}$	$1.27*10^{-3}$
Infilling Zone n, t (m)	0%, 0	5.5%, 0.003
Altered Zone n, t (m)	0%, 0	2%, 0.02
Unaltered Zone n, t (m)	0%, 0	0.01%, 10
Dispersion Length (m)	1	1

Test A5d	Structure	Simulation 1	Simulation 2	Simulation 3	Simulation 4
Transport Aperture (m)	22 20	0.3*0.00122 0.3*0.00196	0.3*0.00122 0.3*0.00196	0.3*0.00122 0.3*0.00196	0.3*0.00122 0.3*0.00196
Pipe Width (m)	22 20	0.13 0.08	0.13 0.08	0.13 0.08	0.13 0.08
Velocity (m/s)	All	$3.82*10^{-4}$	$4.75*10^{-4}$	$4.75*10^{-4}$	$1.27*10^{-4}$
Infilling Zone n, t (m)	22 20	0%, 0	10%, 0.003 5.5%, 0.003	40%, 0.003 40%, 0.003	10%, 0.003 5.5%, 0.003
Altered Zone n, t (m)	22 20	0%, 0	2%, 0.02 2%, 0.02	2%, 0.02 2%, 0.02	2%, 0.02 2%, 0.02
Unaltered Zone n, t (m)	22 20	0%, 0	0.1%, 10 0.01%, 10	0.1%, 10 0.1%, 10	0.1%, 10 0.01%, 10
Dispersion Length (m)	All	2.8	2.8	2.8	4.1
FIZ Pipe Width (m)	FIZ Pipe	Na	Na	Na	0.09
Mass lost to FIZ		Na	Na	Na	46.9%

Test A5e	Structure	Simulation 1	Simulation 2	Simulation 3	Simulation 4
Transport Aperture (m)	22 20	0.3*0.00122 0.3*0.00196	0.3*0.00122 0.3*0.00196	0.3*0.00122 0.3*0.00196	0.3*0.00122 0.3*0.00196
Pipe Width (m)	22 20	0.13 0.08	0.13 0.08	0.13 0.08	0.13 0.08
Velocity (m/s)	All	$6.31*10^{-5}$	$7.92*10^{-5}$	$7.92*10^{-5}$	$7.92*10^{-5}$
Infilling Zone n, t (m)	22 20	0%, 0	10%, 0.003 5.5%, 0.003	3%, 0.003 3%, 0.003	5%, 0.003 5%, 0.003
Altered Zone n, t (m)	22 20	0%, 0	2%, 0.02 2%, 0.02	0.5%, 0.02 0.5%, 0.02	0.5%, 0.02 0.5%, 0.02
Unaltered Zone n, t (m)	22 20	0%, 0	0.1%, 10 0.01%, 10	0.01%, 10 0.01%, 10	0.01%, 10 0.01%, 10
Dispersion Length (m)	All	2.8	2.8	2.8	2.8

Table 4-17 Sink Location KI0025F03:P5 Path (Test A5a, A5b, A5c, A5d, A5e) Simulated and Measured t5, t50, t95, and Percent Recovery.

Test A5a	t_5 (hours)	t_{50} (hours)	t_{95} (hours)	Recovery %
Measured Data	19.6	81.8	Na	72%
Simulation 1	50	88	160	100%
Simulation 2	16	42	310	100%
Simulation 3	20	60	Na	100%
Simulation 4	16	63	Na	65%

Test A5b	t_5 (hours)	t_{50} (hours)	t_{95} (hours)	Recovery %
Measured Data	Na	Na	Na	Below background levels
Simulation 1	520	900	Na	100%
Simulation 2	Na	Na	Na	10%

Test A5c	t_5 (hours)	t_{50} (hours)	t_{95} (hours)	Recovery %
Measured Data	1.9	7.8	17.0	>100%
Simulation 1	8	19	55	100%
Simulation 2	4	15	59	100%

Test A5d	T5 (hours)	T50 (hours)	T95 (hours)	Recovery %
Measured Data	25.0	Na	Na	60%
Simulation 1	124	220	400	100%
Simulation 2	22	62	Na	100%
Simulation 3	41	142	Na	95%
Simulation 4	27	500	Na	55%

Test A5e	T5 (hours)	T50 (hours)	T95 (hours)	Recovery %
Measured Data	86.0	153.6	469.6	100%
Simulation 1	85	148	270	100%
Simulation 2	92	210	Na	100%
Simulation 3	128	750	Na	80%
Simulation 4	81	158	670	100%

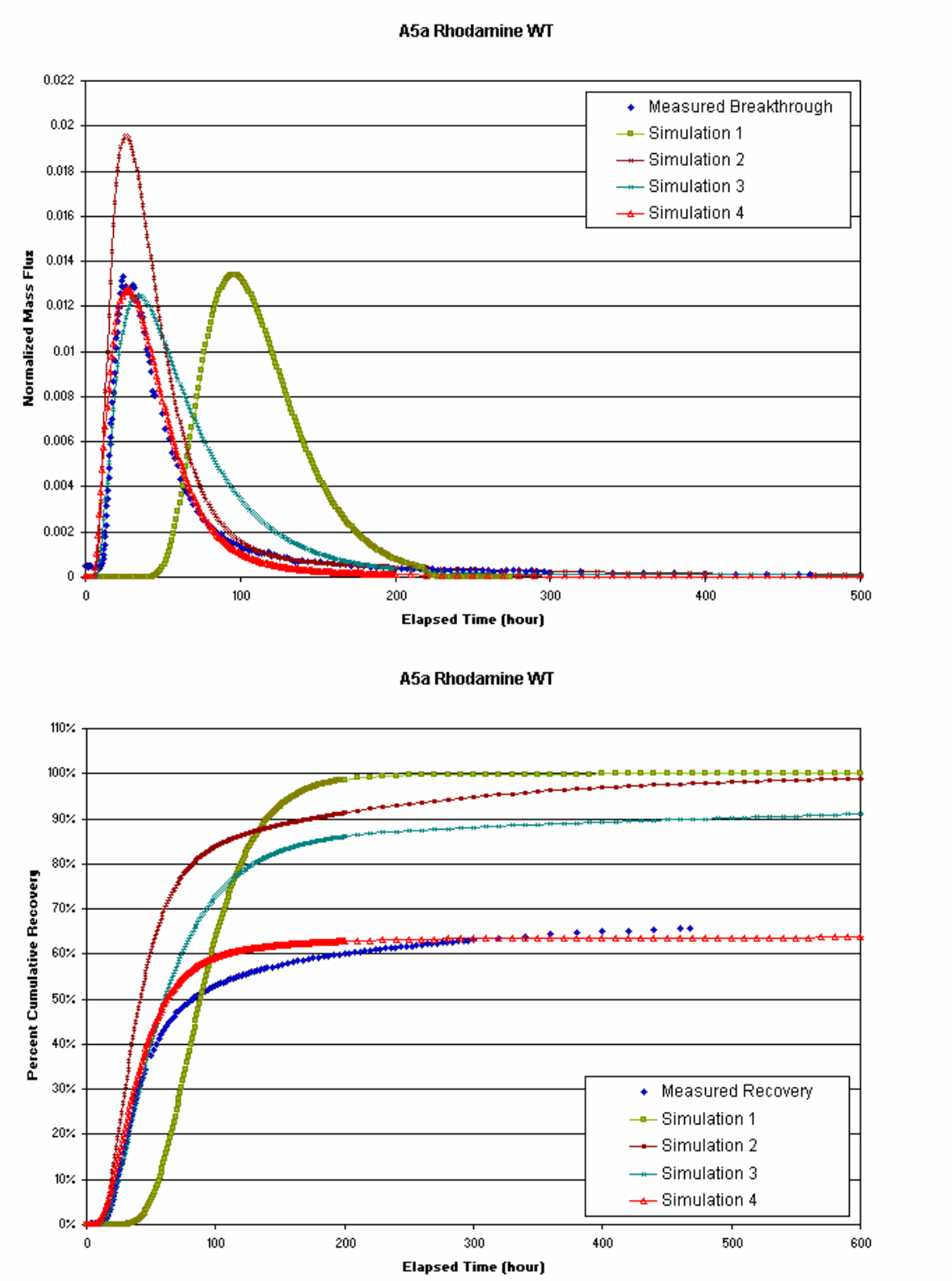

Figure 4-20 *Tracer Test A5a (Rhodamine WT): Simulations and Measured Data.*

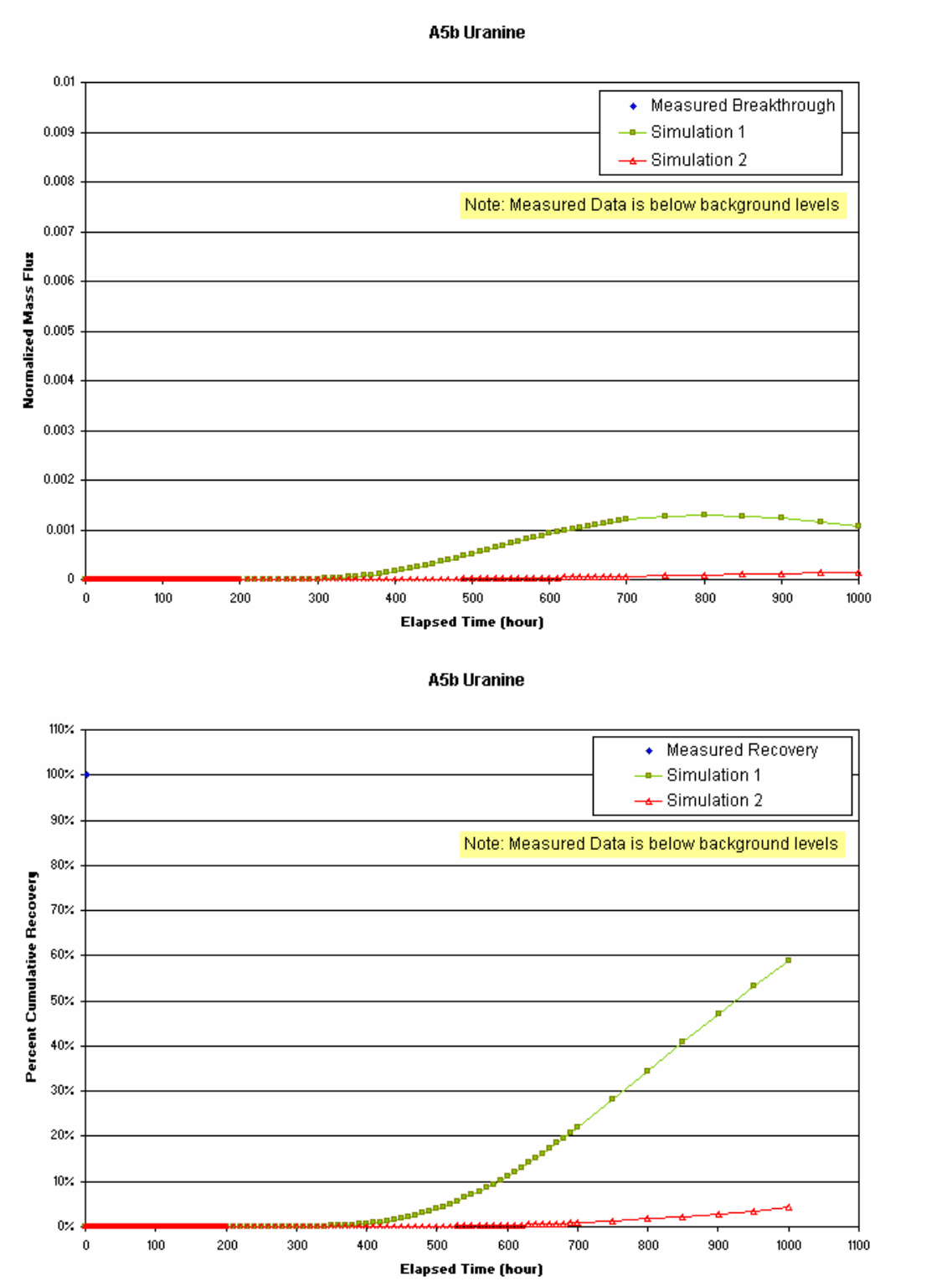

Figure 4-21 *Tracer Test A5b (Uranine): Simulations and Measured Data.*

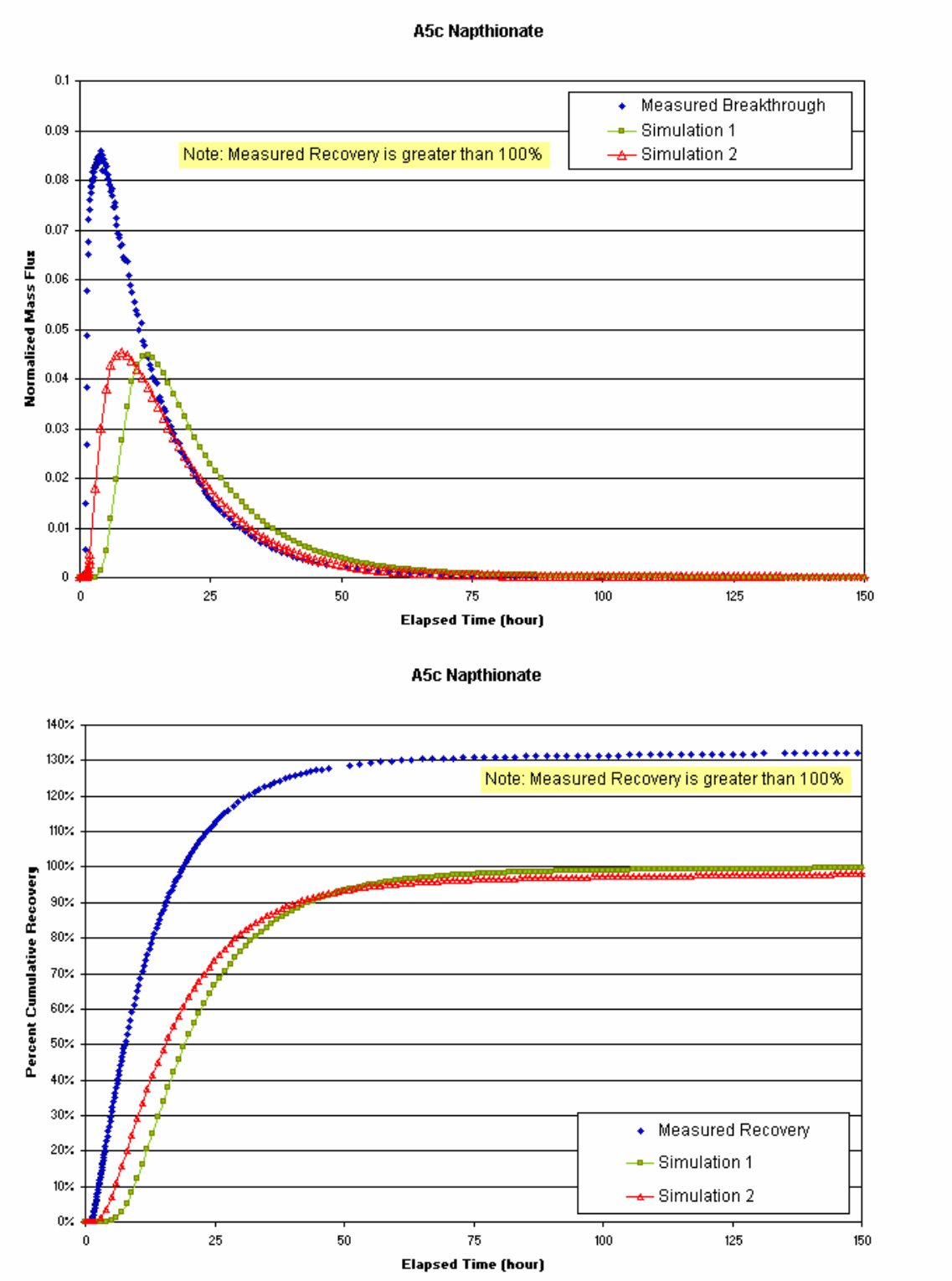

Figure 4-22 *Tracer Test A5c (Napthionate): Simulations and Measured Data.*

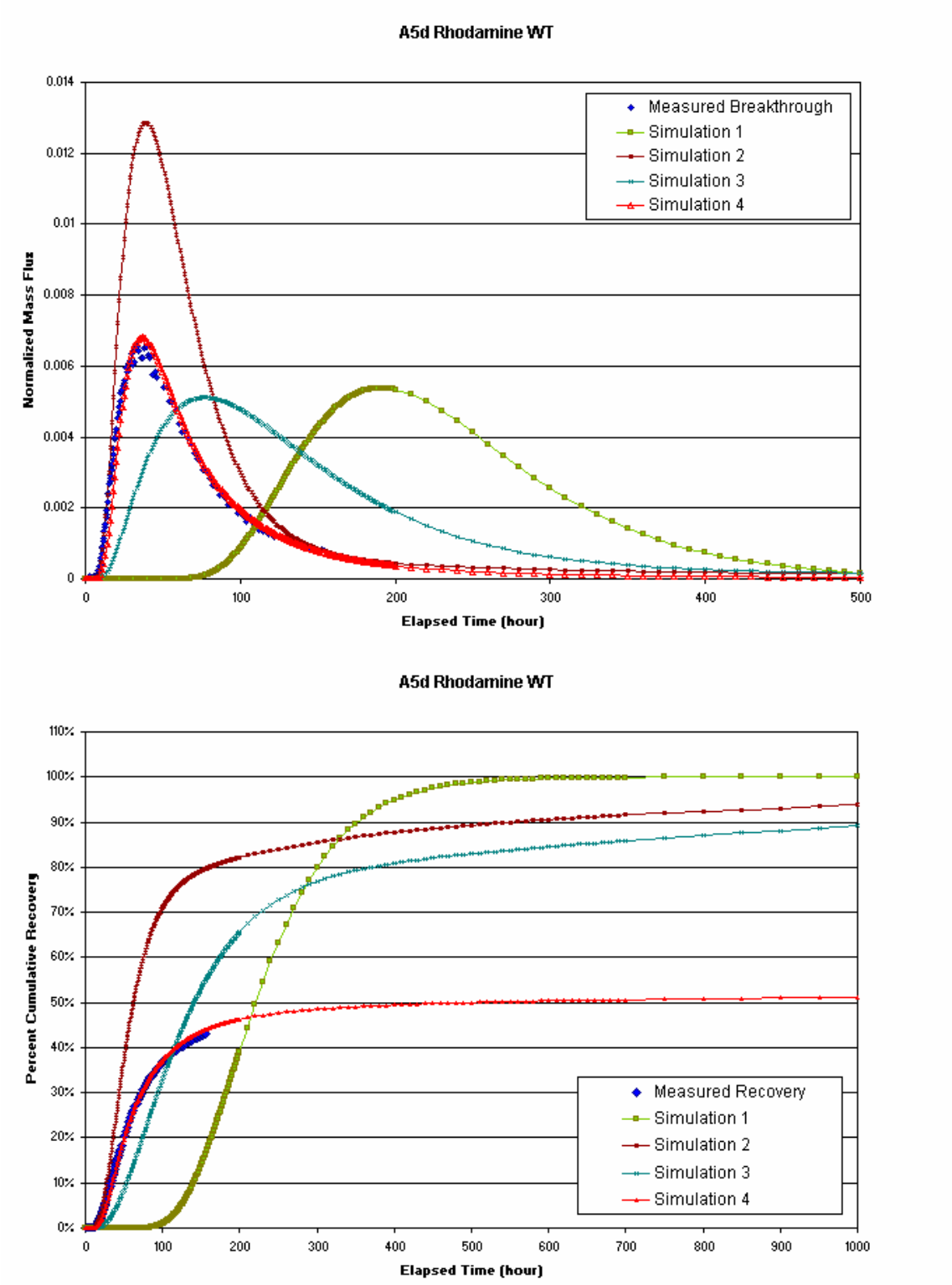

Figure 4-23 *Tracer Test A5d (Rhodamine WT): Simulations and Measured Data.*

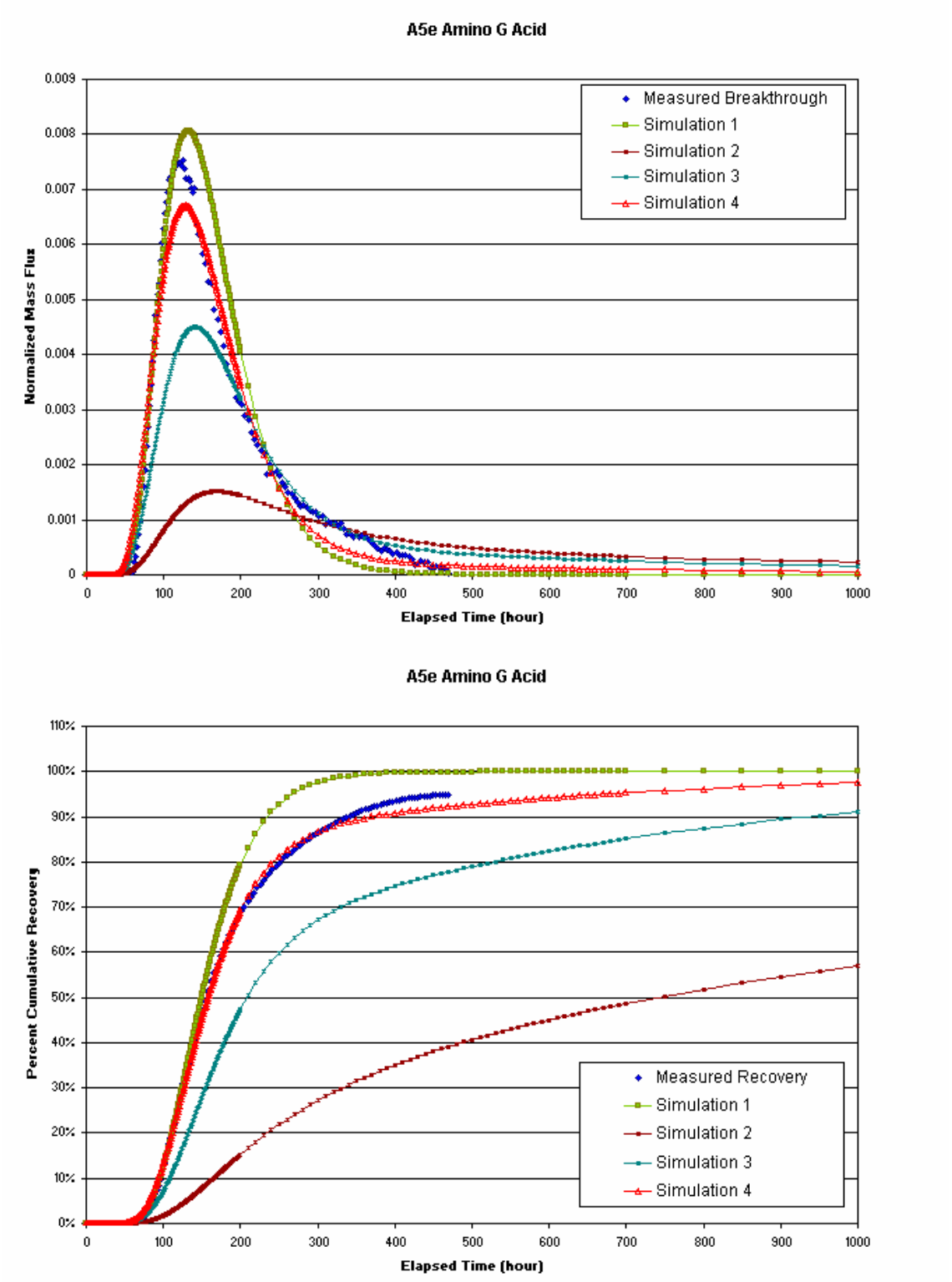

Figure 4-24 *Tracer Test A5e (Amino G): Simulations and Measured Data.*

4.3 Pathway Sorption Properties

Simple pathway effective sorption properties were derived by simulating transport of the Phase C tracer tests. Three simulations were carried out for each test: K_d value of zero, Byegård laboratory K_d values, and finally a sensitivity study to determine the effective value of K_d. The pathway parameters of conservative tests along the same pathway, as identified in Section 4.2, were used in the simulations of the Phase C sorbing tracer tests. This procedure was previously used by Dershowitz et al. (2000) to derive effective K_d values for "Feature A" at the 'TRUE-1" rock block.

4.3.1 Sorbing Tracer Test C1

Table 4-18 lists the sorption parameters simulated for the simple pipe channel pathway for the simple pipe pathway model of Pathway I (KI0025F03:P5 to KI0023B:P6) for sorbing tracer test C1. The tracer simulations are presented in Figure 4-25 through Figure 4-29. Simulation 1 is run with K_d=0, Simulation 2 with Byegård K_d values, and Simulation 3 with enhanced sorption. The conservative transport parameters for this simulation are those shown for Simulation 5 of Table 4-2.

Table 4-18 K_d values for Test C1 Sorbing Tracers.

Tracer	Byegård K_d (kg/m^3) (Simulation 2)	Calibration K_d (kg/m^3) (Simulation 3)	K_d Multiplier for Simulation
Na-24	$1.40*10^{-6}$	$2.38*10^{-5}$	17
K-42*	$2.00*10^{-4}$	$4.40*10^{-4}$	2.2
Ca-47	$5.20*10^{-6}$	$1.56*10^{-4}$	30
Rb-86	$4.00*10^{-4}$	$2.40*10^{-3}$	6
Cs-134	$8.00*10^{-4}$	$2.80*10^{-2}$	35

*K-42 K_d value referenced to CRC. Laboratory value was not reported in Byegård et al., 1998.

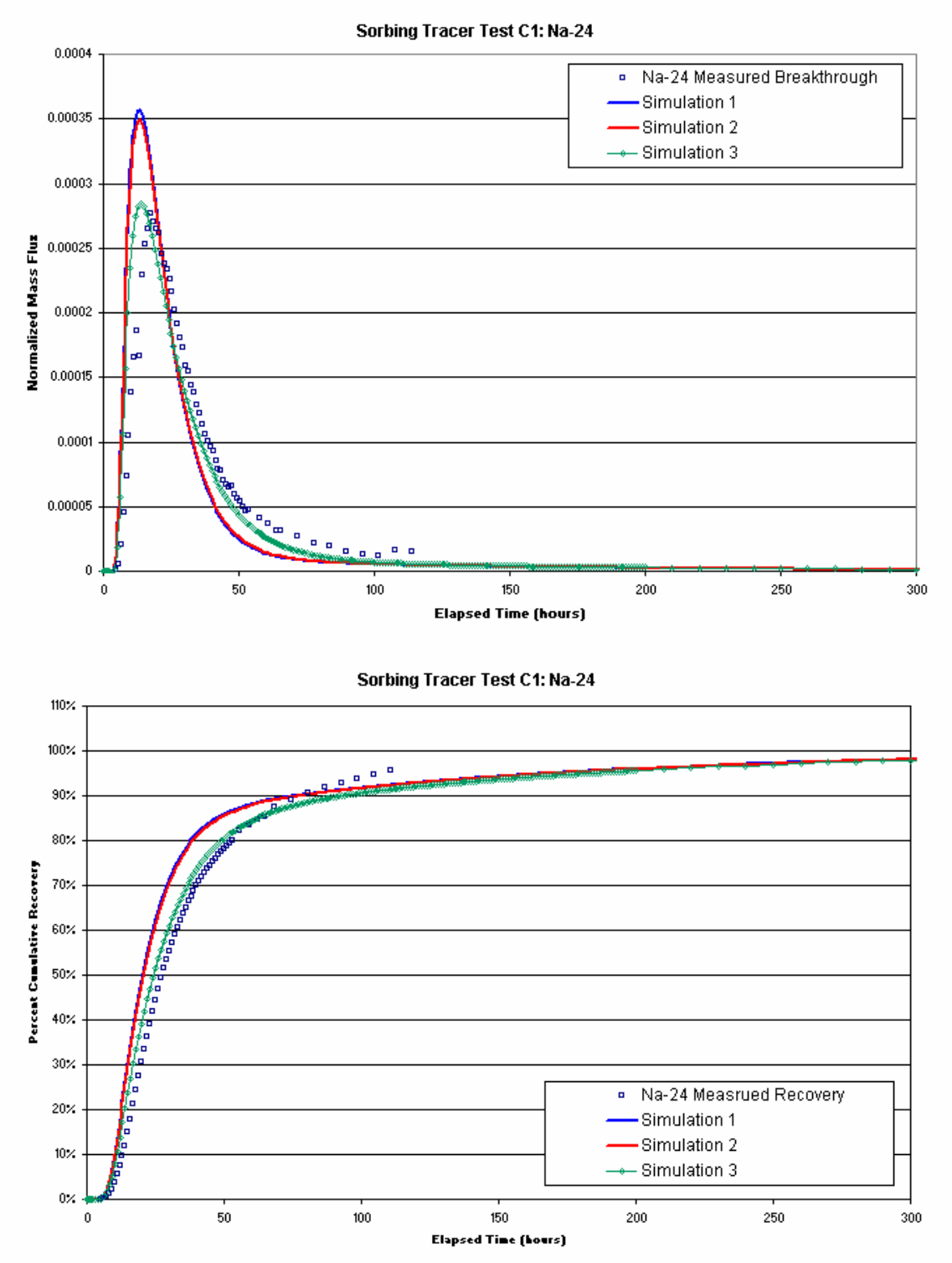

Figure 4-25 *Tracer Test C1 (Na-24): Simulations and Measured Data.*

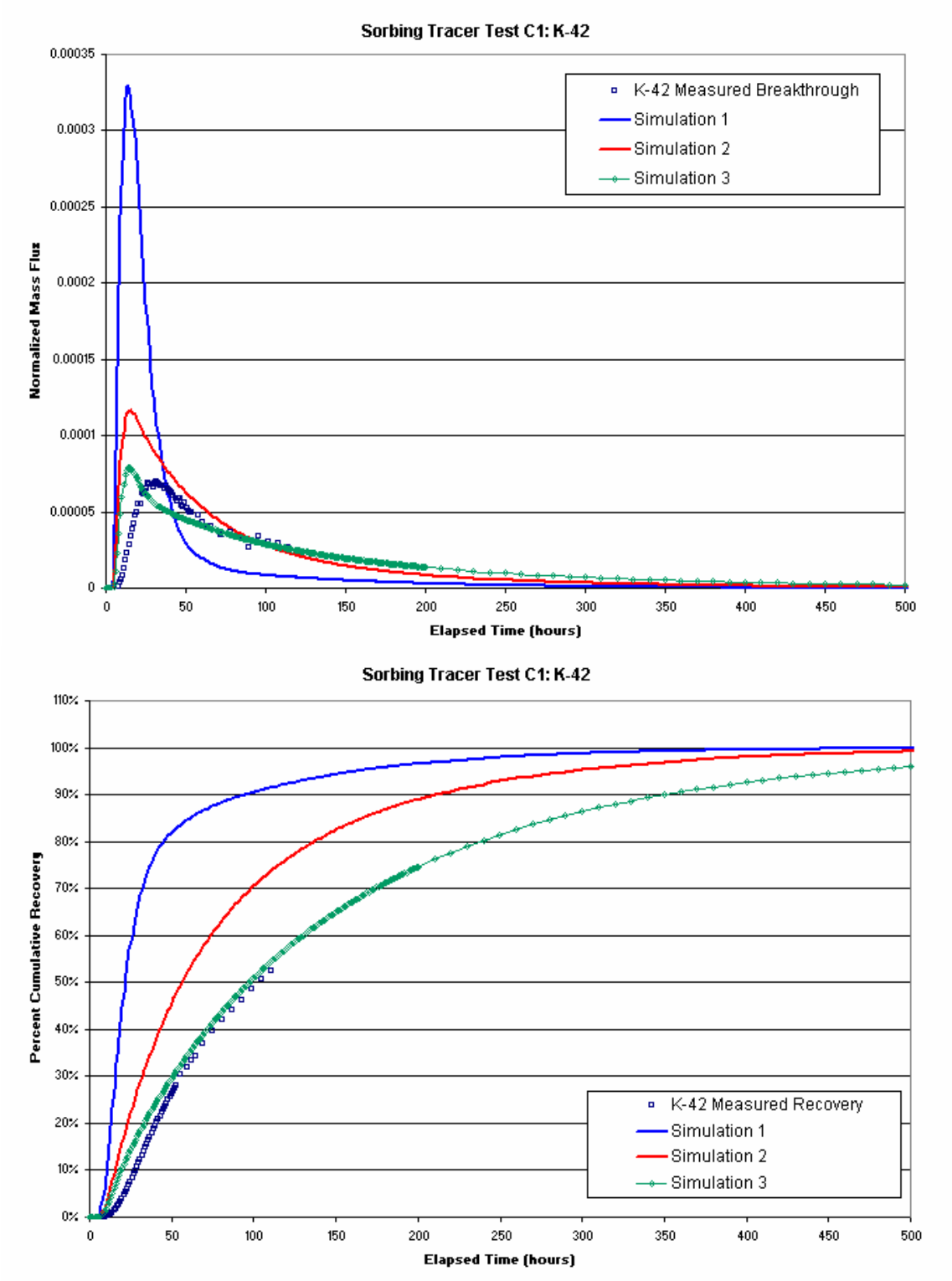

Figure 4-26 *Tracer Test C1 (K-42): Simulations and Measured Data.*

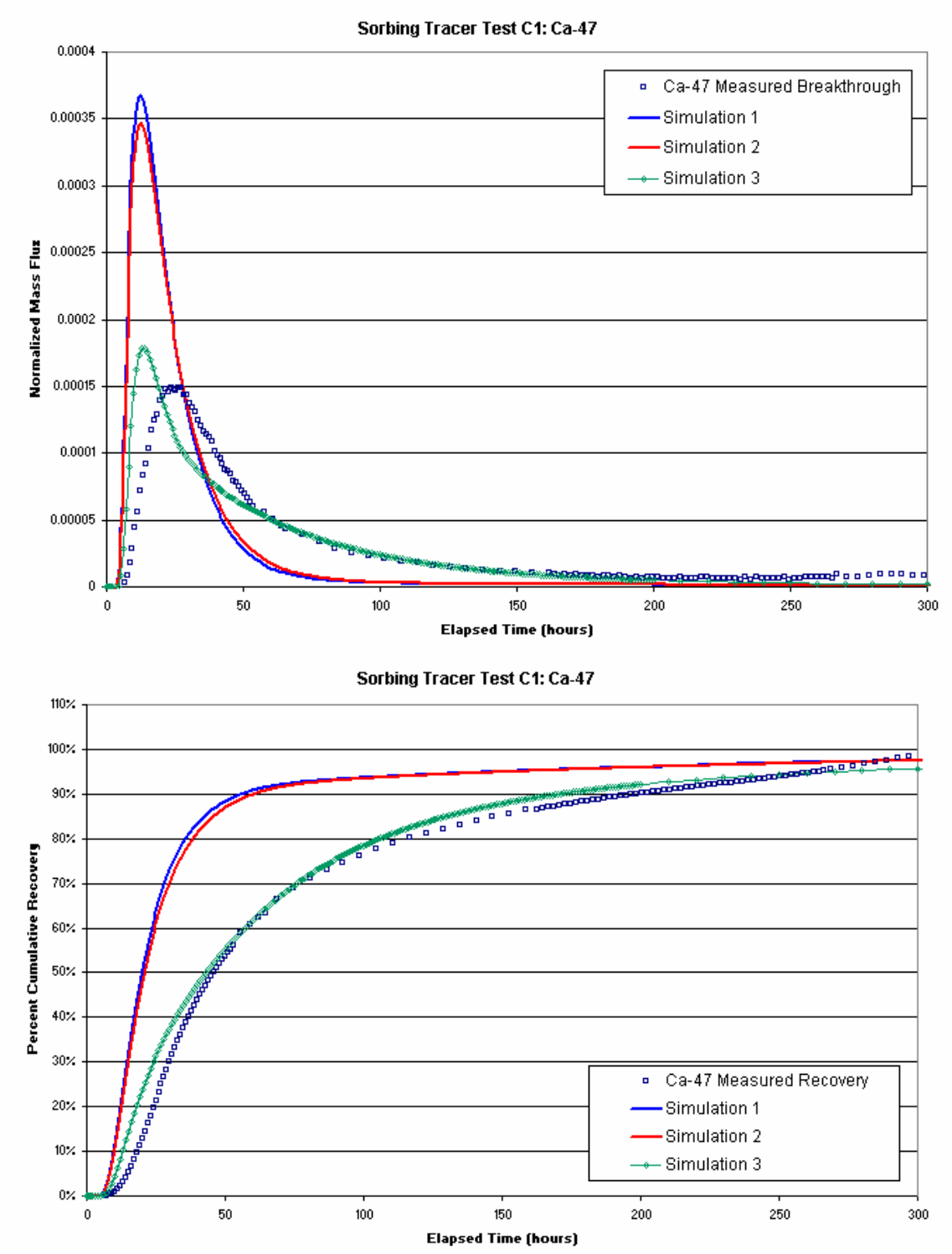

Figure 4-27 *Tracer Test C1 (Ca-47): Simulations and Measured Data. Tracer.*

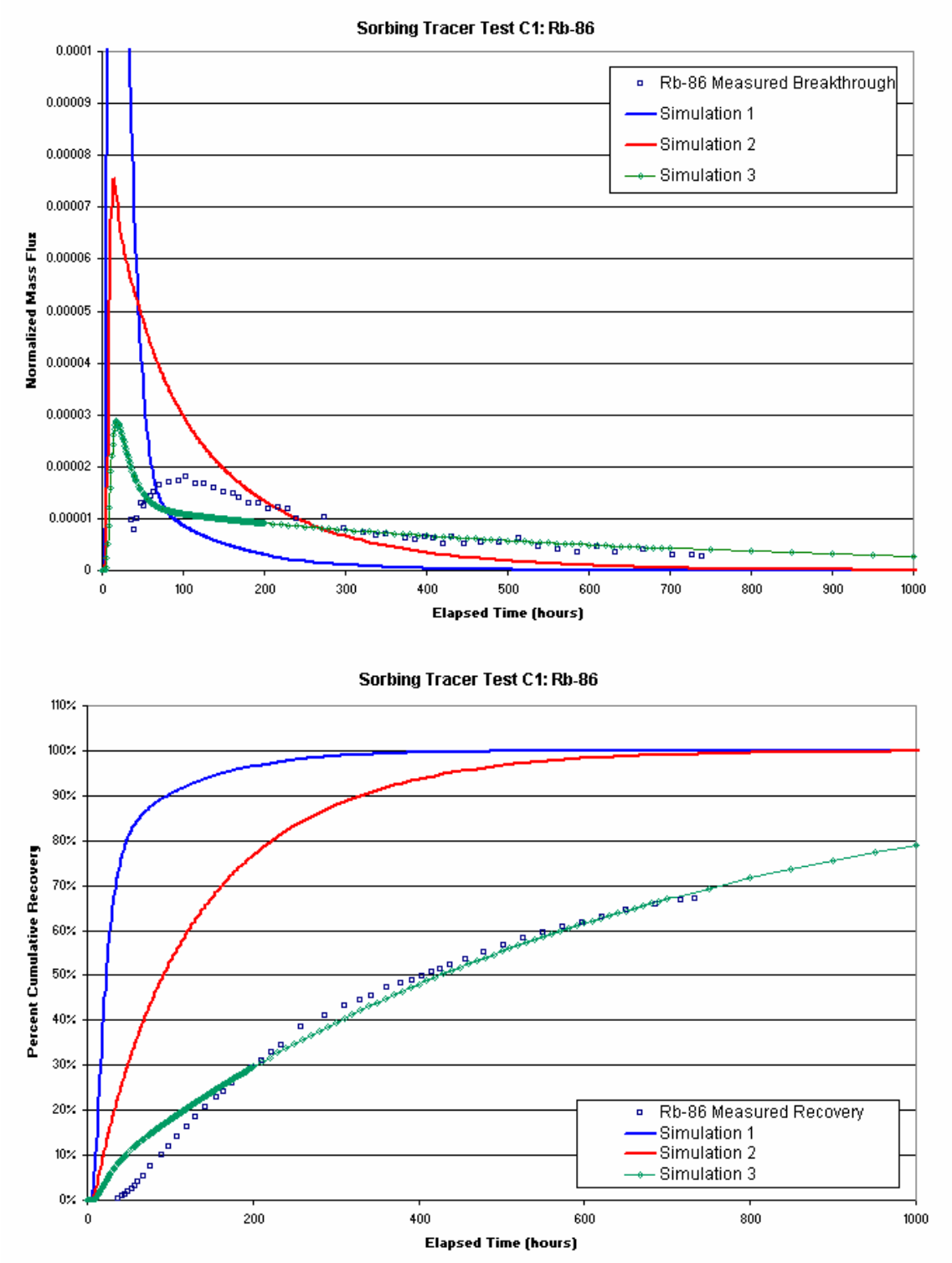

Figure 4-28 *Tracer Test C1 (Rb-86): Simulations and Measured Data.*

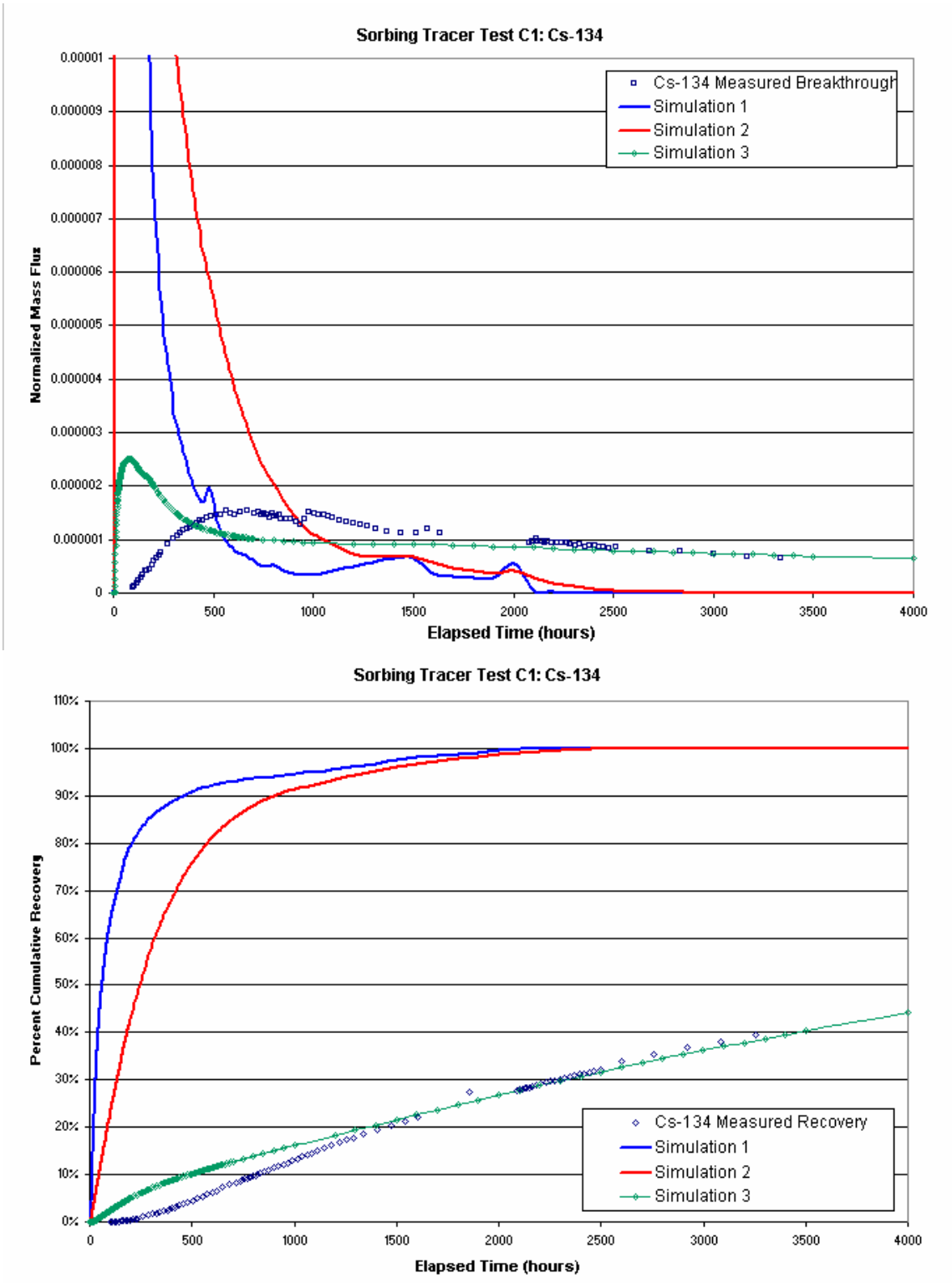

Figure 4-29 *Tracer Test C1 (Cs-134): Simulations and Measured Data.*

4.3.2 Sorbing Tracer Test C2

The following sorbing tracer study, injected as part of Test C2, travel along Pathway II (KI0025F03:P7 to KI0023B:P6). Pathway II conservative tracers have enigmatic results. The projected ultimate recovery for conservative tracer test B2d is only 80%, while test A5c was not recovered at measurable levels. Therefore the model for B2d and A4c includes a F1Z pathway. However, the later C2 tracer test recovered 100% of the conservative tracer, inconsistent with the results for B2d and A4c. Nevertheless, the F1Z model for C2 provided a good match, as only <1% of the tracer mass was lost to the F1Z pipe.

The tracer simulations carried out for sorbing tracer test C2 are presented in Figure 4-30 through Figure 4-32. Simulation 1 is run with K_d=0, Simulation 2 with Byegård K_d values, and Simulations 3 and 4 with enhanced sorption. The conservative transport parameters for this simulation are those shown for Simulation 5 in Table 4-12. Table 4-19 provides the K_d values studied in the simulations for tracer test C2.

Of the three sorbing tracers, Ca-47 was the only tracer which showed recovery during the monitoring period. Simulations of Ca-47 were run with K_d value of 0, Byegård K_d, a K_d value that best matched the mass flux, and the Ca-47 K_d value found during the sensitivity study in Test C1 (Simulation 4). The Ca-47 breakthrough had an initial delay, which could not be explained by any of the advection-diffusion-dispersion processes modeled. Ba-133 has a recovery of 42.4% when run with the Byegård K_d value and would require a K_d value 6 times the lab value to obtain a recovery of less than 2% after a 1000-hour simulation. Cs-137 has a recovery of 3.6% after 1000 hours and would need a K_d value 1.3 times the lab value to have less than 2% recovery after 1000 hours. Test C2 conservative and sorbing tracers result in unclear conclusions regarding the effective sorption.

Table 4-19 K_d values for Test C2 Sorbing Tracers.

Tracer	Byegård K_d (kg/m^3) (Simulation 2)	Calibration K_d (kg/m^3) (Simulation 3)	K_d Multiplier for Simulation
Ca-47	$5.2*10^{-6}$	$6.24*10^{-5}$	12
Ba-131	$2.0*10^{-4}$	$1.2*10^{-3}$	6
Cs-137	$8.0*10^{-4}$	$1.04*10^{-3}$	1.3

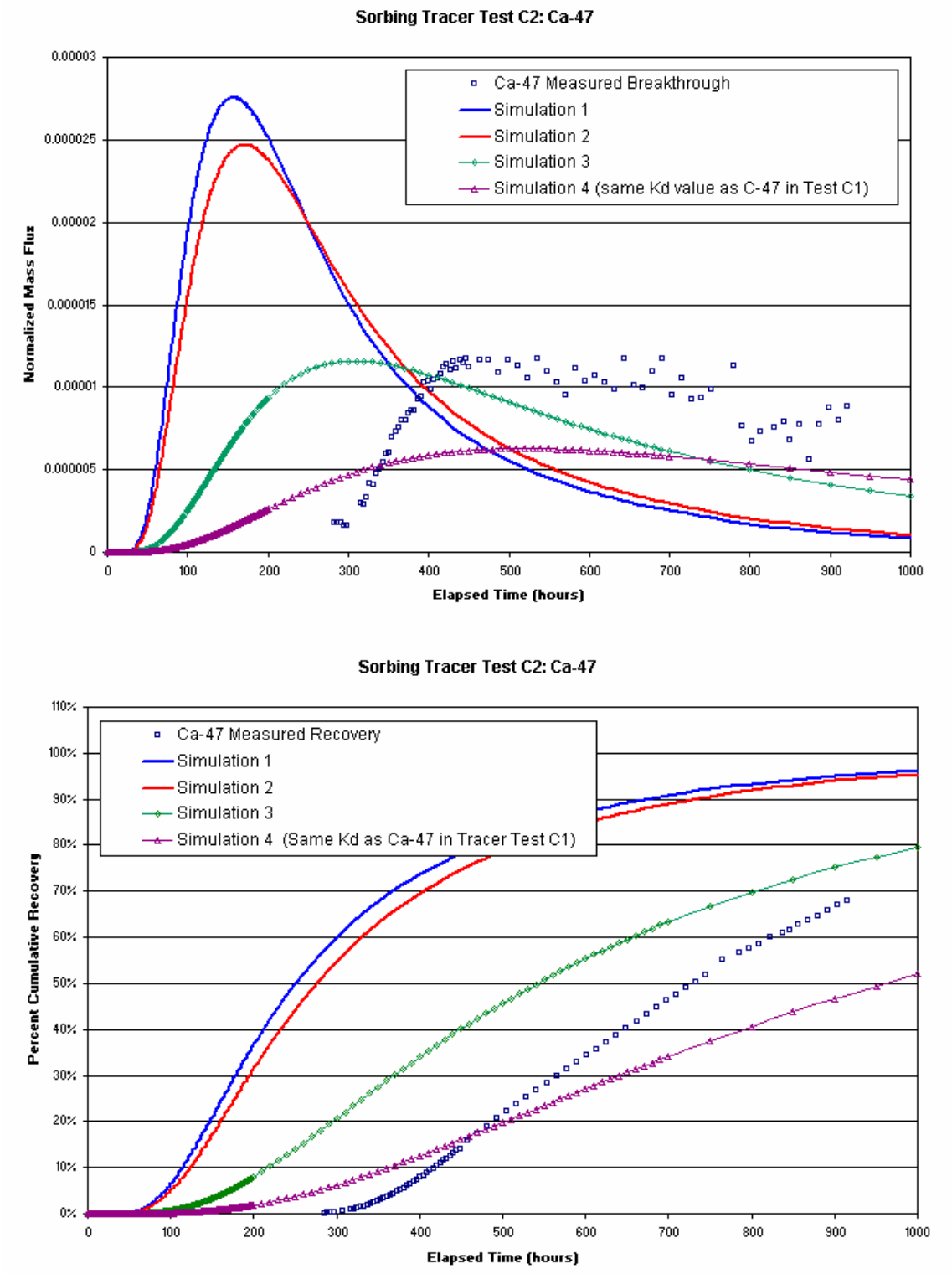

Figure 4-30 *Tracer Test C2 (Ca-47): Simulations and Measured Data.*

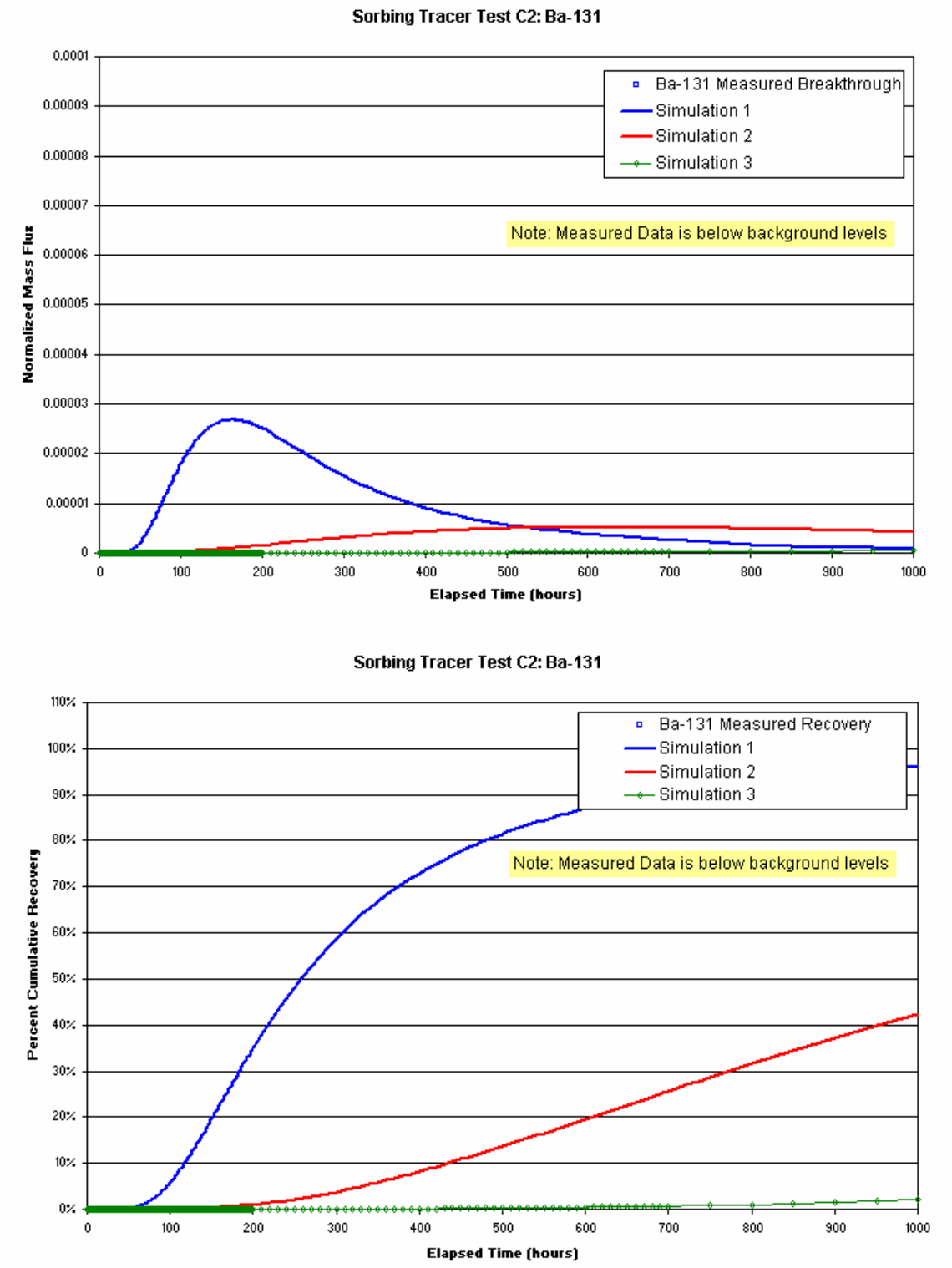

Figure 4-31 *Tracer Test C2 (Ba-131): Simulations and Measured Data Measured Data is below background levels.*

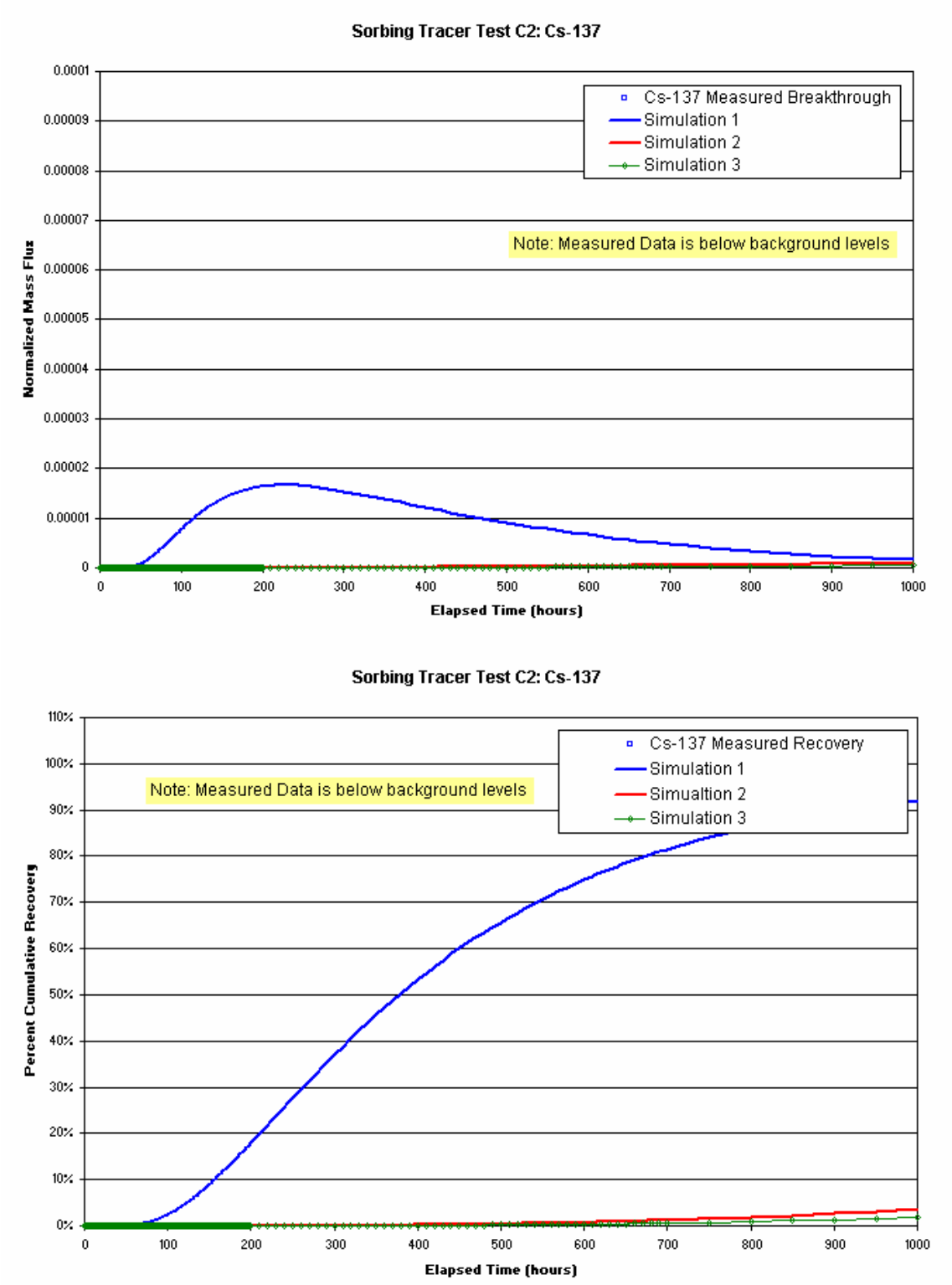

Figure 4-32 *Tracer Test C2 (Cs-137): Simulations and Measured Data. Measured Data is below background levels.*

4.3.3 Sorbing Tracer Test C3

Table 4-20 lists the sorption parameters for tracers used in Test C3 for the pipe model of Pathway III (KI0025F02:P3 to KI0023B:P6). The conservative tracer transport parameters used for these simulations are from Simulation 5 of Table 4-6. Test C3 was carried out on a transport path 32.5 meters in length, generally within Structure 21. The question for this tracer test is how the sorption in Structure 21 compares to the sorption in Structure 20, which was tested in tracer test C1. Structure 21 was a lower transmissivity, is a less prominent structure, more akin to a "background fracture" than Structure 20.

Figure 4-33 through Figure 4-36 display simulations of Test C3 sorbing tracer transport. Simulation 1 is run with K_d=0, Simulation 2 with Byegård K_d values, and Simulation 3 with enhanced sorption. Enhanced sorption/diffusion processes of 15 to 100% are consistent with the observations. This is generally greater than the values for Test C1, indicating a relative enhancement of retention processes for the lower transmissivity, smaller scale Structure 21.

Table 4-20 Lab K_d values for Test C3 Sorbing Tracers and Simulation K_d value.

Tracer	Byegård K_d (kg/m^3) (Simulation 2)	Calibration K_d (kg/m^3) (Simulation 3)	K_d Multiplier for Simulation
Na-22	$1.4*10^{-6}$	$7.14*10^{-5}$	51
Sr-85	$4.7*10^{-6}$	$4.7*10^{-4}$	100
Rb-83	$4.0*10^{-4}$	$2.4*10^{-2}$	60
Ba-133	$2.0*10^{-4}$	$3.0*10^{-3}$	15

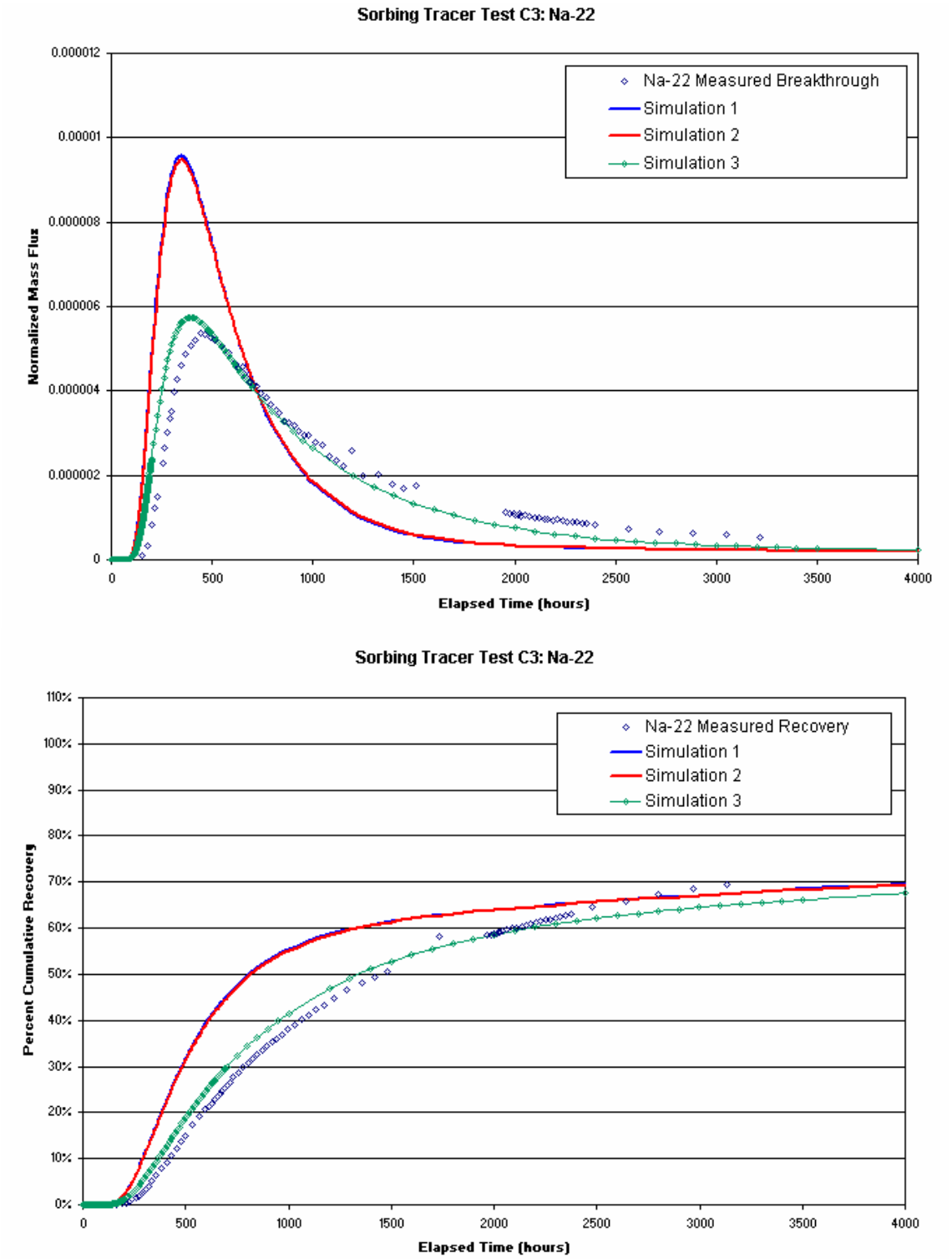

Figure 4-33 *Tracer Test C3 (Na-22): Simulations and Measured Data.*

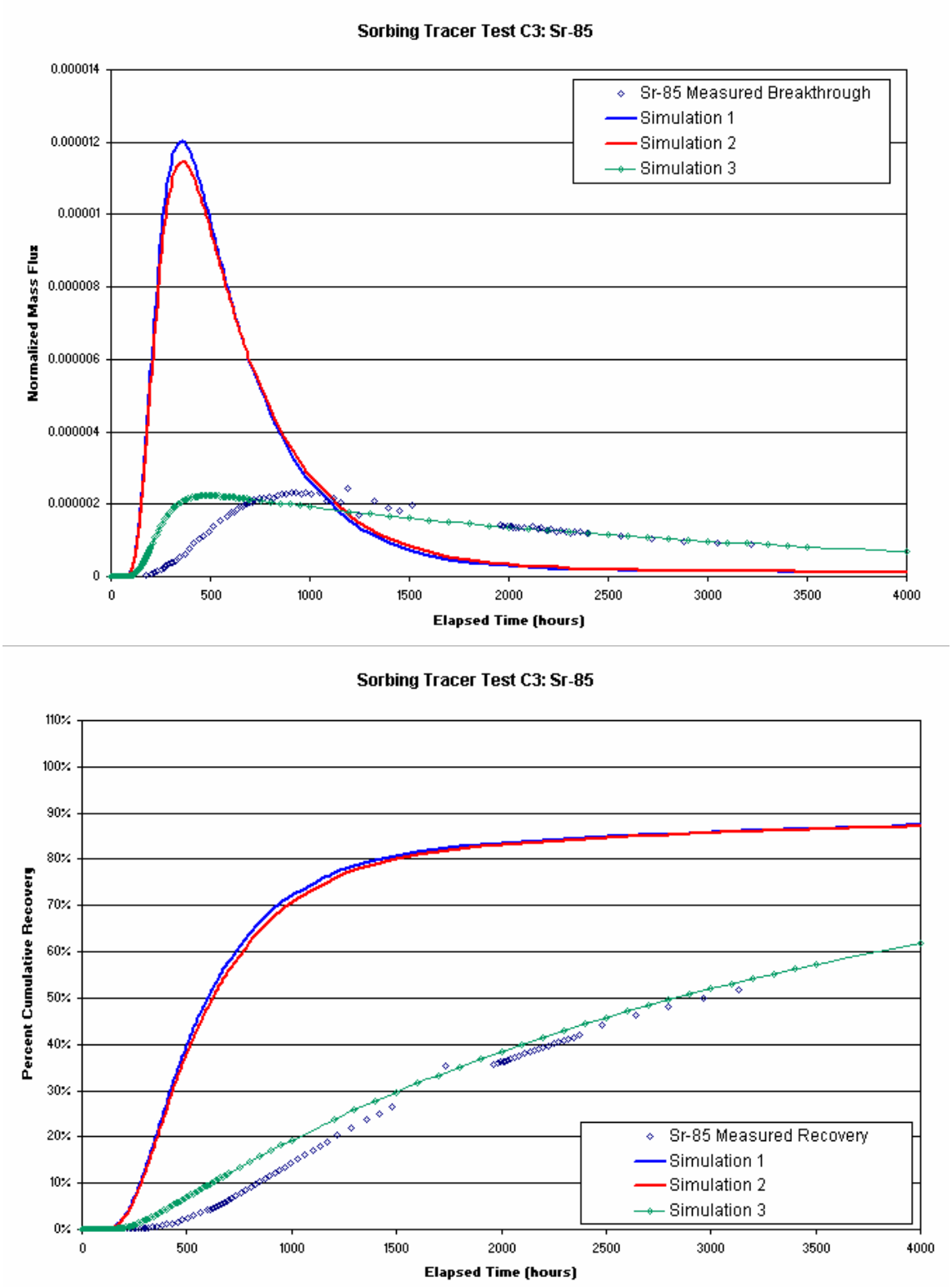

Figure 4-34 *Tracer Test C3 (Sr-85): Simulations and Measured Data.*

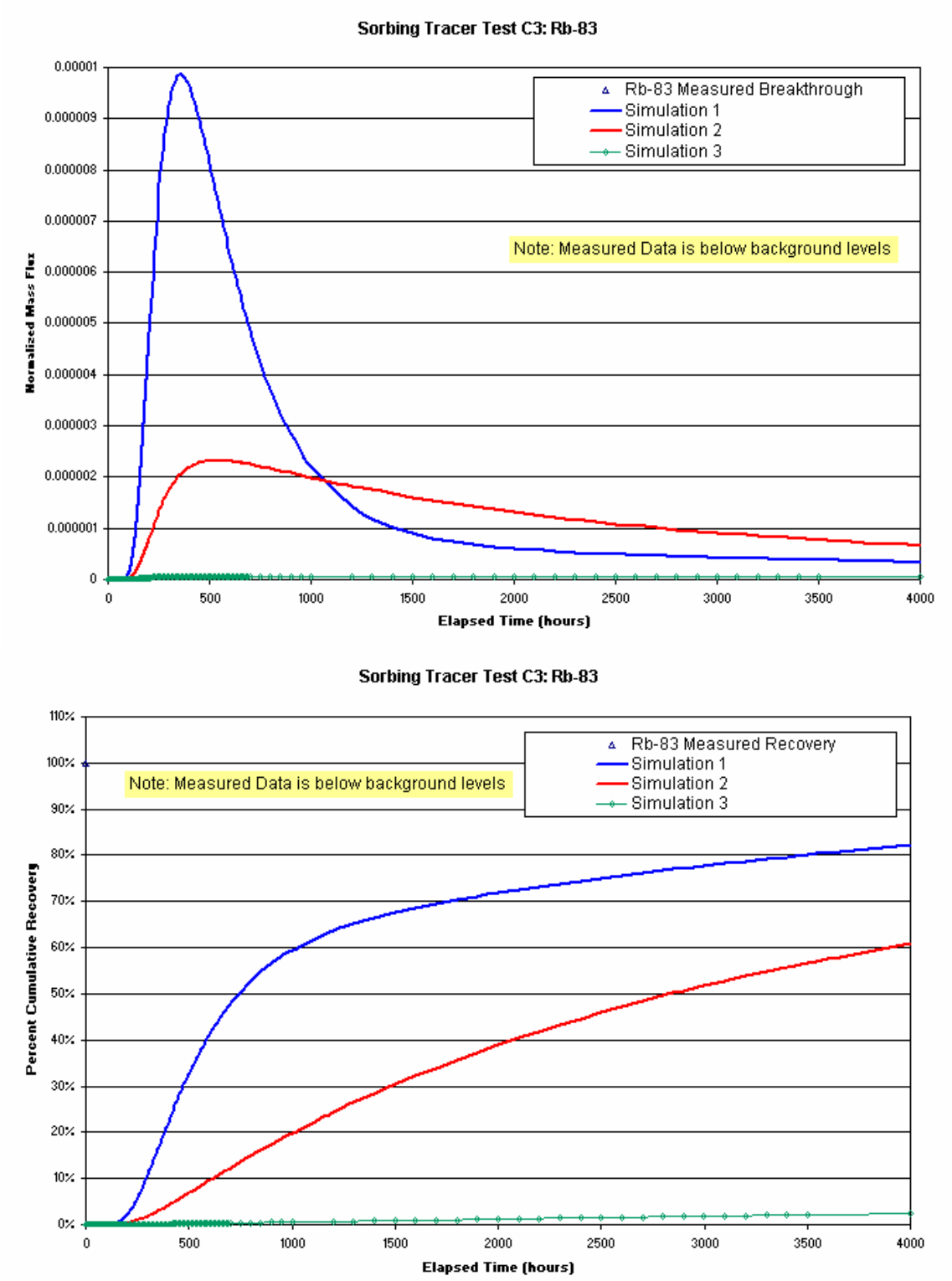

Figure 4-35 *Tracer Test C3 (Rb-83): Simulations and Measured Data. Measured Data is below background levels.*

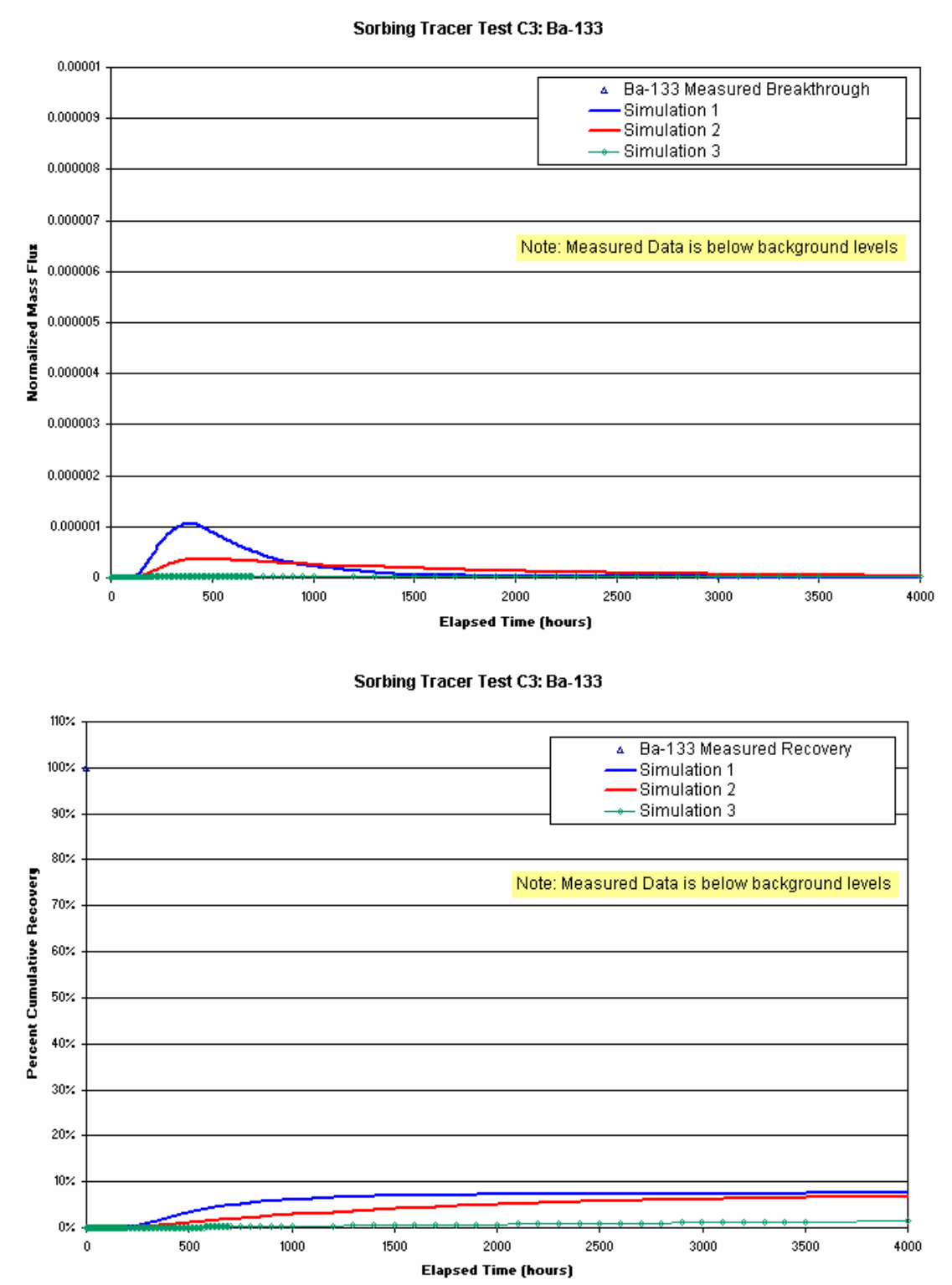

Figure 4-36 *Tracer Test C3 (Ba-133): Simulations and Measured Data. Measured Data is below background levels.*

4.3.4 TRUE-1 Sorption Parameter Comparison

The TRUE-1 sorbing tracer experiments were carried out in a reactivated mylonite "Feature A" which is structurally similar to many of the structures tested in the TRUE Block Scale tracer experiments. It is therefore interesting to examine how the calibrated K_d values from the TRUE-1 experiment (Dershowitz et al., 2000) compare with those reported above in Section 4.2.

Table 4-21 through Table 4-23 present a comparison of K_d values from calibration of TRUE-1 and TRUE Block Scale sorbing tracer experiments. For Test C1 (Table 4-21) and C2 (Table 4-22), the K_d value found is very similar to that for TRUE-1. This indicates that pathway and retention properties of "Structure 20" which provides the primary pathway in tests C1 and C2 has similar retention properties to those of "Feature A" which was the focus of the TRUE-1 experiments.

Test C3 was carried out on pathway III, which was primarily through Structure 21 rather than Structure 20. The retention K_d found in test C3 (Table 4-23) is significantly greater than that found for "Feature A" in the TRUE-1 experiments. This indicates that the fracture infillings, mineralogy, or pathway geometry for Structure 21 are different from those of "Feature A". The effective K_d derived for Test C3 is 2.3 to 12 times greater than that of "Feature A". It would be useful to examine the microstructure of "Structure 21" to determine why it exhibits enhanced retention relative to "Structure 20".

Table 4-21 TRUE-1 K_d (Dershowitz et al., 2000) comparison to Test C1 sorbing parameter calibration.

Tracer	Byegård K_d (kg/m^3)	TRUE-1 K_d (kg/m^3)	Calibration K_d (kg/m^3)	K_d Multiplier (Byegård)	K_d Multiplier (TRUE-1)
Na-24	$1.40*10^{-6}$	$2.70*10^{-5}$	$2.38*10^{-5}$	17.0	0.9
K-42*	$2.00*10^{-4}$	--	$4.40*10^{-4}$	2.2	--
Ca-47	$5.20*10^{-6}$	$6.30*10^{-5}$	$1.56*10^{-4}$	30.0	2.5
Rb-86	$4.00*10^{-4}$	$2.00*10^{-3}$	$2.40*10^{-3}$	6.0	1.2
Cs-134	$8.00*10^{-4}$	$8.30*10^{-3}$	$2.80*10^{-2}$	35.0	3.4

Table 4-22 TRUE-1 K_d (Dershowitz et al., 2000) comparison to Test C2 sorbing parameter calibration.

Tracer	Byegård K_d (kg/m^3)	TRUE-1 K_d (kg/m^3)	Calibration K_d (kg/m^3)	K_d Multiplier (Byegård)	K_d Multiplier (TRUE-1)
Ca-47	$5.2*10^{-6}$	$6.30*10^{-5}$	$6.24*10^{-5}$	12.0	1.0
Ba-131	$2.0*10^{-4}$	$1.30*10^{-3}$	$1.2*10^{-3}$	6.0	0.9
Cs-137	$8.0*10^{-4}$	$8.30*10^{-3}$	$1.04*10^{-3}$	1.3	0.1

Table 4-23 TRUE-1 K_d (Dershowitz et al., 2000) comparison to Test C3 sorbing parameter calibration.

Tracer	Byegård K_d (kg/m^3)	TRUE-1 K_d (kg/m^3)	Calibration K_d (kg/m^3)	K_d Multiplier (Byegård)	K_d Multiplier (TRUE-1)
Na-22	$1.4*10^{-6}$	$2.70*10^{-5}$	$7.14*10^{-5}$	51.0	2.6
Sr-85	$4.7*10^{-6}$	$1.00*10^{-4}$	$4.7*10^{-4}$	100.0	4.7
Rb-83	$4.0*10^{-4}$	$2.00*10^{-3}$	$2.4*10^{-2}$	60.0	12.0
Ba-133	$2.0*10^{-4}$	$1.30*10^{-3}$	$3.0*10^{-3}$	15.0	2.3

4.4 Effective Pathway Transport Parameters

The results of pathway transport property studies with conservative tracers are summarized in Table 4-24. From the conservative tracers, the pathway properties are generally as follows:

- Flow aperture: 0.17 to 2.7 mm (A = 2; B=0.5 from Equation 1)
- Transport Aperture: 30% of Flow Aperture
- Path Width: 5 to 22 cm
- Fracture Infilling/Fault Gouge Porosity: 0.5% to 40%
- Fracture Infilling/Fault Gouge Thickness: 0.1 to 3 mm
- Altered Rock Zone Porosity: 0.5% to 2%
- Altered Rock Zone Thickness: 0.5 to 2 cm.
- Unaltered Rock Zone Porosity: 0.01% to 0.1%
- Unaltered Rock Zone Thickness: 10m

The porosity and thickness values are at the upper end of the studied ranges. These values do, however, provide reasonable matches to observed breakthroughs within experimental accuracy and consistent with the microstructure conceptual model of Figure 4-2. Smaller values of immobile zone thickness and porosity were not able to reproduce the observed tails of the breakthrough curves.

The tracer experiments with conservative tracers indicate enhanced retention, since they seem to require values of immobile zone porosity on the high end of the physically reasonable range. The tracer experiments with sorbing tracers also seem to indicate enhanced retention, since the calibrated values of K_d are significantly higher than the K_d values reported by Byegård et al. (1998) which were used as reference values for this study. Byegård and calibrated K_d values are compared in Table 4-21 through Table 4-23 above.

During the TRUE Block Scale project, the primary theories put forward to explain this enhanced retention were:

a) increased area available for diffusion along the transport pathway, due to for example multiple reactive surfaces within the fracture or increased transport pathway width
b) increased effective diffusion considering porosity and tortuosity effects

Neither of these explanations was considered satisfactory, as we have no direct or indirect evidence to support them. Following the conclusion of the simulations reported above, an additional study was carried out which calculated K_d values for fracture coatings, fault gouge, cataclasite, altered rock, as well as intact rock (Dershowitz et al., 2003). These results were based on laboratory experiments using TRUE Block Scale groundwater.

The calibrated K_d values are compared against these laboratory based K_d values in Table 4-25 through Table 4-27. Transport parameters from the sorbing tracer simulations are summarized in Table 4-28. The calibrated K_d values are almost all between the Dershowitz et al. (2003) values for cataclasite and gouge based on laboratory experiments.

This provides a strong indication that the major retention processes for the TRUE Block Scale experiments occurred in fault gouge and in fracture minerals such as cataclasite. This is also consistent with the results shown in Sections 4.1 through 4.3 above, where high gouge and altered rock porosities were necessary to explain observed tracer breakthrough.

The calibrated K_d values from the TRUE-1 project (Table 4-21 through Table 4-23) are also consistent with the Dershowitz et al. (2003) gouge and cataclasite K_d values. This indicates that TRUE-1 experiments may also have been strongly influenced by fracture infillings.

Table 4-24 Calibrated Immobile Zone Parameters, Conservative Tracer Experiments.

Test	Test Length (m)	Dispersion Length (m)	Structure	Transport Aperture (m)	Pipe Width (m)	Advective Velocity (m/s)	Fracture Infill Porosity, Thickness	Altered Rock Porosity, Thickness	Unaltered Porosity, Thickness	FIZ	Mass Lost to FIZ after 1000 hours	FIZ Width (m)
A4a	17.9	1.5	20	$0.3*1.96*10^{-3}$	0.1	$6.18*10^{-5}$	5.5%, 0.003	2%, 0.02	0.1%, 10	Na	Na	Na
A4b	52.7	2.0	22	$0.3*1.22*10^{-3}$	0.16	$2.85*10^{-4}$	5.5%, 0.003	1.5%, 0.02	0.1%, 10	20/21	0.1%	0.1
			20	$0.3*1.96*10^{-3}$	0.1	$2.85*10^{-4}$	5.5%, 0.003	1.5%, 0.02	0.01%, 10			
			21	$0.3*1.80*10^{-3}$	0.11	$2.85*10^{-4}$	17%, 0.003	0.2%, 0.02	0.08%, 10			
A4c	68.6	2.9	23	$0.3*1.65*10^{-4}$	0.19	$8.87*10^{-4}$	5.5%, 0.003	0.5%, 0.02	0.01%, 10	20/21	94.8%	0.01
			22	$0.3*1.22*10^{-3}$	0.07	$3.17*10^{-4}$	5.5%, 0.003	0.5%, 0.02	0.01%, 10			
			20	$0.3*1.96*10^{-3}$	0.05	$3.17*10^{-4}$	5.5%, 0.003	0.5%, 0.01	0.01%, 10			
			21	$0.3*1.80*10^{-3}$	0.05	$2.54*10^{-4}$	17%, 0.003	0.2%, 0.02	0.01%, 10			
A5a	38.4	2.3	20	$0.3*1.96*10^{-3}$	0.1	$8.87*10^{-4}$	5.5%, 0.003	2%, 0.02	0.01%, 10	20/21	36.3%	0.1
A5b	55.9	4.5	21	$0.3*1.80*10^{-3}$	0.11	$1.55*10^{-5}$	17%, 0.003	0.2%, 0.02	0.08%, 10	Na	Na	Na
			20	$0.3*1.96*10^{-3}$	0.1	$1.55*10^{-5}$	5.5%, 0.003	2%, 0.02	0.01%, 10			
A5c	12.9	1	20	$0.3*1.96*10^{-3}$	0.1	$1.27*10^{-3}$	5.5%, 0.003	2%, 0.02	0.01%, 10	Na	Na	Na
A5d	41.1	4.1	22	$0.3*1.22*10^{-3}$	0.13	$1.27*10^{-4}$	10%, 0.003	2%, 0.02	0.1%, 10	22/20	46.9%	0.09
			20	$0.3*1.96*10^{-3}$	0.08	$1.27*10^{-4}$	5.5%, 0.003	2%, 0.02	0.01%, 10			
A5e	35.0	2.8	22	$0.3*1.22*10^{-3}$	0.13	$7.92*10^{-5}$	5%, 0.003	0.5%, 0.02	0.01%, 10	Na	Na	Na
			20	$0.3*1.96*10^{-3}$	0.08	$7.92*10^{-5}$	5%, 0.003	0.5%, 0.02	0.01%, 10			
B1a	17.9	1.5	20	$0.3*1.96*10^{-3}$	0.1	$3.42*10^{-4}$	5.5%, 0.003	2%, 0.02	0.1%, 10	Na	Na	Na
B1b	52.7	4.1	22	$0.3*1.22*10^{-3}$	0.16	$1.84*10^{-4}$	5.5%, 0.003	2%, 0.02	0.1%, 10	20/21	10.7%	0.1
			20	$0.3*1.96*10^{-3}$	0.1	$1.84*10^{-4}$	5.5%, 0.003	2%, 0.02	0.01%, 10			
			21	$0.3*1.80*10^{-3}$	0.11	$1.84*10^{-4}$	17%, 0.003	0.2%, 0.02	0.08%, 10			

Table 4-24 (Continued) Calibrated Immobile Zone Parameters, Conservative Tracer Experiments.

Test	Test Length (m)	Dispersion Length (m)	Structure	Transport Aperture (m)	Pipe Width (m)	Advective Velocity (m/s)	Fracture Infill Porosity, Thickness	Altered Rock Porosity, Thickness	Unaltered Porosity, Thickness	FIZ	Mass Lost to FIZ after 1000 hours	FIZ Width (m)
B1c	33.8	3.38	20	$0.3*1.96*10^{-3}$	0.1	$3.42*10^{-4}$	30%, 0.003	2%, 0.02	0.01%, 10	20/21	58.6%	0.05
B2a	52.7	4.1	22	$0.3*1.22*10^{-3}$	0.16	$2.54*10^{-4}$	5.5%, 0.003	2%, 0.02	0.1%, 10	20/21	28.2%	0.1
			20	$0.3*1.96*10^{-3}$	0.1	$2.54*10^{-4}$	5.5%, 0.003	2%, 0.02	0.01%, 10			
			21	$0.3*1.80*10^{-3}$	0.11	$2.54*10^{-4}$	17%, 0.003	0.2%, 0.02	0.08%, 10			
B2b	32.5	2	21	$0.3*1.80*10^{-3}$	0.1	$6.02*10^{-5}$	17%, 0.003	0.2%, 0.02	0.08%, 10	Na	Na	Na
B2c	169.2	13.5	19	$0.3*2.68*10^{-3}$	0.07	$6.65*10^{-5}$	17%, 0.003	0.5, 0.02	0.1%, 10	Na	Na	Na
			13	$0.3*8.25*10^{-4}$	0.22	$6.65*10^{-5}$	17%, 0.003	0.2%, 0.02	0.1%, 10			
			21	$0.3*1.80*10^{-3}$	0.1	$6.65*10^{-5}$	17%, 0.003	0.2%, 0.02	0.1%, 10			
B2d	68.6	2.9	23	$0.3*1.65*10^{-4}$	0.19	$8.87*10^{-4}$	5.5%, 0.003	0.5%, 0.02	0.01%, 10	20/21	23.3%	0.01
			22	$0.3*1.22*10^{-3}$	0.07	$3.17*10^{-4}$	5.5%, 0.003	0.5%, 0.02	0.01%, 10			
			20	$0.3*1.96*10^{-3}$	0.05	$3.17*10^{-4}$	5.5%, 0.003	0.5%, 0.01	0.01%, 10			
			21	$0.3*1.80*10^{-3}$	0.05	$2.54*10^{-4}$	17%, 0.003	0.2%, 0.02	0.01%, 10			
B2e	25.3	1.6	21	$0.3*1.80*10^{-3}$	0.1	$2.22*10^{-5}$	20%, 0.003	1.5%, 0.02	0.08%, 10	Na	Na	Na
B2g	17.9	1.5	20	$0.3*1.96*10^{-3}$	0.1	$5.70*10^{-4}$	5.5%, 0.003	2%, 0.02	0.1%, 10	Na	Na	Na
C1	17.9	1.5	20	$0.3*1.96*10^{-3}$	0.1	$5.70*10^{-4}$	5.5%, 0.003	2%, 0.02	0.1%, 10	Na	Na	Na
C2	68.6	5.9	23	$0.3*1.65*10^{-4}$	0.19	$8.87*10^{-4}$	5.5%, 0.003	0.5%, 0.02	0.01%, 10	20/21	0.1%	0.05
			22	$0.3*1.22*10^{-3}$	0.07	$3.17*10^{-4}$	5.5%, 0.003	0.5%, 0.02	0.01%, 10			
			20	$0.3*1.96*10^{-3}$	0.05	$3.17*10^{-4}$	5.5%, 0.003	0.5%, 0.01	0.01%, 10			
			21	$0.3*1.80*10^{-3}$	0.05	$2.54*10^{-4}$	17%, 0.003	0.2%, 0.02	0.01%, 10			
C3	32.5	2	21	$0.3*1.80*10^{-3}$	0.1	$4.39*10^{-5}$	17%, 0.003	0.2%, 0.02	0.08%, 10	Na	Na	Na

Table 4-25 Gouge and Cataclasite K_d (Dershowitz et al, 2003) Comparison to Test C1 sorbing parameter calibration.

Tracer	Byegård K_d (kg/m^3)	Gouge K_d (kg/m^3)	Calibration K_d (kg/m^3)	Cataclasite K_d (kg/m^3)
Na-24	$1.40*10^{-6}$	$1.1*10^{-4}$	$2.38*10^{-5}$	$1.1*10^{-5}$
K-42*	$2.00*10^{-4}$	$2.9*10^{-3}$	$4.40*10^{-4}$	$2.7*10^{-4}$
Ca-47	$5.20*10^{-6}$	$7.1*10^{-4}$	$1.56*10^{-4}$	$6.7*10^{-5}$
Rb-86	$4.00*10^{-4}$	$1.6*10^{-2}$	$2.40*10^{-3}$	$1.5*10^{-3}$
Cs-134	$8.00*10^{-4}$	$1.6*10^{-1}$	$2.80*10^{-2}$	$1.5*10^{-2}$

Table 4-26 Gouge and Cataclasite K_d (Dershowitz et al, 2003) Comparison to Test C2 sorbing parameter calibration.

Tracer	Byegård K_d (kg/m^3)	Gouge K_d (kg/m^3)	Calibration K_d (kg/m^3)	Cataclasite K_d (kg/m^3)
Ca-47	$5.2*10^{-6}$	$7.1*10^{-4}$	$6.24*10^{-5}$	$6.7*10^{-5}$
Ba-131	$2.0*10^{-4}$	$1.4*10^{-2}$	$1.2*10^{-3}$	$1.3*10^{-3}$
Cs-137	$8.0*10^{-4}$	$1.6*10^{-1}$	$1.04*10^{-3}$	$1.5*10^{-2}$

Table 4-27 Gouge and Cataclasite K_d (Dershowitz et al, 2003) Comparison to Test C3 sorbing parameter calibration.

Tracer	Byegård K_d (kg/m^3)	Gouge K_d (kg/m^3)	Calibration K_d (kg/m^3)	Cataclasite K_d (kg/m^3)
Na-22	$1.4*10^{-6}$	$1.1*10^{-4}$	$7.14*10^{-5}$	$1.1*10^{-5}$
Sr-85	$4.7*10^{-6}$	$7.1*10^{-4}$	$4.7*10^{-4}$	$6.7*10^{-5}$
Rb-83	$4.0*10^{-4}$	$1.6*10^{-2}$	$2.4*10^{-2}$	$1.5*10^{-3}$
Ba-133	$2.0*10^{-4}$	$1.4*10^{-2}$	$3.0*10^{-3}$	$1.3*10^{-3}$

Table 4-28 Comparison of Calibrated K_d, Sorbing Tracer Experiments against Byegård et al (1998) and Dershowitz et al.(2003).

Tracer	Test	K_d (kg/m^3) Byegård et al., 1998	Free Water Diffusion (m^2/s)	Calibrated K_d (kg/m^3)	K_d Multiplier (relative to Byegard)	K_d Multiplier (relative to Gouge Dershowitz et al. 2003	K_d Multiplier (relative to Cataclaste, Dershowitz et al. 2003)
Ba-131	C2	$2.0*10^{-4}$	$0.83*10^{-9}$	$1.2*10^{-3}$	6	0.086	**0.923**
Ba-133	C3	$2.0*10^{-4}$	$0.83*10^{-9}$	$3.0*10^{-3}$	15	**0.214**	2.308
Ca-47	C1	$5.2*10^{-6}$	$0.79*10^{-9}$	$1.56*10^{-4}$	30	**0.220**	2.328
Ca-47	C2	$5.2*10^{-6}$	$0.79*10^{-9}$	$6.24*10^{-5}$	12	0.088	**0.931**
Cs-134	C1	$8.0*10^{-4}$	$2.02*10^{-9}$	$2.80*10^{-2}$	35	0.175	**1.867**
Cs-137	C2	$8.0*10^{-4}$	$2.02*10^{-9}$	$1.04*10^{-3}$	1.3	0.007	0.069
K-42*	C1	$2.0*10^{-4}$	$2.00*10^{-9}$	$4.40*10^{-4}$	2.2	0.152	**1.630**
Na-22	C3	$1.4*10^{-6}$	$1.33*10^{-9}$	$7.14*10^{-5}$	51	**0.649**	6.491
Na-24	C1	$1.4*10^{-6}$	$1.33*10^{-9}$	$2.38*10^{-5}$	17	0.216	**2.164**
Rb-83	C1	$4.0*10^{-4}$	$2.03*10^{-9}$	$2.4*10^{-2}$	60	**1.500**	16.000
Rb-86	C3	$4.0*10^{-4}$	$2.03*10^{-9}$	$2.40*10^{-3}$	6	0.150	**1.600**
Sr-85	C3	$4.7*10^{-6}$	$0.79*10^{-9}$	$4.7*10^{-4}$	100	**0.662**	7.015

5 Conclusion

This report presents a series of studies to improve our understanding of flow and transport in the TRUE Block Scale rock mass based on an integrated study of hydraulic and tracer test results through December 2000. These studies address key issues regarding transport properties based on conservative and sorbing tracer tests, the possibility of special flow and transport properties at fracture intersection zones (FIZ), and the possibility to improve the project hydro-structural model through minor changes in connectivity and transmissivity.

The major conclusions of this study are as follows:

Tracer Transport and Retention

- Conservative tracer transport properties (transport aperture and flow width) are fairly consistent between the three major transport pathways studied (I, II, and III). The power law relationship between feature transmissivity and transport aperture could be applied consistently to all the transport pathways studied.
- Conservative and sorbing tracer retention on pathways I and II, which primarily involved Structure #20, is similar to that seen on "Feature A" in the TRUE-1 experiments. Both Structure #20 and "Feature A" are reactivated mylonites. Pathway III (Structure #21) has enhanced retention relative the pathways I and II.
- Sorbing tracer retention on pathways I, II, and III is consistent with K_d values calculated for gouge and cataclasite, rather than intact wall rock. This indicates that at the TRUE Block Scale experimental conditions, the primary retention is occurring in these or similar materials.
- By using gouge and cataclasite K_d values, there is no need to invoke enhanced reactive surface area to explain observed sorbing tracer breakthrough.

Hydrostructural Model and Fracture Intersection Zones

- Mass loss during tracer tests show a statistical correlation to the pathways crossing fracture intersection zones (FIZ). However, these paths tend to be the longer pathways, such that it cannot be definitively stated that this is a FIZ effect.
- There are several unexplained contradictions in the experimental results, such as the low conservative tracer (HTO) recovery for the C3 transport pathway, and the high conservative tracer (Br) recovery for the C2 transport pathway which appear to lose mass in earlier experiments.
- The hydro-structural model can be improved to match complex hydraulic interference responses through relatively minor changes to structure transmissivity and connectivity. In particular, the use of flow barrier "anti-fractures" within structures or at structure intersections has the potential to explain several observed responses.

Background Fractures

- Many hydraulic interference and tracer dilution measurements indicate that much of the rock block is not well interconnected. This lack of connection can be explained by the local absence of background fractures, or the presence of flow barrier structures. This indicates that background fractures may have less hydraulic significance than was assumed in the original DFN/CN model implementation.
- A small number of background fractures are necessary to explain hydraulic connections not provided by the deterministic structures
- Models containing a large number of ubiquitous background fractures are measurably over-connected when compared to hydraulic interference measurements.
- A less well connected, more heterogeneous background fracture population would be more consistent with the variety of hydraulic interference responses seen.

6 References

Andersson P., Ludvigsson J-E., Wass E. and Homqvist M., 2000a. Interference tests, dilution tests and tracer tests, Phase A, Swedish Nuclear Fuel and Waste Management Company (SKB), International Progress Report IPR-00-28.

Andersson P., Wass E., Holmqvist M. and Fierz T., 2000b. Tracer Tests, Phase B. Swedish Nuclear Fuel and Waste Management Company (SKB), Äspö Hard Rock Laboratory, International Progress Report IPR-00-29.

Andersson P., Ludvigsson J-E., Wass E. and Holmqvist M., 2001b. Detailed Characterisation Stage - Interference tests and tracer tests PT-1 - PT-4. Swedish Nuclear Fuel and Waste Management Company (SKB), Äspö Hard Rock Laboratory, International Progress Report IPR-01-52.

Andersson P., Byegård J., Dershowitz W., Doe T., Hermanson J., Meier P., Tullborg E-L., Winberg A., 2002a. TRUE Block Scale Project Final Report. 1. Characterization and model development. Swedish Nuclear Fuel and Waste Management Company. SKB Technical Report TR-02-13.

Andersson P., Byegård J. and Winberg A., 2002b. TRUE Block Scale Project Final Report 2. Tracer tests in block scale. Swedish Nuclear Fuel and Waste Management Company. SKB Technical Report TR-02-13.

Byegård J., Johansson H., Skålberg M. and Tullborg E-L. 1998. The interaction of sorbing and non-sorbing tracers with different Äspö rock types. Sorption and diffusion experiments in the laboratory scale. SKB TR-98-18. ISSN 0284-3757.

Dershowitz W., Foxford T., Sudicky E., Shuttle D.A. and Eiben T.,1998. PAWorks: Pathways analysis for discrete fracture networks with LTG solute transport. User Documentation, Version 1.5. Golder Associates Inc.

Dershowitz W., Fox A. and M. Uchida, 2000. Understanding of Sorbing Transport in Fracture Network at the 10 Meter Scale. Unpublished document.

Dershowitz W., 2000. Conductive background fractures in the area investigated in the Tracer Test Stage (TTS). Äspö Hard Rock Laboratory, International Technical Document ITD-00-03.

Dershowitz, W., Winberg A., Hermanson J., Byegård J., Tullborg E.L., Andersson P. and Mazurek M., 2003. A Semi-synthetic Model of Block Scale Conductive Structures at the Äspö Hard Rock Laboratory. SKB, Stockholm.

Hermanson J.; Follin S. and Wei L., 1997. Structural analysis of fracture traces in boreholes KA2563A and KA3510 and in the TBM tunnel. Swedish Nuclear Fuel and Waste Management Company, Äspö Hard Rock Laboratory, Technical Note TN-97-31b. SKB, Stockholm.

Hermanson J. and Doe T., 2000. March '00 structural and hydraulic model based on borehole data from KI0025F03. Swedish Nuclear Fuel and Waste Management Company (SKB), Äspö Hard Rock Laboratory, International Progress Report IPR-00-34.

Lide D., 1972. CRC Handbook of Chemistry and Physics, Volume 74.

Miller I., Lee G. and Dershowitz W., 1999. MAFIC: Matrix/Fracture Interaction Code with heat and solute transport. User Documentation Version 1.6, Golder Associates Inc.

Winberg A., Andersson P., Hermanson J., Byegård J., Cvetkovic V. and Birgersson L., 2000. "Final report of the first stage of the tracer retention understanding experiments." Swedish Nuclear Fuel and Waste Management Company (SKB), Technical Report TR-00-07. ISSN 1404-0344.

Winberg A., Andersson P., Byegård, J., Poteri A., Cvetkovic V., Dershowitz W., Doe T., Hermanson J., Gómez-Hernández J., Hautojärvi A., Billaux D., Tullborg E-L., Holton D., Meier P. and Medina A., 2003. Final report of the TRUE Block Scale project. Swedish Nuclear Fuel and Waste Management Company (SKB), Äspö Hard Rock Laboratory, Technical Report TR-02-16.